INVESTIGATION OF SLOW COOK-OFF CHARACTERISTICS OF SELF-IGNITING ENERGETIC MATERIALS

A THESIS SUBMITTED TO
THE GRADUATE SCHOOL OF NATURAL AND APPLIED SCIENCES
OF
MIDDLE EAST TECHNICAL UNIVERSITY

BY

ZEKERİYA TANER KAYA

IN PARTIAL FULFILLMENT OF THE REQUIREMENTS
FOR
THE DEGREE OF MASTER OF SCIENCE
IN
CHEMICAL ENGINEERING

FEBRUARY 2022

Approval of the thesis:

INVESTIGATION OF SLOW COOK-OFF CHARACTERISTICS OF SELF-IGNITING ENERGETIC MATERIALS

submitted by **ZEKERİYA TANER KAYA** in partial fulfillment of the requirements for the degree of **Master of Science** in **Chemical Engineering, Middle East Technical University** by,

Prof. Dr. Halil Kalıpçılar
Dean, Graduate School of **Natural and Applied Sciences** _____

Prof. Dr. Pınar Çalık
Head of the Department, **Chemical Engineering** _____

Prof. Dr. Görkem Külah
Supervisor, **Chemical Engineering, METU** _____

Prof. Dr. Murat Köksal
Co-Supervisor, **Mechanical Engineering, Hacettepe Uni.** _____

Examining Committee Members:

Assoc. Prof. Dr. Erhan Bat
Chemical Engineering, METU _____

Prof. Dr. Görkem Külah
Chemical Engineering, METU _____

Prof. Dr. Murat Köksal
Mechanical Engineering, Hacettepe Uni. _____

Assoc. Prof. Dr. Özgür Ekici
Mechanical Engineering, Hacettepe Uni. _____

Assist. Prof. Dr. Harun Koku
Chemical Engineering, METU _____

Date: 08.02.2022

I hereby declare that all information in this document has been obtained and presented in accordance with academic rules and ethical conduct. I also declare that, as required by these rules and conduct, I have fully cited and referenced all material and results that are not original to this work.

Name, Last name : Zekeriya Taner Kaya
Signature :

ABSTRACT

INVESTIGATION OF SLOW COOK-OFF CHARACTERISTICS OF SELF-IGNITING ENERGETIC MATERIALS

Kaya, Zekeriya Taner
Master of Science, Chemical Engineering
Supervisor: Prof. Dr. Görkem Külah
Co-Supervisor: Prof. Dr. Murat Köksal

February 2022, 174

In this study slow heating response of small-scale test items and full-scale munitions due to thermal decomposition of explosives was investigated. Thermal decomposition parameters of the four most prevalent explosive formulations (from P1 to P4) used in defense industry were determined using non-isothermal thermogravimetric analysis and differential scanning calorimetry. Considering these parameters, an igniter formulation was developed to burn the explosive formulations in a predefined temperature before the undesired deflagration and detonation in slow heating test.

A small-scale heating chamber was designed according to slow heating test standard requirements to determine the slow heating response (ignition temperature and ignition time) of the explosive formulations and of the developed igniter for 5, 15 and 25 °C/h heating rates in forced convection conditions. Coupling of igniter with P1 explosive configuration led to controlled burn response between 142.5-153.6 °C before the violent response of bare explosive formulation configurations (P1 to P4 without igniter) between 174.8-217.2°C at 5, 15 and 25°C/h heating rates. Cook-off temperature of the igniter, P1 (64% RDX by weight) and P2 (87% HMX by weight) explosive rose with increasing heating rate (from 5 to 25°C/h), whereas cook-off temperature of the P3 (45% HMX by weight) and P4 (20% RDX by weight)

explosive decreased with increasing heating rate (from 5 to 25°C/h). Cook-off temperature trend observed for different explosive formulations was attributed to ratio of heat generation due to thermal decomposition in explosive formulations to heat dissipation. This ratio is higher for the formulations that contains more energetic material such as P1 (64% RDX by weight) and P2 (87% HMX by weight). Numerical simulations of small-scale slow heating tests carried out with ANSYS Fluent software were validated by comparing the experimental temperature measurements with calculated results at different heating rates. Maximum temperature difference between experiments and simulations for cook-off temperature was calculated as 0.2, 0.4, and 1.2% for Igniter, P1 and P4 explosives and 1.8-7.5% for P3 and P2 explosives for suggested 15°C/h heating rate in literature.

In the second part of the study, a large-scale slow heating test with full-scale munition was conducted in a heating chamber under forced convection conditions. Flow in the heating chamber and around the full-scale munition coupled with the heat transfer in the munition was also modeled with ANSYS Fluent software. Cook-off temperature of P1 explosive was measured as 173.4°C in full-scale test. Cook-off temperature and cook-off time were calculated with 2.7% and 2.2% error in numerical simulations in addition to correct calculation of temperature profile and ignition point.

Developed methodology for determining the response of munitions against slow-heating threat by computer modeling is expected to facilitate the munition design phase and reduce the test risks and test costs at TUBITAK SAGE and domestic defense industry.

Keywords: Slow Heating, Cook-Off, Energetic Materials, Heat Transfer, Numerical Modelling.

ÖZ

KENDİLİĞİNDEN TUTUŞAN ENERJİK MALZEMELERİN YAVAŞ ISINMA (İNG. SLOW COOK-OFF) ÖZELLİKLERİNİN İNCELENMESİ

Kaya, Zekeriya Taner
Yüksek Lisans, Kimya Mühendisliği
Tez Yöneticisi: Prof. Dr. Görkem Külah
Ortak Tez Yöneticisi: Prof. Dr. Murat Köksal

Şubat 2022, 174

Bu çalışmada küçük ölçekli test kalemlerinin ve tam ölçekli mühimmatların, patlayıcıların ısıl bozunmasından kaynaklanan yavaş ısınma tepkisi araştırılmaktadır. Savunma kaynaklarında en çok kullanılan dört patlayıcı bileşiminin (P1'den P4'e) ısıl bozunma parametreleri izotermal olmayan termogravimetrik analiz ve diferansiyel taramalı kalorimetre ile belirlenmiştir. Bu parametreler dikkate alınarak yavaş ısınma testinde patlayıcı bileşimlerini istenmeyen şiddetli yanma (*ing.* deflagrasyon) ve infilak (*ing.* detonasyon) öncesinde yakacak bir ateşleyici (*ing.* igniter) bileşimi geliştirilmiştir.

Geliştirilen ateşleyici ve patlayıcı bileşimlerinin yavaş ısınma tepkisinin (tutuşma sıcaklığı ve tutuşma zamanı) 5, 15 ve 25°C/saat ısıtma hızlarında zorlamalı taşınım koşullarında belirlenmesi amacıyla yavaş ısınma test standart gereksinimlerine göre küçük ölçekli bir ısıtma kabini tasarlanmıştır. Ateşleyicinin P1 patlayıcısı ile birlikte kullanıldığı konfigürasyon 5, 15 ve 25°C/saat ısıtma hızlarında patlayıcıların tek başına kullanıldığı (ateşleyici olmadan) konfigürasyonun 174.8-217.2°C arasındaki şiddetli tepkisinden önce 142.5-153.6 °C arasında kontrollü bir yanmaya sebep olmuştur. Ateşleyicinin, P1 (ağırlıkça %64 RDX) ve P2 (ağırlıkça %87 HMX) patlayıcılarının tutuşma (*ing.* cook-off) sıcaklığı artan ısıtma hızı (5'ten 25 °C/saate) ile yükselmiş, ancak P3 (ağırlıkça %45 HMX) ve P4 (ağırlıkça %20 RDX)

patlayıcılarının tutuşma sıcaklığı artan ısıtma hızı (5'ten 25 °C/saate) ile azalmıştır. Farklı patlayıcı bileşimleri için gözlenen tutuşma sıcaklığı eğilimi patlayıcı bileşimlerinin ısıl bozunması sonucu oluşan ısı üretiminin ısı kaybına oranına bağlanmıştır. Bu oran daha fazla enerjik malzeme içeren bileşimlerde örneğin P1 (ağırlıkça %64 RDX) ve P2 (ağırlıkça %87 HMX) daha yüksektir. Küçük ölçekli test kalemleri için Ansys Fluent yazılımı ile gerçekleştirilen yavaş ısınma sayısal benzetimleri, deneysel sıcaklık ölçümleri ile hesaplanan sonuçlar karşılaştırılarak farklı ısıtma hızları için doğrulanmıştır. Literatürde önerilen 15°C/saat ısıtma hızı için deneyler ve benzetimler arasındaki en yüksek tutuşma sıcaklığı farkı ateşleyici, P1 ile P4 için %0,2, 0,4, 1.2 ve P3 ile P2 için %1,8-7,5 olarak hesaplanmıştır.

Çalışmanın ikinci kısmında büyük ölçekli yavaş ısınma testi tam ölçekli mühimmat ile bir ısıtma kabininde zorlamalı taşınım koşullarında gerçekleştirilmiştir. Isıtma kabinindeki ve tam ölçekli mühimmat çevresindeki akış da mühimmat içindeki ısı transferi ile birleştirilerek ANSYS Fluent yazılımıyla modellenmiştir. Tutuşma sıcaklığı tam ölçekli testte P1 patlayıcısı için 173,4°C olarak ölçülmüştür. Sayısal benzetimlerde sıcaklık profilinin ve tutuşma noktasının doğru hesaplanmasına ek olarak tutuşma sıcaklığı ve tutuşma zamanı da %2,7 ve %2,2 hata ile hesaplanmıştır.

Mühimmatların yavaş ısınma tehdidine karşı tepkisinin bilgisayar modellemesi ile belirlemesi için geliştirilen yaklaşım mühimmat tasarım aşamasını kolaylaştırması ve TÜBİTAK SAGE ile yerli savunma sanayisindeki test riskleri ile test maliyetlerini büyük ölçüde azaltması beklenmektedir.

Anahtar Kelimeler: Yavaş Isınma, Kendiliğinden Ateşlenme, Enerjik Malzemeler, Isı Transferi, Sayısal Modelleme.

To My Family

ACKNOWLEDGMENTS

I would like to thank my advisors, Prof. Dr. Görkem Külah and Prof. Dr. Murat Köksal, for their constant guidance, patience and support in this prolonged study.

I would like to express my gratitude for the encouragement from Dr. Emrah Konokman and M.Sarper Yavuz, current and former supervisors of the Terminal Ballistics Division during this study at The Scientific and Technological Research Council of Turkey (TUBITAK) Defense Industries Research and Development Institute (SAGE).

I would like to appreciate answers of Muharrem Özgün on Fluent software, suggestions of Emre Erten and Anıl Tatlıdilli on thermal decomposition studies, effort of İbrahim Yılmaz for the large-scale slow heating test and previous studies performed by Hakan Şahin and Erdoğan Aydemir on insensitive munitions at TUBITAK SAGE. I would also thank to leaders and members of my previous division notably Dr. Gürkan Atınç Yılmaz, Dr. Değer Çetin, Tarık Yücel and Hülya Kanbur with whom I developed the explosive formulations used in this study at TUBITAK SAGE for various projects.

Finally, my deepest gratitude to my family and friends for their unfailing support and continuous encouragement.

TABLE OF CONTENTS

LIST OF TABLES

LIST OF FIGURES

LIST OF ABBREVIATIONS

ALE3D	Arbitrary Lagrangian–Eulerian three-dimensional analysis
AP	Ammonium perchlorate
ASTM	American Society for Testing and Materials
ATEX	Explosive Atmosphere
CAD	Computer-aided Design
CFD	Computational Fluid Dynamics
DBTL	Dibutyltin dilaurate or [dibutyl(dodecanoyloxy)stannyl] dodecanoate
DHE	Di–(2–Hydroxyethyl)–5, 5-Dimethylhydantoin
DOA	Dioctyl adipate or di(octyl) hexanedioate
DSC	Differential Scanning Calorimetry
EM	Energetic Material
FEM	Finite Element Method
FVM	Finite Volume Method
F/W/O	Flynn/Wall/Ozawa Isoconversional Decomposition Model
HDPE	High Density Polyethylene
HMX	Cyclotetramethylenetetranitramine or 1,3,5,7-Tetranitro-1,3,5,7-tetrazocane
HNS	Hexanitrostilbene or 1,1′-[(*E*)-Ethane-1,2-diyl]bis(2,4,6-trinitrobenzene)
HTPB	Hydroxyl-terminated polybutadiene
ID	Inside Diameter
IDP	Isodecyl pelargonate or 8-methylnonyl nonanoate
IM	Insensitive Munition
IPDI	Isophorone diisocyanate or 5-isocyanato-1-(isocyanatomethyl)-1,3,3-trimethylcyclohexane
K/A/S	Kissinger/Akahira/Sunose Isoconversional Decomposition Model
MP	Melting Point
NATO	North Atlantic Treaty Organization

OD	Outside Diameter
ODTX	One-Dimensional Time to Explosion
PBX	Polymer Bonded Explosive
PETN	Pentaerythritol tetranitrate or 2,2-Bis[(nitrooxy)methyl]propane-1,3-diyl dinitrate
PP	Polypropylene
RAM	Random Access Memory
RANS	Reynold Averaged Navier-Stokes Equations
RDX	Cyclotrimethylenetrinitramine or 1,3,5-Trinitro-1,3,5-triazinane
SAGE	Defense Industries Research and Development Institute
SITI	Sandia Instrumented Thermal Ignition
SST	Shear Stress Transport
STANAG	Standardization Agreement
STEX	Scaled Thermal Explosion Experiment
TATB	Triaminotrinitrobenzene or 2,4,6-Trinitrobenzene-1,3,5-triamine
TGA	Thermogravimetric Analysis
TNT	Trinitrotoluene or 2-Methyl-1,3,5-trinitrobenzene
TPB	Triphenylbismuth or triphenylbismuthane
TÜBİTAK	Scientific and Technological Research Council of Turkey
UDF	User Defined Function
UN	United Nations
US	United States
VCCT	Variable Confinement Cook-Off Test

LIST OF SYMBOLS

$\dot{q}$	Volumetric Heat Generation, W/m^3
A	Pre-Exponential Factor, 1/s
B(t)	Baseline Signal in DSC Studies, mW/mg
C_p	Specific Heat Capacity, J/(kg.K)
D	Diameter, m
E	Energy term, W/m3
E_A	Activation Energy, J/(mol.K)
h	Convective Heat Transfer Coefficient, $W/(m^2.K)$
g	Gravitational acceleration, m/s^2
k	Rate Constant
I	Unit Tensor
J_j	Diffusion Flux of Species
L	Length, m
Nu	Nusselt Number
p	Pressure, MPa
Pr	Prandtl Number
Q	Decomposition Enthalpy, J/kg
q	Heat Flux, W/m^2
r	Radius, m
R	Universal Gas Constant, J/(mol.K) 8.314
r^2	Coefficient of Determination
r_{burn}	Burn Rate, mm/s
Re	Reynolds Number
R_{ij}	Reynolds Stress Tensor
S	Source Term, W/m^3
S(t)	Signal in DSC Studies, mW/mg
T	Temperature, °C, °F, K
t	Time, s
T_c	Critical Temperature, °C, K

Y_j Mass Fraction of Species

Greek Symbols

$\bar{u}$ Time Average Velocity, m/s

u' Fluctuating Velocity, m/s

δ_{ij} Kronecker Delta

$\bar{\varphi}$ Time Average Scalar Quantities (energy, pressure etc.)

φ' Fluctuating Scalar Quantities (energy, pressure etc.)

f (α) Reaction Model (Derivative Form)

g (α) Reaction Model (Integral Form)

α Extent of the Conversion

β Heating Rate in Thermal Analysis Devices, °C/minute

λ Thermal Conductivity, W/(m.K)

μ Dynamic Viscosity, Pa.s

μ_T Turbulent (Eddy) Viscosity

ρ Density, kg/m^3

u Instantaneous Velocity, m/s

δ Shape Factor for Critical Temperature Calculation

κ Turbulence Kinetic Energy

τ Shear Stress, Pa

φ Instantaneous Scalar Quantities (energy, pressure etc.)

ω Specific Dissipation Rate of Turbulent Kinetic Energy into Thermal Energy

CHAPTER 1

INTRODUCTION

Munition and missile systems used in defense industry contain different types of energetic materials (explosives, pyrotechnics, and propellants) for the implementation of mission. Pyrotechnics are used for the initiation of the other energetic materials and generation of smoke and light. Propellants are adopted for generating thrust that is required to transfer the payload and explosives are utilized for the intended blast and fragment performance. During the mission, performance of the munition and missile is the primary factor to be considered. However, during the storage and handling, which usually takes years to decades, sensitivity of the systems is the primary factor to be considered. Safe storage and handling are the dominant design factors for a munition system and several undesired external stimuli are considered during the design phase. External stimuli that threaten the munition and missile systems can be heat effects (fire and slow heating), impact and shock (bullet, fragment, shaped charged etc.). These stimuli and the potential response of the systems are summarized in Table 1.1 and energetic components of the systems are illustrated in Figure 1.1

Table 1.1 External Stimuli and Potential Response of the Munitions [1], [2]

<table>
<tr><th colspan="2">Stimuli</th><th colspan="2">Potential Responses</th></tr>
<tr><td>Thermal</td><td>• Fire
• Slow Heating
• Hot Spall Fragments</td><td rowspan="2">• Ignition
• Burning
• Propulsion
• Explosion
• Detonation
• Heat
○ Radiant
○ Hot Gases
○ Plasma</td><td rowspan="2">• Blast
○ Shockwaves
○ Overpressure
• Fragments
○ Small, High Speed
○ Large, Lower Speed
• Combinations of the above
• None</td></tr>
<tr><td>Impact and Shock</td><td>• Bullet
• Fragment
• Shaped Charge Jet
• Drop</td></tr>
</table>

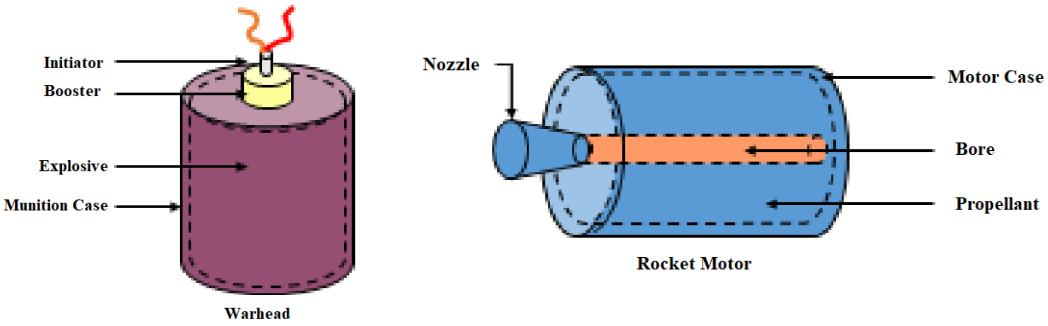

Figure 1.1. Energetic Components of Munition and Missile Systems

Thermal effects are the primary external stimuli or threat in insensitive munition design among fragment and shock stimuli. In a heated medium, heat generation of energetic material due to exothermic thermal decomposition can easily surpass the heat dissipation to the environment, which leads to violent response (rapid pressure rise, deflagration) especially for energetic material in a confined volume such as munitions or missiles. Thermal effects that lead to self-ignition of energetic material in a munition can be considered in two sub-groups which are fast heating and slow heating. Fast heating test simulates an undesired or accidental fire condition that can occur in a ship deck or storage compartment. Slow heating test, on the other hand, simulates an undesired or accidental fire condition between the adjacent compartments of a ship or storage facility. Fragment impact threat occur from an accidental fragment coming from detonation of other munitions, bullet impact threat results from a deliberate bullet coming from a rifle and shaped-charge jet threat originated from a deliberate shaped charge jet coming from an antitank or penetrating warhead. Sympathetic reaction simulates initiation or detonation of a pallet of a munition and considers the threat of a munition poses to other munitions in pallet. To define the stimuli and response, several test methods were developed for insensitive munitions in literature [3]. These stimuli and test methods are given in Table 1.2.

Table 1.2 External Stimuli and Test Methods for Insensitive Munitions [3]

Stimuli	Test
Thermal	• Slow Heating [4] • Fast Heating [5]
Impact and Shock	• Bullet Impact [6] • Sympathetic Reaction [7] • Fragment Impact [8] • Shaped Charge Jet [9]

When a designed munition system is tested against the external stimuli, responses in sensitivity tests are categorized in six groups (Figure 1.2) from worst to best case scenario which are, 1-Detonation, 2-Partial Detonation, 3-Explosion, 4-Deflagration, 5-Burning, 6- No Reaction. For the worst-case scenarios 1 to 3 (detonation to explosion), blast or fragment from the test item can detonate the adjacent munitions in a depot and this can affect greater area or facility. In an open area, produced blast and fragment because of detonation can cause equipment/platform damage or collateral damage to personnel. To prevent these undesired results, safer scenarios 4 or 5 (deflagration or burning of test item) is desired for the minimum effect and damage. It should be noted that for slow and fast heating tests, munitions are subjected to heat flux and any munition that contains energetic material (explosive or propellant) would always burn at the end of the test. Because of the burning of energetic material, most desired response for heating (cook-off) tests are type 5-Burning instead of type 6-No Reaction.

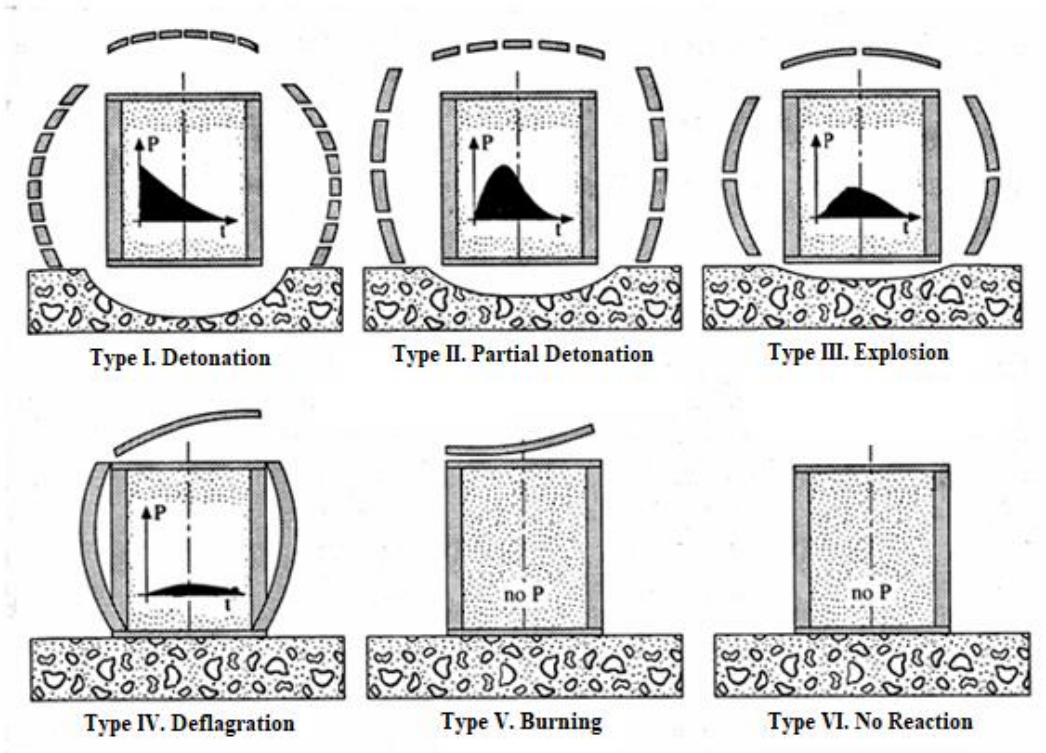

Figure 1.2. Typical Responses in Sensitivity Tests [10]

Since outcome of these stimulants summarized in Table 1.1 can be devastating, both international and domestic authorities require munitions to be tested for possible threats [3]. Insensitive munition (IM) concept is introduced in military literature that categorizes the degree of insensitiveness of the munition in response to the thermal, impact and shock threats. An IM munition is defined as "a munition that minimizes inadvertent initiation and severity of subsequent collateral damage when subjected to unplanned stimuli while reliably fulfilling its performance, readiness and operational requirements on demand" [11]. To simplify, a munition that responds as type 4-deflagration and type 5-burning to the threats can be considered as an insensitive munition (IM). IM approach in literature drew attention as a result of serious accidents between World War II and 1970s due to violent response of conventional munitions to the external threats (Figure 1.3). In this period, several accidents due to different external stimulants led to death or injury of personnel, damage, or loss of aircraft, ship, submarine, depot, military base. Stimulants and test

methods have been suggested as guidelines or policies since 1990s by different organization such as United Nations (UN) and North Atlantic Treaty Organization (NATO) for transport, handling, and storage of energetic materials for civil and military use [2], [10]. Turkey has also started considering these guidelines and policies especially after the accident in Kırıkkale that led to loss of munition plant in which conventional TNT explosive was cast into munitions in 1997 (Figure 1.4).

Figure 1.3. Accident due to Munitions from Various US Aircraft Carriers from 1960s [13], [14]

Figure 1.4. Accident due to Munitions Containing Conventional TNT Explosive in Kırıkkale-Turkey, 1997 [15]

IM assessment of munitions is considered as vital in munition design with the performance assessment. Knowing response of a munition system against a threat or external stimuli or response in an accident enable designers to protect personnel or launch platform in a mission in addition to facilitating the storage, handling, and transportation.

Heat effects summarized in previous paragraphs pose a great threat in storage, handling and transportation of energetic materials and munitions. It takes days or a week to control accidental fire in a munition depot and adjacent magazines (compartments) in depot may heat-up for prolonged time which slowly heats the munition or missile systems. Because of the confinement of energetic materials in munitions and missiles, decomposition due to heating and self-ignition is observed considerably lower than the autoignition temperature (which is measured in unconfined test tubes) of energetic materials. It is vital to store and handle munitions safely and to achieve this, modelling and testing of fast/slow heating response of the munition is required. Fast heating response of a munition can be tested in a liquid fuel fire pool that generates at least 800°C average flame temperature and at least 80 kW/m^2 heat flux to the test item. Slow heating response of a munition can be tested in a special test chamber that can heat the test item or munition in forced convection conditions with predefined slow heating rate 5, 15, 25 °C/hour. In this study, slow heating response of a munition is investigated.

1.1 Literature Review

Investigation of slow heating response of a munition requires proficiency in four subtopics which are (i) test set-up design, (ii) thermal decomposition of energetic materials, (iii) slow heating modelling and (iv) mitigation measures for slow cook-off.

1.1.1 Test Set-Up for Slow Heating

Slow heating test-setups are used to observe the response of energetic materials and generic test items to limit test risks and costs. Slow heating test standards in literature suggest heating with forced convection configuration in an air circulated test chamber [4]. Different laboratories (US Lawrence Livermore and Sandia National Laboratories) and companies have been using small-scale test set-ups from 6 g to 750 g range with different heating methods i.e., conduction or convection under different set-up names (Sandia instrumented thermal ignition (SITI), Variable confinement cook-off test (VCCT), Scaled Thermal Explosion Experiment, (STEX)). These small-scale set-ups were designed to measure decomposition, critical temperature, and ignition of energetic materials in ambient conditions or under confinement.

SITI was used for up to 6 g energetic materials having dimensions of 25.4 (diameter)*12.7 mm (length) [16]. VCCT on the other hand measures up to 50 g samples by heating bands with 3.3-25°C/h heating rate under confinement [17]–[19]. Both test set-ups employ conduction for heating and are illustrated in Figure 1.5.

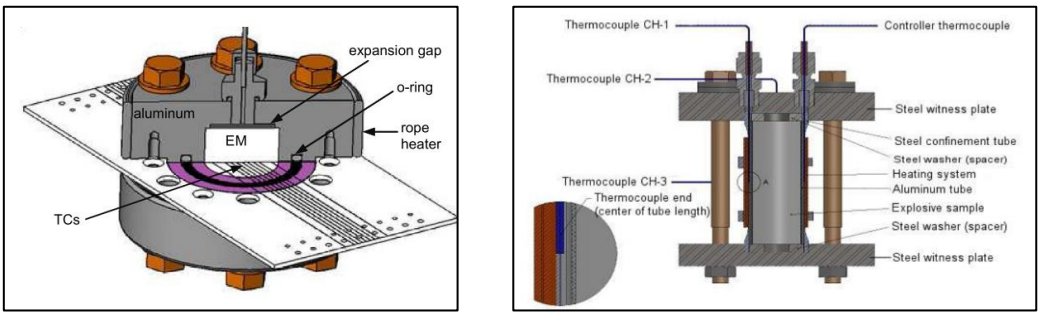

Figure 1.5. SITI (left) and VCCT (right) Slow-Heating Test Set-Ups [16], [17]

A medium-scale test set up called STEX was used at United States Lawrence Livermore National Laboratory to test polymer bonded explosive compositions that has a length/diameter ratio of 4 with a diameter of ≈5cm up to 750 g [20]–[23]. The

design of the STEX set-up is similar to VCCT test set-up in terms of confinement but heating is performed with radiative heaters instead of heating bands. Another medium-scale commercial heating chamber was used for testing of 0.35 kg of polymer bonded explosives in forced convection conditions with a 3.3°C/h heating rate [24] (Figure 1.6).

Figure 1.6. Medium (left) and Large-Scale (right) Slow-Heating Test Set-Ups [24]–[26]

In addition to chamber design, test parameters such as conditioning time and heating rate were also investigated in literature. Conditioning time that is required for uniform temperature distribution in test item with respect to diameter at the start of slow heating test was calculated by assuming 1D heat transfer among cylindrical test items [27]. Moreover, the effect of heating rate on temperature gradient in test chamber as well as ignition temperature and test response was investigated [28]. Effect of chamber isolation materials that contributes to uniform temperature distribution and reducing the cost of tests were also studied with large-scale test set-ups [26].

Majority of the small-scale set-ups mentioned above heat the test items with conduction contrary to recommended forced convection in the test standard [4]. Moreover, each large-scale test set-up requires modelling of air flow and heat transfer since unique design of the set-up (air flow) depends on the test item shape and dimensions. However, numerical simulation of large-scale test set-ups that couple heat transfer in the munition and fluid flow around the is not available in

literature. Therefore, small-scale experiments under forced convection heating can be conducted and large-scale test set-up can be simulated to fill the gaps in the literature. Furthermore, effect of heating rate on cook-off temperature for different explosives with the same test item at the same test conditions is also a useful addition to literature, which was studied at different conditions with different test items previously.

1.1.2 Thermal Decomposition of Energetic Materials

Exothermic thermal decomposition of energetic materials that leads to cook-off in slow/fast heating tests were also investigated in literature. In literature, it was shown that thermal decomposition of energetic materials could be investigated by the reaction rate data obtained from conventional thermal analysis devices that used Differential Scanning Calorimetry (DSC) and Thermogravimetric Analysis (TGA) methods. By using DSC and/or TGA parameters such as specific heat (C_p), activation energy (E_A) and pre-exponential factor (A) could be calculated which were used to obtain the heat generated due to self-decomposition considering Arrhenius equation [29] with several standardized calculation methods [30]–[37].

Trinitrotoluene (TNT), triaminotrinitrobenzene (TATB), pentaerythritol tetranitrate (PETN), hexanitrostilbene (HNS), cyclotrimethylenetrinitramine (RDX) and cyclotetramethylenetetranitramine (HMX) are the prevalent energetic materials employed for explosive formulations in literature. Energetic materials used in literature, especially nitramines such as RDX and HMX, were investigated by either thermal analysis devices in mg scale or by small-scale test set-ups such as One-Dimensional time to Explosion (ODTX) and Scaled Thermal Explosion Experiment (STEX) in g scale [38]–[47]. These nitramines (RDX and HMX) constitute majority (up to 87 % by weight) of the polymer bonded explosive (PBX) formulations also used in this study. Investigation of decomposition kinetics were conducted either by (i) analyzing the solely pure energetic material or nitramine [38]–[40], [42] (ii) nitramine with the presence of binder up to 10% by weight [41], [43], [48] or (iii)

nitramine in a PBX mixture with the presence of binder, plasticizer, bonding agent and metal powder up to 20% by weight [44]–[46]. For pure TNT and TATB three step autocatalytic thermal decomposition reaction was reported. For pure RDX and HMX three step decomposition reaction was observed, the first step being the slowest step. It was reported that for the third case (nitramine in PBX mixture), also investigated in this study, calibration was required for the kinetic data obtained from different test set-ups for the PBX mixtures [46]. In addition, decomposition of PBX mixtures that only contains ≈ 64 % by weight nitramine was attributed to nitramine only ignoring other constituents such as aluminum powder (≈ 20 % by weight) and polyurethane binder (≈ 16 % by weight) [20], [49]. Considering the calculation methods of thermal decomposition of energetic materials, it was understood that calculation of decomposition parameters of prevalent PBX mixtures using model-based kinetics could be a useful contribution to the literature in which decomposition is calculated with various simplified approaches (i, ii and iii) summarized above.

Thermal ignition of energetic materials also needs to be studied to calculate the critical temperature above which a given energetic material violently self-heats due to thermal decomposition. As slow cook-off begins after the critical temperature, calculation of critical temperature for different explosives are required for safe storage of munitions. In addition to this, critical temperature of the explosives investigated in this study is not covered in literature and calculation of critical temperature and comparison with slow cook-off temperature of those would be a contribution to literature.

Calculation methods of critical temperature of the conventional energetic materials (TNT etc.) were studied by various simplification and assumptions in literature. Nikolay Semenov, also awarded Nobel Prize in chemistry, concluded that ignition occurs when heat generation exceeds convective heat dissipation in a solid material that has a uniform temperature distribution by formulating heat generation and heat dissipation lines [50]. As uniform temperature distribution in a material is not

attainable due to imperfect mixing; Frank-Kamenetskii, also a student of Semenov, focused on the temperature gradient on the surface and center of the energetic materials to calculate critical temperature region of energetic materials for different shapes [51]. Induction periods before thermal explosions [52] and the application of Frank-Kamenetskii approach to RDX and TNT based formulations were also investigated in literature [53]. In addition to these studies, effect of energetic material reactant consumption, novel approaches to thermal initiation theory and critical ignition temperature of energetic materials were also investigated [54]–[56]. By implementing Frank-Kamenetskii approach in military standards, it was also shown in literature that this approach, which utilizes temperature gradient and conduction in solid energetic materials, could be applied for fast and slow heating purposes as well as determination of critical temperature [57]. Critical temperature calculation approach and calculated critical temperature values for test items are summarized in section 5.6.

1.1.3 Modelling of Slow Heating

Several commercial software packages that utilize finite element method (FEM) and finite volume method (FVM) were encountered in literature to simulate fast and slow heating in munition systems. Comsol Multiphysics and Abaqus FEA implements FEM, whereas Ansys Fluent implements FVM. Several in-house developed software such as ALE3D and CALORE can be used along with commercial software for 2D and 3D geometries in addition to basic 1D software reported in the literature for slow cook-off modelling. However, due to their proprietary nature, the methodology in modelling or software used in several studies were not reported in literature.

Ansys Fluent software has been used for slow and fast heating (cook-off) simulations of polymer bonded explosive formulations or TNT based melt-cast explosives to simulate convective heat transfer [58]–[60] Also, for the same and similar cases, COMSOL Multiphysics software was used considering Arrhenius decomposition

kinetics in addition to convective heat transfer [25], [61]. In addition, same software can be employed to calculate heat generation due to thermal decomposition of TNT based melt cast explosives with a 15% overestimation of the small-scale test data [17]. Abaqus FEA software was also utilized to simulate small-scale test set-up by using Arrhenius decomposition kinetics for a solid propellant [23].

Arbitrary Lagrangian–Eulerian three-dimensional analysis (ALE3D) code, an in-house multi-physics software, which was developed in United States (US) Lawrence Livermore National Laboratory has been used in several studies to model slow heating in energetic materials and munitions by considering Arrhenius type decomposition of energetic materials, strength model of solid materials and thermal expansion of constituents [20], [62]–[64]

1D and 2D FEA codes were also utilized in literature in addition to commercial software. CALORE code, a 2D finite element code, which was developed in US Sandia National Laboratory used for slow cook-off heating scenario considering the thermal decomposition data obtained from thermal analysis devices (DSC and TGA) [21]. REACON was another 2D finite element code developed at TUBITAK SAGE for simple geometries assuming zero order kinetics for energetic materials [65]. This code utilizes surface temperature profile of the test item as boundary condition instead of convective heat transfer around test item and requires additional meshing update for igniter configurations. Furthermore, 1D transient heat transfer equation was used to develop a simple Fortran code (TEPLO) considering zero order kinetics to solve to heat generation with respect to Arrhenius kinetics for cylinders, slabs and spheres by US Los Alamos National Laboratory [66], [67] . Moreover, similar approach in TEPLO code was used to form a simple Microsoft Excel spreadsheet [68] or to develop a 1D computer code (THERMEX) for solving heat generation and thermal initiation for different shapes in 1D [69].

Also undisclosed software similar to Abaqus and COMSOL were used to calculate slow heating in a munition by considering two-phase flow model with compressible solid and gas phases or to verify slow heating of polymer bonded in small-scale Variable confinement cook-off test (VCCT) test-setup or to calculate ignition point of a polymer bonded explosive containing sea-mine in slow and fast heating simulation or to calculate slow heating response of a warhead [70]–[75]. Investigation of the literature showed that commercial software packages readily available in literature could be utilized in slow cook-off studies.

1.1.4 Mitigation Measures for Slow Heating

Mitigation of cook-off in fast and slow heating tests are required to prevent violent behavior of munition or test item in IM design. Mitigation is achieved either by passive or active mitigation techniques. Passive mitigation techniques consider increasing the venting area by implementing parts that melt in elevated temperatures (≥100°C). Active mitigation techniques intend to burn the energetic material (explosive or propellant) in munition or test item from a predefined location near vents at specific temperature in a controlled manner. By burning the energetic material from a specific vent location, pressure rise due to ignition at an undesired location is prevented.

Passive mitigation techniques utilize meltable polymeric (high density polyethylene, HDPE, polypropylene, PP) or eutectic parts (plugs/aft closures). Different binary and tertiary eutectic mixtures were proposed in literature which are, 70 % Lithium + 30 % Zinc (Melting Point, (MP):164°C) [76], 40% Bismuth and 60 % Tin (MP:138°C) [77]. Active mitigation techniques use self-igniting energetic materials that have 20-40 °C lower ignition temperature than the energetic materials in munitions or test items. Boron and barium chromate based pyrotechnic mixtures or pentaerythritol tetranitrate (PETN) based igniter mixtures [78]–[82] (as well as undisclosed proprietary mixtures) were proposed for mitigation against slow heating threat for different type of munitions such as penetrator warheads and sea-mines [83].

Although use of igniters was suggested in literature, thermal decomposition and behavior of igniters in slow heating tests were not revealed. These parameters will also be calculated in this study and will be presented as contributions to the open literature.

As summarized above in four subtopics, literature survey reveals that decomposition and thermal initiation of the energetic materials can be modeled by using conventional thermal analysis devices and Arrhenius kinetics. Several commercial solvers or in house software were used for simulating heat transfer and decomposition of energetic materials in slow heating for 2D and 3D geometry. However, these studies rather focused on conductive heat transfer by defining temperature ramp (for instance 3, 5, 15 °C/hour) for the test item in simulations than the real problem that consists of forced convective heat transfer in small or large-scale test set-up. Furthermore, numerical simulation of large-scale test set-ups that couple heat transfer in the munition and fluid flow around the is not available in literature. In addition, modelling of slow heating of energetic materials with active mitigation methods such as igniters are not also studied in literature.

1.2 Motivation and Objectives

Assessment of insensitive munitions (IM) response of munitions and missiles used in defense industry has critical importance for safety of personnel and launch platforms as well as handling, storage, and transportation. IM assessment requires mild or non-violent response to several threats such as impact, shock, and heat. From these threats, external heating is considered as the most prevalent threat in literature. Possible violent behavior due to external fast or slow heating threat may lead to detonation or explosion which may cause severe damage to personnel or launch platform or storage. As fast and slow heating tests contain risk of detonation, computer modelling of heating and decomposition is required to decrease the test risks and costs.

The main objective of this study was to investigate the slow heating response of munitions in small and large-scale set-ups by experimental and numerical modelling studies. To achieve this objective, firstly, thermal decomposition of recently developed explosive formulations by thermal analysis devices was investigated. Secondly, a new igniter composition was developed for non-violent burning of explosives formulations in confined munitions. After that, explosive formulations and igniter decomposition kinetics were investigated in small-scale slow-heating test chamber at different heating rates under forced convection heating conditions. Ignition temperatures and time to ignition of different explosive formulations and igniter are intended to be simulated with a computational fluid dynamics software for different heating rates under these conditions. Finally, it was aimed to test and simulate slow heating response of a full-scale munition in a large-scale test chamber in the presence of axial asymmetric air flow. The scope of this study and the steps to be followed are summarized in Figure 1.7.

By completing these steps, a methodology for determining response of munitions and missiles to slow-heating threat will be achieved by gaining modelling capabilities of thermal decomposition of recently developed energetic materials and developed igniter composition under different heating rates and modelling of full-scale munitions under forced convection conditions. This methodology is expected to facilitate the design and IM assessment of full-scale munition and missile systems by implementing numerical modelling capabilities for decomposition and heat transfer, which in turn significantly decrease the full-scale testing of munitions. Decreasing the number of full-scale slow heating tests would eliminate the risks and costs of the testing in domestic defense industry considerably. In addition, for polymer bonded explosives and igniter composition; thermal decomposition parameters, critical temperature and slow cook-off temperature for several heating rates are presented as contributions to the literature as well as numerical simulation of large-scale slow heating test set-up.

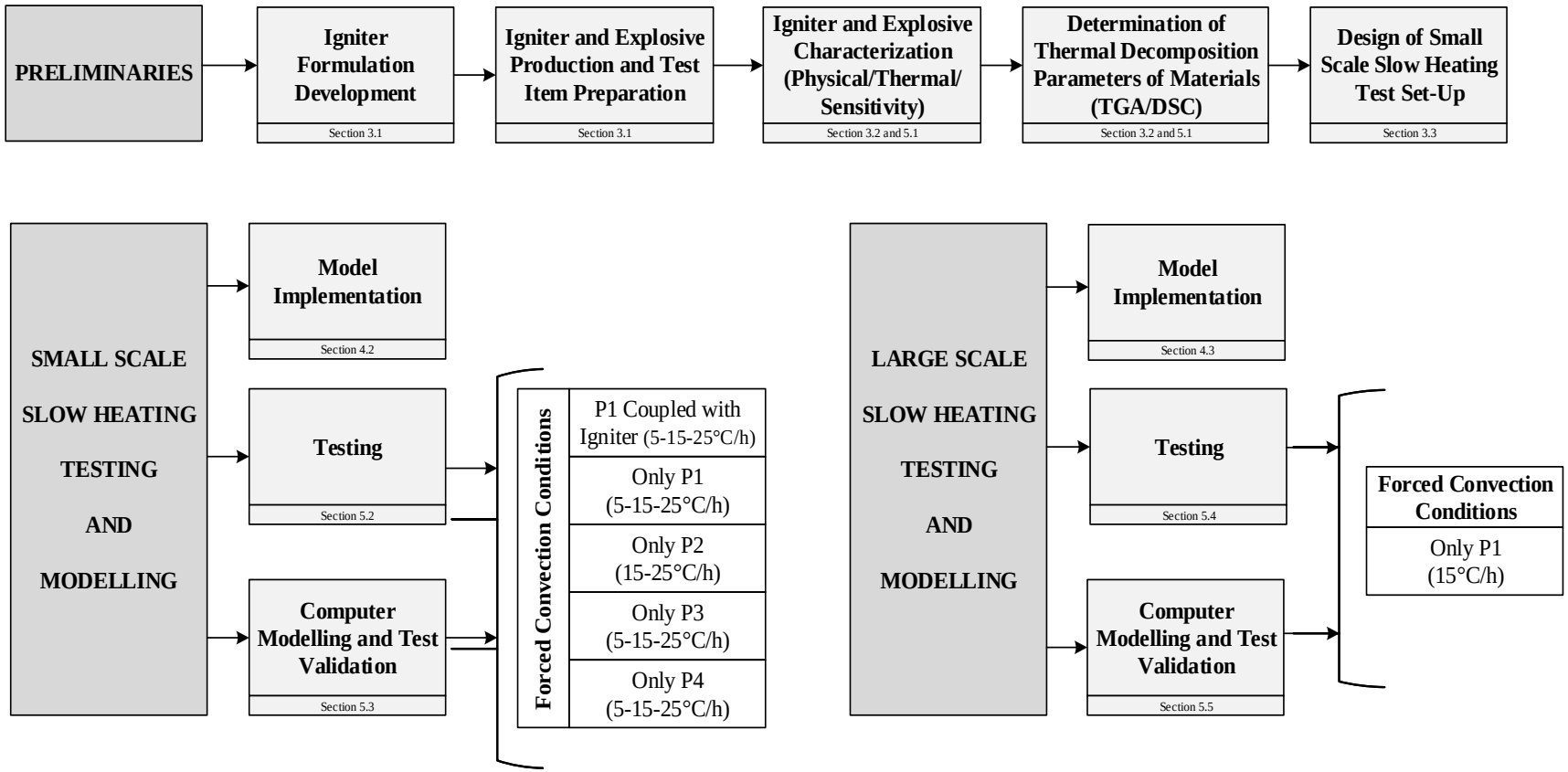

Figure 1.7 Scope of This Study

CHAPTER 2

MODELLING OF SLOW HEATING

The aim of the modelling efforts is to calculate the transient temperature distribution in explosive containing test items and test chambers as well as predict the temperature profile, self-ignition temperature and time. By modelling the slow heating test and slow cook-off process it is intended to limit the number of tests, test risks and cost.

2.1 Energy Balance for Selected Geometries

With slow heating (cook-off) tests, it is intended to simulate the response of a munition against prolonged adjacent heating source (fire etc.) that heats up the test item slowly in a depot, on a ship or on a railcar. Slow heating test method requirements were defined in literature with test standard, and it was recommended to conduct the test using forced convection heating method with 15°C/hour heating rate in a disposable test chamber [4]. Figure 2.1 illustrates the recommended test set-up for slow heating test. Test requires temperature measurements from various locations of the insulated test chamber and test item, while heating the test item with a hot air inlet stream and discharging the air through air outlet ports. Slow heating tests is a destructive test that includes the risk of detonation/explosion and it is desired to limit the scale and number of the conducted tests. To reduce the test risks and costs, modelling of slow heating is required. In this study a small-scale test item and a large-scale (full-scale) munition is selected for heating and cook-off investigations.

Small-scale test item was used for testing four type of explosives (from P1 to P4) and an igniter at different heating rates (5, 15, 25°C/h) and validation of tests with

computer modelling. Large-scale test item was used for determining slow heating response of a full-scale penetrator warhead and modelling temperature profile of the test. To model the selected geometries, it is required to tabulate the governing equations and boundary conditions. Governing equations for small and large-scale test items are revealed in section 2.1.1 and 2.1.2 respectively, while experimental details about test items and test set-ups are summarized in section 3.3. In addition, implementation of governing equations to computer model is presented in section 4.2 (small-scale simulation model) and 4.3 (large-scale simulation model) respectively.

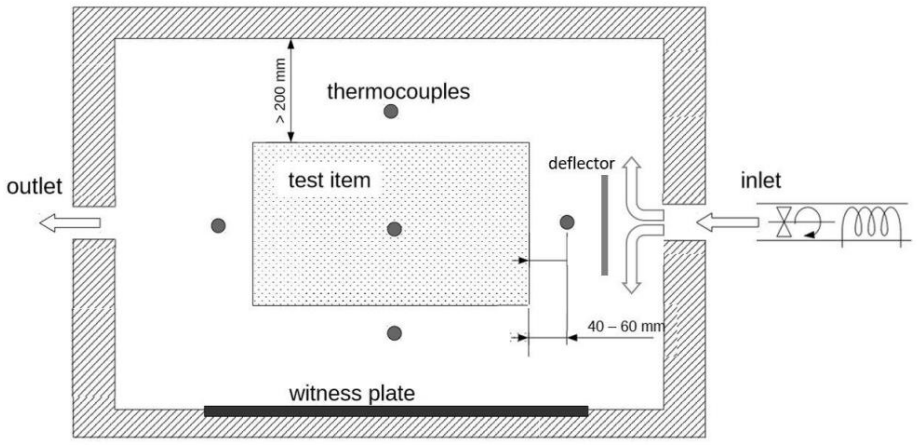

Figure 2.1. Slow Heating Set-Up From Test Standard [4]

2.1.1 Small-Scale Test Item

Small-scale test item consists of 34.2 mm diameter explosive in a 42.2 mm diameter cylinder Aluminum casing. Length of the explosive is 68 mm and length of the casing is 85 mm. Explosive is enclosed with Teflon plug (5 mm thickness) and other end of the explosive is open to air to discharge the burn products during cook-off. Small-scale test item is illustrated in Figure 2.2. Illustrated test item is heated in a small-scale test chamber that complies with test standard and Figure 2.1. Forced convection in the small-scale test chamber is provided with an air fan that produces

0.4 m/s constant velocity around test item. Test item is located parallel to chamber door that consists of a transparent polycarbonate window to observe the cook-off process. The test item is placed in the test chamber in such a way that crossflow air flow takes place around it. The position of the test item is selected deliberately to protect the chamber window against the possible violent response (thrust, deflagration, explosion, detonation etc.) in tests. Detailed photograph of the small-scale test item and test set-up is presented in section 3.3.1.

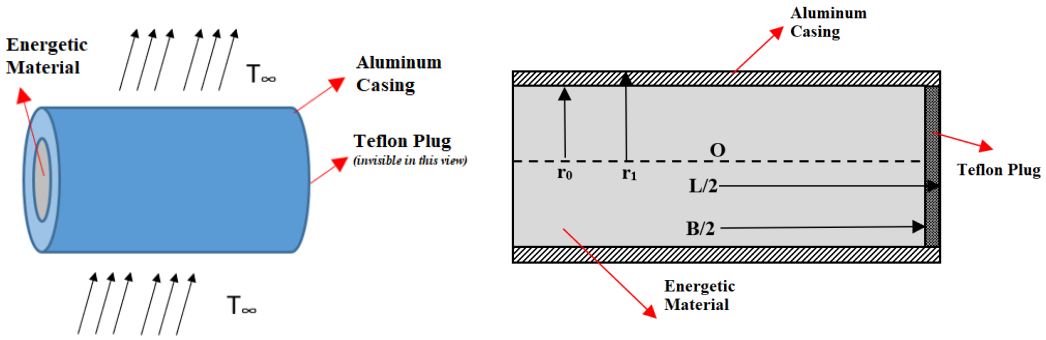

Figure 2.2. Small-Scale Slow Heating Test Item Illustration

Small-scale test item in a cross air flow can be modeled in 3D using general energy equation (Eq. 1) for a stationary system considering convective heat transfer around test item but ignoring the contact resistance around test item and between test item-explosive interface. Radiation is also neglected as radiation is not the dominant mode of heat transfer in the temperature range of study. Contact resistance can be neglected because explosive is firmly attached to casing by compressing the casing with a clamp. In addition, casing material is Aluminum that has a relatively high thermal conductivity. Radiative heat transfer is also neglected considering the relatively low maximum air temperature (150-200°C) inside test chamber. "$\dot{q}$" is considered as the source term (volumetric heat generation) due to exothermic thermal decomposition of the explosive in elevated temperature (between 130-200°C). It should be noted that the air flow around the test item was not solved and convective heat transfer boundary condition was imposed on the test item surface. The general energy equation reads as:

$$\rho C_p \frac{\partial T}{\partial t} = \frac{\lambda}{r}\left(\frac{\partial T}{\partial r} + \frac{r\partial^2 T}{\partial r^2}\right) + \frac{\lambda}{r^2}\frac{\partial^2 T}{\partial \theta^2} + \lambda \frac{\partial^2 T}{\partial z^2} + \dot{q}(t, r, \theta, z) \qquad \text{Eq. 1}$$

Energy equation should be solved as set of equations for 3D geometry for Aluminum casing and Teflon plug (Eq. 2) and explosive (Eq. 3).

$$\rho_0 C_{p_0} \frac{\partial T}{\partial t} = \frac{\lambda_0}{r}\left(\frac{\partial T}{\partial r} + \frac{r\partial^2 T}{\partial r^2}\right) + \frac{\lambda_0}{r^2}\frac{\partial^2 T}{\partial \theta^2} + \lambda_0 \frac{\partial^2 T}{\partial z^2} \qquad \text{Eq. 2}$$

$$\rho_0 C_{p_1} \frac{\partial T}{\partial t} = \frac{\lambda_1}{r}\left(\frac{\partial T}{\partial r} + \frac{r\partial^2 T}{\partial r^2}\right) + \frac{\lambda_1}{r^2}\frac{\partial^2 T}{\partial \theta^2} + \lambda_1 \frac{\partial^2 T}{\partial z^2} + \dot{q}(t, r, \theta, z) \qquad \text{Eq. 3}$$

Initial and boundary conditions for these equation sets are illustrated in Appendix A in detail ignoring the radiative heat transfer. To simplify, initial condition at time=0 is set as T_0=50°C (323.15 K) (recommended by test standard) for both Eq. 2 and Eq. 3. For Aluminum casing and Teflon plug (Eq. 2) boundary condition at r=r_1 and z=L/2 is conductive heat transfer being equal to convective heat transfer ($q_{conduction}=q_{convection}$= h(T)($T_\infty$(t)-T(t,r,θ,z)) and coupled conduction terms are equal to each other between contact surfaces of (i) explosive perimeter and Aluminum inner wall (r=r_0) and (ii) explosive right end and Teflon plug (z=L/2). For explosive (Eq. 3) coupled conduction terms are equal to each other (i) between contact surfaces of explosive perimeter and Aluminum inner wall (r=r_0) and (ii) explosive right end and Teflon plug (z=L/2). Also boundary condition at z=-L/2 (explosive left end is open to air) is conductive heat transfer being equal to convective heat transfer ($q_{conduction}=q_{convection}$= h(T)($T\infty$(t)-T(t,r,θ,z)). Convective heat transfer coefficient for small-scale simulations can be calculated by using correlations available in the literature for cross air flow around cylinder. Hilbert, Zukauskas and Churchill-Bernstein correlations were recommended in literature for cross air flow around cylinder [84]–[87]. While the first and second correlations suggests different coefficients with respect to increasing Re_D, Churchill and Bernstein correlation

reveals a generalized correlation for Re_D.Pr>0.2 given in Eq. 4. These correlations correspond to 9.03±0.05, 8.25±0.05, 9.3±0.05 W/m^2.K average convective heat transfer coefficient respectively for the small-scale test chamber used in this study (between 50-220°C air temperature and 400-1000 Re_D). Initially, Churchill-Bernstein correlation that leads to highest average convective heat transfer coefficient (9.3±0.05 W/m^2.K) is selected for this study. It is decided that if the selected correlation leads to higher simulation temperature results compared to experimental results due to highest heat transfer coefficient value; correlation with lowest heat transfer coefficient (Zukauskas) can be used for simulations. Selected Churchill-Bernstein correlation is used to calculate instantaneous average convective heat transfer from air to test item in small-scale simulations considering the film temperature for cross air flow for Re_D.Pr>0.2 (which is 300-600 in this study). Velocity of cross air flow around small-scale test item in test chamber is measured as 0.4 m/s using Kestrel 4000 anemometer. Implementation of governing energy equations to small-scale simulation model is presented in section 4.2.

$$\overline{Nu}_D = \frac{\bar{h}D}{\lambda} = 0.3 + \frac{0.62 Re_D^{1/2} Pr^{1/3}}{[1+(0.4/Pr)^{2/3}]^{1/4}} \left[1 + \left(\frac{Re_D}{282000}\right)^{5/8}\right]^{4/5} \qquad \text{Eq. 4}$$

for Re_D.Pr>0.2

2.1.2 Large-Scale Test Item

Large-scale test item is located parallel to asymmetric air inlet and air outlet streams due to longitudinal design of test chamber shown in Figure 2.3. Initially, similar to small-scale test item; convective heat transfer coefficient was intended to be calculated by correlations from the literature for axial flow around cylinders. However, it was encountered that majority of the correlations were available for crossflow configuration and the available correlations for axial flow were either for different L/D ratio or different Reynolds number [88]–[91]. Moreover, even a correlation for this geometry is available, location of air inlet/outlet, test fixture and

test item does not allow to calculate an average air velocity around test item. Furthermore, velocity measurements in the same time frame results in between 0.20-0.85 m/s around test item. Considering the lack of reliable correlation for convective heat transfer coefficient, it was decided to simulate whole test set-up including test chamber, air flow in/out, test fixture and test item.

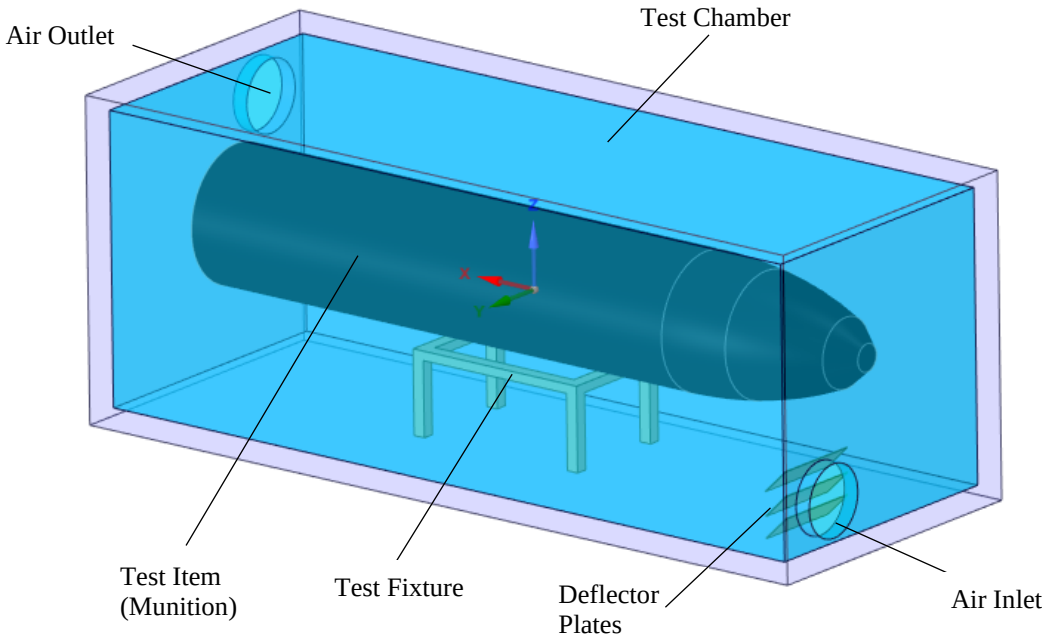

Figure 2.3. Large-Scale Slow Heating Test Item Illustration

To model air flow in the large-scale slow heating test set-up, continuity (Eq. 5) and incompressible momentum conservation equations (Eq. 6) should be used in addition to energy equations (Eq. 7 and Eq. 8) [92]. For the transport equations given, bold notations are used for vectors and $\bar{\bar{}}$ accent is used for tensors.

$$(\nabla \cdot \boldsymbol{u}) = 0 \qquad \text{Eq. 5}$$

$$\rho \frac{D\boldsymbol{u}}{Dt} = \rho \left(\frac{\partial \boldsymbol{u}}{\partial t} + \boldsymbol{u} \cdot \nabla \boldsymbol{u} \right) = -\nabla \mathrm{p} + \nabla \cdot \bar{\bar{\boldsymbol{\tau}}} + \rho \boldsymbol{g} + \boldsymbol{F} \qquad \text{Eq. 6}$$

$$\bar{\bar{\tau}} = \mu\left[(\nabla \boldsymbol{u} + \nabla \boldsymbol{u}^{T}) - \frac{2}{3}\nabla \cdot \boldsymbol{u}\bar{\bar{I}}\right] \quad \text{Eq. 7}$$

$$\frac{\partial(\rho E)}{\partial t} + \nabla \cdot \left(\boldsymbol{u}(\rho E + p)\right) = \nabla \cdot \left((\lambda \nabla \mathrm{T} - \sum_{j}\left(\int_{T_{ref}}^{T} c_{p,j} dT\right)\boldsymbol{J_j} + \bar{\bar{\tau}} \cdot \boldsymbol{u}\right) + \dot{q} \quad \text{Eq. 8}$$

$$E = \sum_{j}\left(\int_{T_{ref}}^{T} c_{p,j} dT\right)\boldsymbol{Y_j} - \frac{p}{\rho} + \frac{u^2}{2} \quad \text{Eq. 9}$$

$\bar{\bar{\tau}}$ given in Eq. 6 is stress tensor defined in Eq. 7. $\rho \boldsymbol{g}$ and **F** given in Eq. 6 is gravitational and external body forces respectively. μ is viscosity and $\bar{\bar{I}}$ is the unit tensor in Eq. 7. First three terms on the right side of the Eq. 8 denotes conduction, species diffusion and viscous dissipation respectively $\boldsymbol{J_j}$ being the diffusion flux of species (only air in this study). Energy term (E) given in Eq. 8 is defined in Eq. 9 and Y_j used in Eq. 9 is mass fraction of species.

Initial condition for the large-scale test item (munition) and test fixture was selected as 51.5°C (324.65 K) and experimental air temperature for the air which is 55.1°C (328.25 K) before the start of heating. Boundary conditions for the system illustrated in Figure 2.3 was defined considering the inlet and outlet air streams. Inlet air stream velocity (10 m/s) and inlet air temperature profile (measured in large-scale experiment) can be defined as "velocity inlet" boundary condition for the solver and outlet stream can be defined as "pressure outlet" boundary condition. Other components in the simulation such as air inside chamber, test item (munition) casing and test fixture were identified as coupled surfaces by the software. By doing so interface of the munition case and air is solved according to convective heat transfer and interface of the munition case, liner and explosive is solved according to conductive heat transfer. Implementation of governing energy equations to large-scale simulation model is presented in section 4.3.

Air flow entering the large-scale test chamber leads to laminar flow along deflector plates (Re=45,000-100,000; L_c=0.2 m), transient flow on bottom of the test chamber (Re=300,000-600,000; L_c=1.25 m) and laminar flow around the test item (Re=30,000-80,000 changes with respect to air velocity and temperature, minimum 10,000 and maximum 230,000; L_c=1.50 m). These different flow regimes simultaneously existing in the test chamber can be handled using a low Reynolds number turbulence model which can perform in the transition region. For this purpose, shear stress transport (SST) κ-ω empirical turbulence model was chosen since it is known to provide accurate predictions at low Reynolds number conditions compared to other models [93]. SST κ-ω turbulence model with coupled solution method is used for the large-scale slow heating test set-up considering the model and solver capabilities [92], [93]. The details of the SST κ-ω turbulence model is given in Appendix B.

2.2 Determination of Source Term

The temperature distribution in the test items and munitions during the slow cook-off process depends on the transient heat generation, and accurate determination of this source term is critical for successful prediction of the cook-off temperature. Thermal decomposition of materials is analyzed with the data derived from thermal analyses using differential scanning calorimetry (DSC) and thermogravimetric analysis (TGA) systems in literature. These systems can also be used for the energetic materials by carefully considering their highly exothermic decomposition reactions and by limiting the sample size with 5.0 mg as well as performing open pan thermal analysis tests [36]. Kinetic analysis in thermal decomposition studies concentrates on measurements and parametrization of the process rates on temperature and pressure [33]. Rate can be related to temperature (T), pressure (P) and the extent of the conversion (α) or reaction model f (α) as can be seen in Eq. 10 [33], [94]. Usually, the effect of pressure is ignored in solid explosives for ambient conditions contrary to propellants. For instance, burn rate of the P1 explosive can be expressed with Eq. 11 and is less than 1 mm even in 10 MPa (100 bar) considering

the r_{burn}(mm/s)=0.24.$p^{1.32}$(MPa) relation from literature [95]. Accordingly, the dependence of rate constant (k) can be considered to be only function of two variables which are α and T as shown in Eq. 12 where rate constant (k) can be related to temperature (T) with well-known Arrhenius equation (Eq. 13) [29]. Also, for a non-isothermal analysis, heating rate (β) can be related to temperature and time with Eq. 14. Then for constant heating rate non-isothermal analysis, Eq. 15 is obtained. This equation can be used for determining the thermal decomposition in non-isothermal conditions. In addition, reaction model f (α) can be rearranged to give integral of reaction model as g(α) to replace time dependent temperature function (Eq. 16). Depending on the type of the analysis method and data available, both reaction models can be used in calculations. Usually differential data dα/dt is available for DSC and integral data is available for TGA. α_i (α at $t=t_i$) value given in Eq. 17 can be calculated by using TGA data where m_0 is initial mass, m_i is mass at $t=t_i$ and m_f is final mass. α_i (α at $t=t_i$) given in Eq. 18 can also be obtained by DSC knowing that S(t) is signal, and B(t) is baseline.

$$\frac{d\alpha}{dt} = k(T)f(\alpha)h(P) \qquad \text{Eq. 10}$$

$$h(P) = a.P^n \qquad \text{Eq. 11}$$

$$\frac{d\alpha}{dt} = k(T)f(\alpha) \qquad \text{Eq. 12}$$

$$k(T) = Ae^{-E/RT} \qquad \text{Eq. 13}$$

$$\beta = \frac{dT}{dt} \qquad \text{Eq. 14}$$

$$\beta\frac{d\alpha}{dT} = Ae^{\left(-\frac{E}{RT}\right)}f(\alpha) \qquad \text{Eq. 15}$$

$$g(\alpha) = \frac{A}{\beta}\int_0^{\alpha}\frac{d\alpha}{f(\alpha)} = \frac{A}{\beta}\int_0^{T} e^{(-E/RT)}dT \qquad \text{Eq. 16}$$

$$\alpha_i = \frac{m_0 - m_i}{m_0 - m_f} \quad \text{Eq. 17}$$

$$\alpha_i = \frac{\int_0^i [S(t) - B(t)]dt}{\int_0^f [S(t) - B(t)]dt} \quad \text{Eq. 18}$$

General thermal decomposition equation (Eq. 15) can be solved by considering model-based and isoconversional (model-free) kinetics. Model based kinetics assumes that f (α) or g (α) can be fitted to a simple kinetics model. For instance, 1st, 2nd or nth order reaction model can be assumed (f (α)=(1- α)^n for n=1,2 or n) as well as many more reaction models are available in literature such as power law, 1/2/3D diffusion, 1/2/3D nucleation (Avrami-Erofeev), autocatalytic or Prout-Tompkins [33], [94]. Isoconversional (model-free) kinetics, on the other hand, assumes that conversion (α) is only function of temperature (T). This assumption leads to calculation of activation energy without determining any reaction model. Due to this assumption, this approach is also called model-free method. Isoconversional methods lead to general Eq. 19. For b=0 and c=1, this equation further simplifies to Eq. 20 which is known as Flynn/Wall/Ozawa equation [32], [33], [37], [96]–[98]. Furthermore, Eq. 21 is also available in literature for b=2 and c=1 which is known as Kissinger/Akahira/Sunose equation [30], [33], [99]. It should be noted that either by using DSC or TGA methods, activation energy for any conversion (α) can be calculated. However, model-free methods do not suggest any correlation for preexponential factor (A) and a reaction order assumption have to be made to calculate A value for given conversion value. For instance, for a DSC or TGA data set, if it is desired to calculate E and A for given peak temperature value, E can be calculated by model free methods either by using Eq. 20 or Eq. 21. But to calculate pre-exponential factor (A), a reaction order should be assumed (preferably first order). By assuming first order decomposition for a given peak temperature value where decomposition is the fastest along the thermogram, pre-exponential factor (A) can be calculated using Eq. 22. Once the thermal decomposition parameters are

calculated source term "$\dot{q}$" in equation Eq. 23 can be derived using equation Eq. 1 in section 2.1, Q being the decomposition enthalpy that can be measured with DSC.

$$\ln\left(\frac{\beta}{T_\alpha^b}\right) = \text{Constant} - \text{c}\left(\frac{E_\alpha}{RT_\alpha}\right) \quad \text{Eq. 19}$$

$$\ln(\beta) = \text{Constant} - \left(\frac{E_\alpha}{RT_\alpha}\right) \quad \text{Eq. 20}$$

$$\ln\left(\frac{\beta}{T_\alpha^2}\right) = \text{Constant} - \left(\frac{E_\alpha}{RT_\alpha}\right) \quad \text{Eq. 21}$$

$$A = \beta \frac{E_A e^{E_A/RT}}{RT^2} \quad \text{Eq. 22}$$

$$\dot{q} = \rho Q A e^{-E_A/RT} \quad \text{Eq. 23}$$

It should be noted that thermal analysis methods such as DSC and TGA do not depend on species in the mixture and result cannot be directly linked with a specific reaction of molecule [33]. Furthermore, even if an explosive mixture decomposes in a multi-step kinetics, decomposition kinetics can be determined with single-step model-based approaches [33]. This usually means that multi-step reaction contains several steps and slowest step of the multi-step reaction complies with the single-step model-based approach [33]. For instance, RDX and HMX molecules which constitute the energetic material content of P1, P2, P3 and P4 actually decomposes with multi-step kinetics, however slowest step in the multi-step kinetics comply with first order decomposition [38], [39], [100], [101].

CHAPTER 3

EXPERIMENTAL

3.1 Energetic Materials

Four types of explosive formulations and an igniter composition were investigated in experimental studies. Studied explosive formulations in the experiments are the most prevalent ones used in defense literature. P1 gives the optimum blast and heat effect, P2 produces high blast for fragment and shaped charge, P3 is used for enhanced blast for closed and confined volumes and P4 is an oxygen rich composition for underwater applications. In addition to these formulations, to burn these explosive formulations before the critical temperature where heat generation due to thermal decomposition rises exponentially, an igniter can be used. In this study, pentaerythritol tetranitrate (PETN) based polymer bonded explosive was selected as igniter by considering its availability, cost, and critical temperature. Critical temperature of PETN (≥120°C) is lower than the studied explosive compositions but high enough to safely use it in munitions operating conditions.

Igniter and P1 explosive formulations consist of energetic solid powders and thermoset polyurethane matrix. These compositions are called polymer (plastic) bonded explosives in literature due to their polyurethane matrix. Crosslinked thermoset polyurethane matrix greatly contributes to insensitiveness, thermal and mechanical properties of explosive formulations while holding the different powders in its matrix. Polyurethane matrix is produced by using a polyol binder (Hydroxyl-terminated polybutadiene, HTPB) and isocyanate curative (isophorone diisocyanate, IPDI) considering the functional groups numbers and equivalent ratios of functional groups with the presence of organometallic catalysts (mainly triphenylbismuth, TPB) and plasticizers (dioctyl adipate, DOA and isodecyl pelargonate, IDP). Other processing agents can also be used (wetting agent, bonding agent etc.) considering

the processing requirements. Cyclic nitramines such as cyclotrimethylenetrinitramine, RDX and cyclotetramethylenetetranitramine, HMX are the main energetic materials used in explosive formulations. These molecules are stable enough to handle and process against friction, impact, and electrostatic discharge but sensitive enough to react rapidly to produce heat and gas that leads to shock in detonation. Nitramine groups (-NH-NO_2) in RDX and HMX provide both the stability in handling and rapid energy release in detonation. Aluminum powder is added to explosive formulations to sustain shockwave with exothermic oxidation after detonation and ammonium perchlorate (AP) is considered for ensuring oxygen balance in reactions in underwater applications. Composition of studied formulations are summarized in Table 3.1. Composition of explosive formulations (P1 to P4) given in table are proprietary formulations and the weight percent of the ingredients are subject to change up to 5 % by weight according to processing and performance requirements. Considering this, only nominal values from literature were revealed for P1 to P4. Values for the igniter composition on the other hand, revealed precisely.

Table 3.1 Composition of Developed Igniter and Studied Explosive Formulations (% by weight)

	Ingredient	Igniter	**P1** [102]	**P2** [103]	**P3**	**P4** [104]
Energetic Content	**RDX**	37.5	64.0	-	-	20.0
	HMX	-	-	88.0	45.0	
	AP	-	-	-	-	43.0
	PETN	42.3	-	-	-	-
	Al	-	20.0	-	35.0	25.0
Inert Content	**Binder (HTPB)**	9.3	7.3	5.4	9.2	5.7
	Plasticizer (DOA)	9.5	7.3	-	9.2	-
	Plasticizer (IDP)	-	-	5.4	-	5.7
	Curative (IPDI)	0.8	1.1	0.5	0.8	0.5
	Bonding Agent (DHE)	-	0.3	-	-	-
	Catalyst (TPB)	-	0.02	-	0.02	0.03
	Catalyst (DBTL)	0.003				
	Wetting Agent (Lecithin)	0.7		0.7	0.7	
Density (g/cm^3)		1.50±0.01	1.66±0.01	1.66±0.01	1.69±0.03	1.81±0.01

3.1.1 Production of Energetic Materials

Production of explosive formulations is performed by mixing the ingredients in state of art mixers, casting the mixture to Teflon molds, and curing the explosive mixture in chambers. Depending on the cross-linked density and catalyst activity, curing takes 3-7 days in 40-70°C. After curing of explosive, elastic explosive test items are obtained. Mixing of explosive is dangerous and proprietary process that is carried out in extreme care and attention. Production progress includes adding of ingredients

in various steps and ratios in a mix bowl and mixing the ingredients in different mixing speed while applying vacuum or purging inert gas in different temperatures. Special explosion proof, remote-controlled mixing system that was designed considering explosive atmosphere (ATEX) requirements of process was used to produce the explosives investigated in this study. AKANA VK-6 double blade vertical planetary mixer that has 3-liter mixing capacity was employed for production and various curing chambers are used for curing of explosive formulations. Mixer employed in this study has two mixing blades that have different planetary orbits which has a minimum distance of ≤1mm with each other and mixing bowl to ensure the best possible mixing quality. Figure 3.1 illustrates the special explosive mixer and Figure 3.2 shows produced igniter and P1 explosive. In Figure 3.2 igniter is shown as blocks; however, it is cut to desired diameter with cylinder punch before slow heating tests.

Figure 3.1. Explosive Mixer Used for Producing Igniter and Explosive Formulations (P1-P4)

Figure 3.2. Igniter (left) and P1 Explosive (right) Used in This Study

3.2 Characterization of Energetic Materials

Characterization of explosives and igniter is vital in understanding their slow cook-off behavior. All the devices used for characterization of explosive formulations are subject to quality assurance procedures of TUBITAK SAGE and either calibration or verification of the devices have been carried out in 6-12 month periods.

3.2.1 Physical and Thermal Characterization

Density of the explosives was determined by using a gas pycnometer (AccuPyc 13330) that calculated the volume change of weighted sample in a calibrated volume by measuring pressure of helium gas. Specific heat of the test items was measured with differential scanning calorimetry (DSC) between 50-120°C. Thermal conductivity of the explosives were obtained by using C-Therm TCI thermal conductivity instrument between 50-100°C. This device uses modified transient plane source technique that employs a one-sided heat reflected sensor to measure thermal conductivity. Sensor consists of a calibrated heating coil element which calculates the thermal conductivity by relating the potential difference (voltage) change due to heat transfer to the test sample for different testing temperatures.

3.2.2 Characterization of Thermal Decomposition Parameters

Thermal decomposition parameters, activation energy and pre-exponential factor (E_A and A), of explosive formulations were calculated by using either differential scanning calorimetry (DSC) or thermogravimetric analysis (TGA). First approach employs differential scanning calorimeter that compares the heat required to increase the temperature of the sample with the reference material with known thermophysical properties. By calculating heat flow with respect to time or temperature, phase transitions (melting, crystallization, glass transition temperature) and decomposition temperatures and enthalpies can be calculated. Second approach employs thermogravimetric analyzer that measures the mass of sample with respect to time for a given heating rate.

Thermal decomposition parameters of energetic materials can be calculated either by DSC or TGA methods by obtaining thermograms for different heating rates preferably between 1-10 °C/min [36]. First method considers heat flow with increasing temperature while latter uses mass loss. Both methods require multiple datasets, because milligram sample size does not always reflect the actual explosive composition due to inadequate mixing and the location of sample in bulk explosive block sample. For five different explosive types and assuming at least four different heating rates, more than 20 measurements is required for each method even for one data set is used for each explosive type. As explosive compositions have high decomposition enthalpy, relatively higher heat and combustion products are evolved during decomposition. This is especially detrimental to differential scanning calorimeter. To protect the calorimeter instead of using 2 mg of sample sizes for DSC methods, up to 4 mg sample size and TGA methods were employed for thermal decomposition studies of explosive. However, DSC method was still used for measuring decomposition enthalpy and specific heat of explosive samples, but it was rather used with 2 mg sample size and with only one heating rate instead of multiple heating rates and several data sets.

Depending on the availability of thermogravimetric analyzers at TUBITAK SAGE, several devices were used to gather data sets for explosive compositions and igniter for different heating rates. Experiment conditions are summarized in Table 3.2 for each specimen type. Thermal decomposition studies by using TGA can be performed by using isothermal or non-isothermal methods. Isothermal studies investigate mass loss in several constant temperature values (between 150-250°C) while non-isothermal studies measure mass loss in several heating rates (1-10°C/h) from room temperature to decomposition temperature. Although both methods reported to be applicable for thermal decomposition studies [33], it is also reported that isothermal methods also require an inevitable heat-up period to reach preset isothermal temperature which can lead to significant conversion value or decomposition [105]. Moreover, isothermal methods require more test duration (>8 hour) that can be detrimental to thermogravimetric analyzer for multiple data sets in long term. Due to these possible drawbacks, non-isothermal methods were selected for thermal decomposition studies of explosive compositions.

Table 3.2 TGA Parameters for Thermal Decomposition Studies

Parameter		**Igniter**	**P1**	**P2**	**P3**	**P4**
Decomposition Kinetics (TGA)	**Device**	TGA (TA Ins.-Q500)	TG/DTA (Hitachi 6300)	TGA (TA Ins.-Q500)	TGA (TA Ins.-Q500)	TGA (Perkin Elmer Pyris 1)
	Heating Rates (°C/min)	2,5,10,20	1,2,5,10,20	2,5,10,15	2,5,8,10,15	2,5,20,35
	Heating Profile	Keep 10 min @50°C Heat Up to 350°C	Keep 10 min @30°C Heat Up to 350°C	Keep 10 min @50°C Heat Up to 350°C	Keep 10 min @50°C Heat Up to 350°C	Keep 1 min @50°C Heat Up to 550°C
	Gas	Nitrogen				
	Flow Rate (ml/min)	50				

Decomposition enthalpy and temperature dependent specific heat of the explosive formulations were measured using differential scanning calorimeter. Test parameters are summarized in Table 3.3.

Table 3.3 DSC Parameters for Decomposition Enthalpy Studies

Parameter		Igniter	P1	P2	P3	P4
Decomposition Enthalpy (DSC)	**Device**	DSC (Perkin Elmer Diamond DSC)	DSC (Perkin Elmer Diamond DSC)	DSC (TA Ins. Q2000)	DSC (Perkin Elmer Diamond DSC)	DSC (Perkin Elmer Diamond DSC)
	Heating Profile	Keep 10 min @50°C Heat Up to 350°C	Keep 10 min @30°C Heat Up to 350°C	Keep 10 min @30°C Heat Up to 300°C	Keep 3 min @50°C Heat Up to 350°C	Keep 3 min @50°C Heat Up to 500°C
	Heating Rate (°C/min)	15	5	5	10	10
	Gas	Nitrogen				

As was mentioned in section 2.2, thermal decomposition of RDX and HMX energetic materials, which constitute the majority of explosive formulations from P1 to P4, have multi-step decomposition reactions. However, slowest step of these reactions comply with the first-order decomposition and model-based kinetics can be applied. It is decided that 1st order decomposition kinetics should be considered for data obtained from TGA. If it is not applicable or there is lack of data due to fast decomposition, isoconversional (model-free) methods should be applied.

3.2.3 Characterization of Sensitivity Parameters

Sensitivity parameters of the explosive formulations were intended to be determined considering two objectives. First objective was to figure out the impact and friction sensitivity of the igniter which showed whether developed igniter composition was safe to process and handle. Second goal of the tests were to compare autoignition

temperature of the igniter and explosive compositions (P1 to P4) with the self-ignition temperature that was obtained in small-scale slow heating (cook-off) test for these formulations.

Impact sensitivity of the explosive formulations (P1 to P4) and igniter was calculated with a 5 kg drop weight using a remote-controlled impact test machine that as designed according to explosive characterization test standards from literature [106]. 4*4*3 mm test samples were put in a small cylinder bearing and 5 kg block was dropped from 0.4 m height onto the bearing that contains test samples (5 kg*0.4 m*9.8 m/s^2=19.6 J). Accordingly, response (positive-ignition, negative-no reaction) drop height was either increased or decreased 20-30 times until expected standard deviation of the response was reached [106]. Once desired standard deviation was reached, impact sensitivity of the specimen was calculated using 20-30 positive/negative test result according to Bruceton statistical method [106].

Friction sensitivity of the explosive formulations (P1 to P4) and igniter was calculated using a friction test device explosive characterization test standards from literature [107]. This device applies force to 5(diameter)*1(height) mm explosive specimen that is put on a porcelain plate. A moving porcelain peg applies 360 N friction force to six specimen as starting value [107]. Applied friction force level is reduced if ignition is observed either of the six specimens by decreasing the weight on moving porcelain peg [107]. Friction level is reduced until all the six specimen gives “no reaction” response.

Autoignition temperature of the explosive formulations (P1 to P4) and igniter was investigated in a heating chamber according to test procedure from literature [108]. 0.2 g sample size was used for each test tube (14 mm diameter and 90 mm length) and four replicate tests were conducted for each explosive formulation. Firstly, samples were passed from 1.4 mm sieve and material that passed through sieve was

filled to test tubes. Then samples were kept at 50°C for 10 minutes and then 5°C/minute heating was applied to test chamber until 250 °C reached.

3.3 Slow Heating (Cook-Off) Test Set-Ups

Slow heating (cook-off) test aims to determine the response of a munition when subjected to prolonged adjacent heating source (fire etc.) that heats-up the munition slowly such as a nearby or adjacent magazine in a depot, on a ship or on a railcar [4]. Test requires keeping the test item that contains energetic material (explosive, propellant etc.) for 50±3°C to reach thermal equilibrium then heat the test item until cook-off is observed [4]. Heating rate was suggested as 3.3°C/h (6°F/h) in previous versions of test standard but recently it is updated as 15°C/h [4].

A disposable oven that can heat the test item with forced convection configuration is suggested by the test standard for slow heating tests [4]. Additionally, at least six thermocouples and at least 200 mm between test item and oven walls are recommended [4]. Recommended test set-up and thermocouple locations are illustrated in Figure 2.1 in section 2.1.

To investigate the self-igniting characteristics of igniter and explosive formulations, slow heating tests were initially performed in a small-scale set-up along with simulations. Once the simulations and small-scale test results were consistent, large-scale test and simulations are conducted. Small-scale slow heating tests were conducted for igniter and four explosive compositions (P1 to P4) for 5-15-25°C/h heating rates. Large-scale slow heating test was performed for P1 explosive with 15°C/h heating rate.

3.3.1 Small-Scale Test Set-Up and Small-Scale Test Item

First group of experiments were performed in a lab-scale test chamber. A regular oven with 120-liter volume was modified by including an air fan for forced

convection and a polycarbonate window was added to oven door for observation of experiments. In addition, controller of the oven was modified by adding a ramp function (5-30 °C/h) for slow heating tests. 4 test-chambers were placed in a thick wall shelter for violent response during the test. For temperature acquisition, Picotech TC-08 thermocouple data logger was employed with mineral insulated k-type thermocouples. Mineral insulated thermocouples are quite robust in high temperature and can be used in multiple tests. Small scale test set-ups are illustrated in Figure 3.3. Two test chambers were used for each test sparing the remaining two for violent response of tests. Two data-logger with total 16 channels (8 channel*2 logger) enabled recording at least 8 temperature data from the chamber. For each test, 3 of the thermocouples were located inside the explosive and igniter, 2 of the thermocouples were placed inner wall of the explosive and 3 of the thermocouples were located inside the test chamber for air temperature measurements. 1 Hz data logging frequency was used as well as motion tracking camera for response detection.

Figure 3.3. Small-Scale Slow Heating Set-Up at TUBITAK SAGE

Small-scale test items were designed with two configurations. First configuration only contained bare explosive (P1 to P4) without the igniter. Second configuration contained both explosive and igniter pellet. For both configurations 42.2/34.2 mm OD/ID aluminum casing with 85 mm length was used with Teflon plug. For first

configuration 68±2 mm explosive, for second configuration 60±2 mm explosive coupled with igniter pellet that had 20 mm diameter and 4±0.5 mm thickness was used. Both configurations are illustrated in Figure 3.4. Test item and locations of the thermocouples are shown in Figure 3.5.

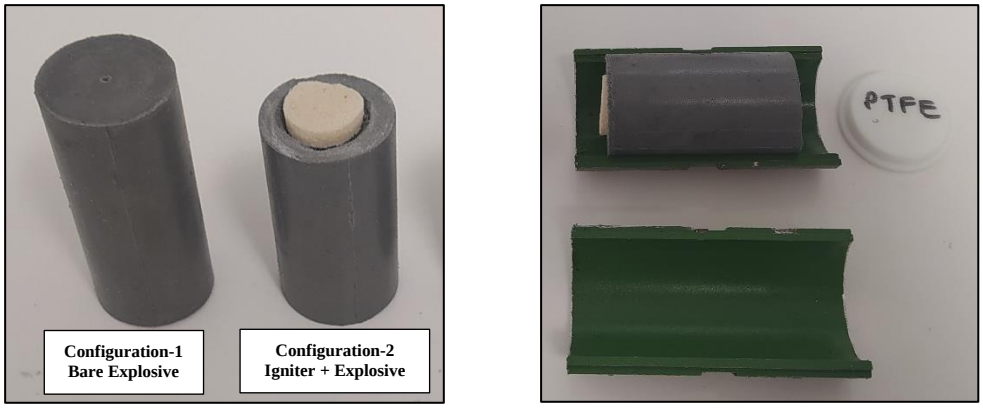

Figure 3.4. Small-Scale Test Item.

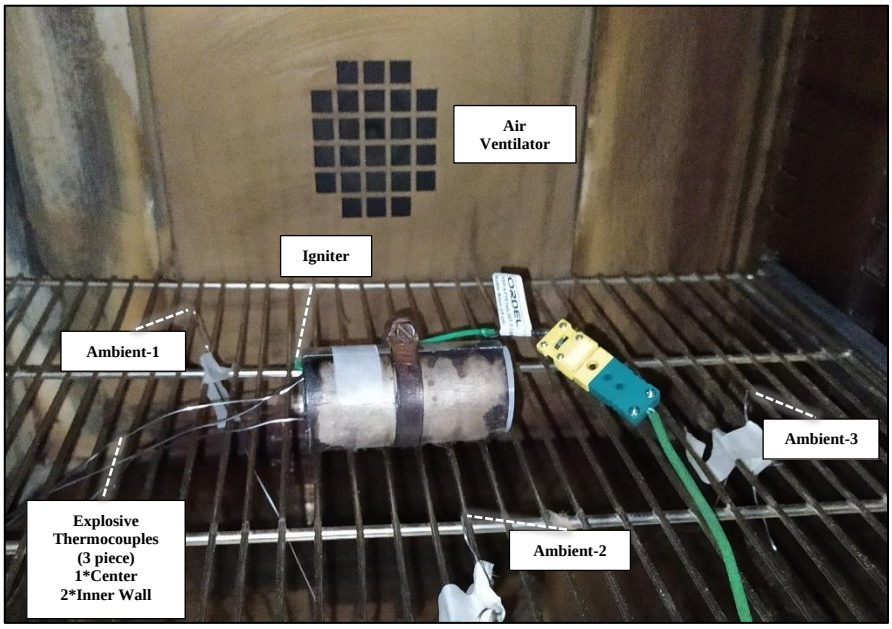

Figure 3.5. Small-Scale Test Item and Thermocouple Locations in Small-Scale Test Chamber

3.3.2 Large-Scale Test Set-Up and Large-Scale Test Item

Large-scale test set-up, shown in Figure 3.6, was designed by considering the test standard requirements. Test chamber consists of disposable plywood test chamber with polyurethane insulation, air inlet/outlet ports and heater/ventilator unit. Test chamber inner dimensions are 0.6*0.6*1.65m. Controller unit can collect 10 thermocouple data with 1 Hz. Large-scale tests consist of detonation risk and requires special test site with constant surveillance.

Figure 3.6. Large-Scale Test Set-Up Components.

Full-scale test item used in large-scale slow heating (cook-off) test was a penetrator munition with ≥20 mm wall thickness and ≥1.5 m length that contained approximately 25 kg P1 explosive (without igniter). Full-scale test item and temperature locations of the large-scale test set-up is shown in Figure 3.7 and Figure 3.8. Six air thermocouple and three surface thermocouples were used for temperature measurements. In addition, a thermocouple was located between the fuzewell and P1 explosive at the rear center of the test item as shown in Figure 3.7.

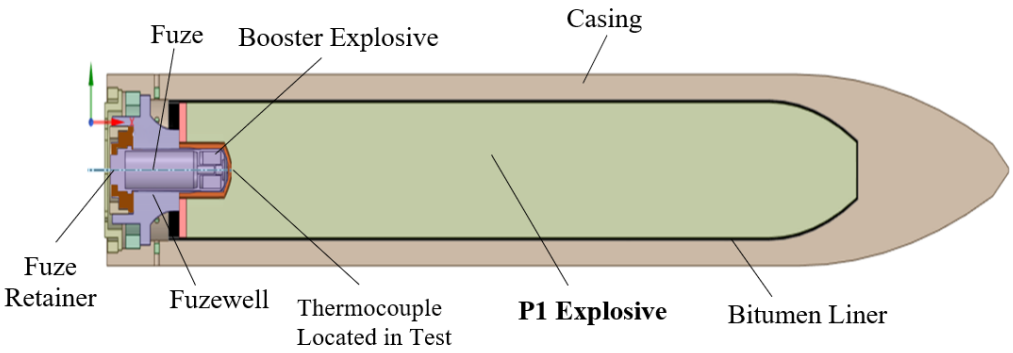

Figure 3.7. Large-Scale Test Item.

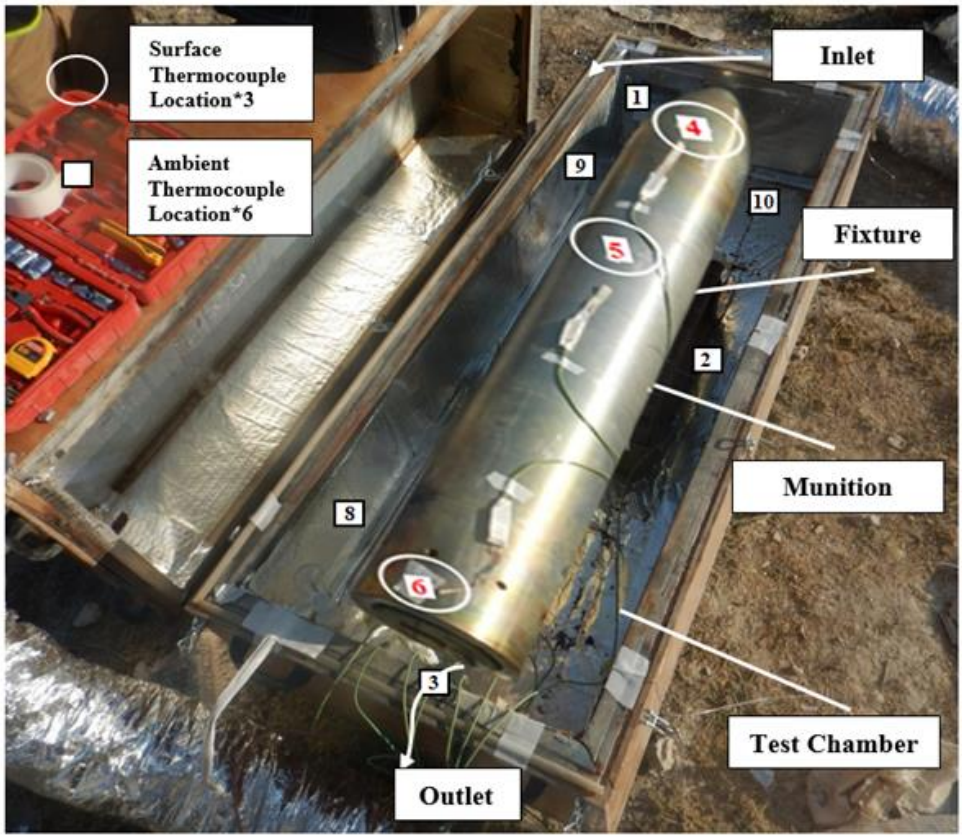

Figure 3.8. Large-Scale Test Item and Thermocouple Locations in Large-Scale Test Chamber

CHAPTER 4

IMPLEMENTATION OF SLOW HEATING MODEL FOR SMALL AND LARGE-SCALE SYSTEMS

4.1 General

In this chapter, the implementation of the slow heating model for small and large-scale systems using a commercial CFD package, ANSYS Fluent is presented. Considering the experimental test configurations, small-scale slow heating simulations were conducted for small-scale test items that contain igniter and four explosive compositions (P1 to P4) for 5,15,25°C/h heating rates and large-scale slow heating simulation was performed for full-scale test item that contained P1 explosive with 15°C/h heating rate.

4.2 Small-Scale Simulation Model

Transient simulations of the slow cook-off process in the small-scale set-up were conducted with Ansys Fluent 19.2 software that uses finite volume method (FVM) for simulations. The air flow around the munition was not solved in the simulation but a convective heat transfer boundary condition was imposed on the surface of the munition as presented in Appendix A. Firstly, solid model was prepared by drawing the model with a computer-aided design (CAD) software. Then 3D geometry was prepared by simplifying the initial geometry. After that solid model was meshed and boundary condition surfaces were defined. The model that was going to be imported to Ansys Fluent was prepared by defining material properties, source term (decomposition parameters), parameters to be reported, contours to be saved and solver methods to be used. Finally, simulation was initialized and started. Transient simulation ran for every time step until desired residual values were reached. Simulation ran until the predefined time.

4.2.1 Solid Geometry Preparation

Solid models were prepared with Ansys SpaceClaim software. Dimensions of the test item and 3D view of test item are illustrated in Figure 4.1 and Figure 4.2 respectively.

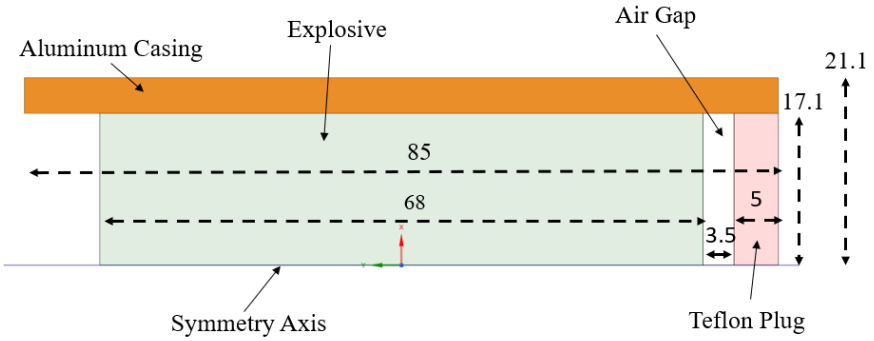

Figure 4.1. Dimensions of Small-Scale Test Item (without igniter) (in mm)

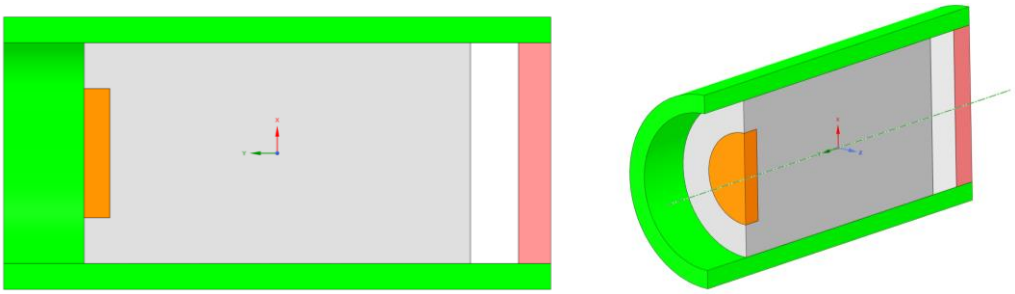

Figure 4.2. 3D Model of Small-Scale Test Item (with igniter)

4.2.2 Meshing and Determination of Heat Transfer Boundaries

Meshing was performed with Ansys Meshing software. Meshed geometries with igniter and without igniter are illustrated in Figure 4.3 and Figure 4.4 respectively. These figures also show boundary condition surfaces selected to define the necessary boundary conditions in Fluent software. Symmetry axis and convective heat transfer surfaces are shown separately.

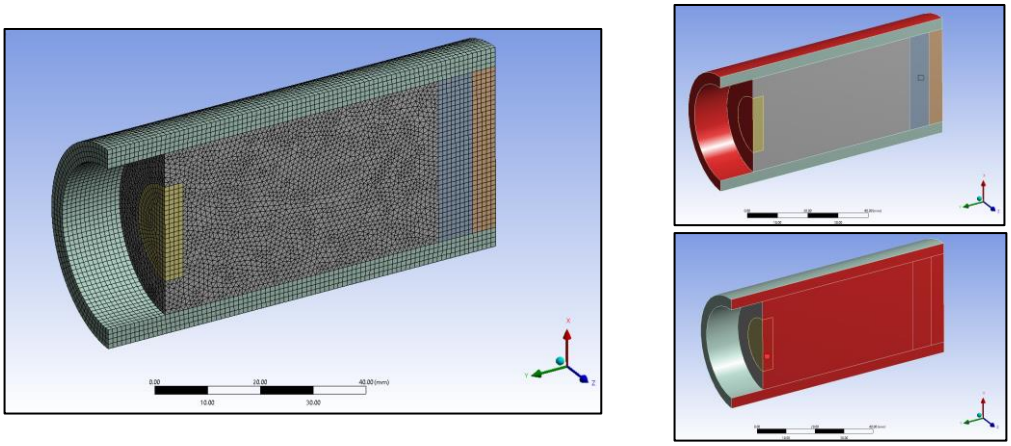

Figure 4.3. Meshed 3D Model of Small-Scale Test Item (with igniter)

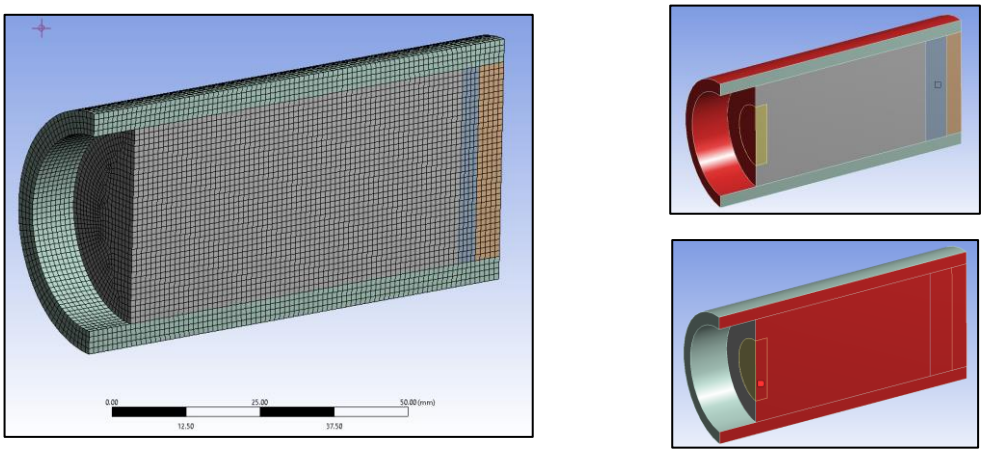

Figure 4.4. Meshed 3D Model of Small-Scale Test Item (without igniter)

To select optimum mesh size and time step for small-scale simulations sensitivity analysis was conducted to small-scale test item with P1 explosive. 16 out of 64 threads of a 2 socket 16 core/socket Intel Xeon Silver 4216 2.10 GHz processor equipped with 64 GB RAM were used for sensitivity analysis. 0.5, 1 and 2 mm mesh size were implemented and these mesh sizes correspond to 555900, 71724 and 9245 elements respectively. In addition, 2, 10, 30 and 60 second time step sizes were investigated for each mesh size. Results of the sensitivity analysis are tabulated in Table 4.1. Calculations for ignition temperature and ignition time compared to experimental values were less than 1.0 % ignoring the 60 s time step as shown in

table. In addition, heating profile of the trials were similar and only an insignificant difference was observed in the thermal decomposition part of the analysis as shown in Figure 4.5.

Selection of the mesh size and time step was carried out by considering the total absolute error (absolute error in ignition time + absolute error ignition temperature). Absolute error for temperature or time was calculated by taking absolute value of (100*[Experimental Value-Calculated Value]/Experimental Value). Smallest absolute error was encountered for 1 mm mesh size and 10 second time step. In addition, it was noted that 0.5 mm mesh contains approximately 8 times more element than 1 mm mesh and 2 second time step has approximately 5 times calculation duration compared to 10 s time step. Considering the increased element number and elevated calculation time that 0.5 mm mesh size and 2 s time step lead respectively, 1 mm mesh size and 10 s time step was selected as optimum simulation parameters also noting that these parameters had the least absolute simulation error in sensitivity analysis.

Table 4.1 Sensitivity Analysis of Small-Scale Test Item with P1 Explosive

Analysis Type	**3D**				**3D**				**3D**			
Element Size	**0.5**				**1**				**2**			
Node (#)	602937				83895				12467			
Element (#)	555900				71724				9245			
Time Step (s)	**2**	**10**	**30**	**60**	**2**	**10**	**30**	**60**	**2**	**10**	**30**	**60**
Calculation Time (min)	**298**	**66**	**27**	**16**	**234**	**46**	**17**	**9**	**223**	**44**	**17**	**8**
Ignition Time (s)	**28928**	**29060**	**29160**	**29460**	**28724**	**28960**	**29070**	**29160**	**28728**	**28700**	**28710**	**28740**
Time (Error %)	-0.2	-0.7	-1.0	-2.1	0.5	**-0.3**	-0.7	-1.0	0.5	0.6	0.5	0.4
Ignition Temperature	173.90	174.07	175.40	178.77	174.71	**174.65**	174.93	174.75	174.81	174.43	174.29	173.53
Temperature (Error %)	0.7	0.6	-0.1	-2.0	0.3	**0.3**	0.1	0.2	0.2	0.4	0.5	0.9
Total Absolute Error (Temperature + Time Errors) (%)	1.0	1.3	1.2	4.1	0.7	**0.6**	0.9	1.3	0.7	1.0	1.0	1.4

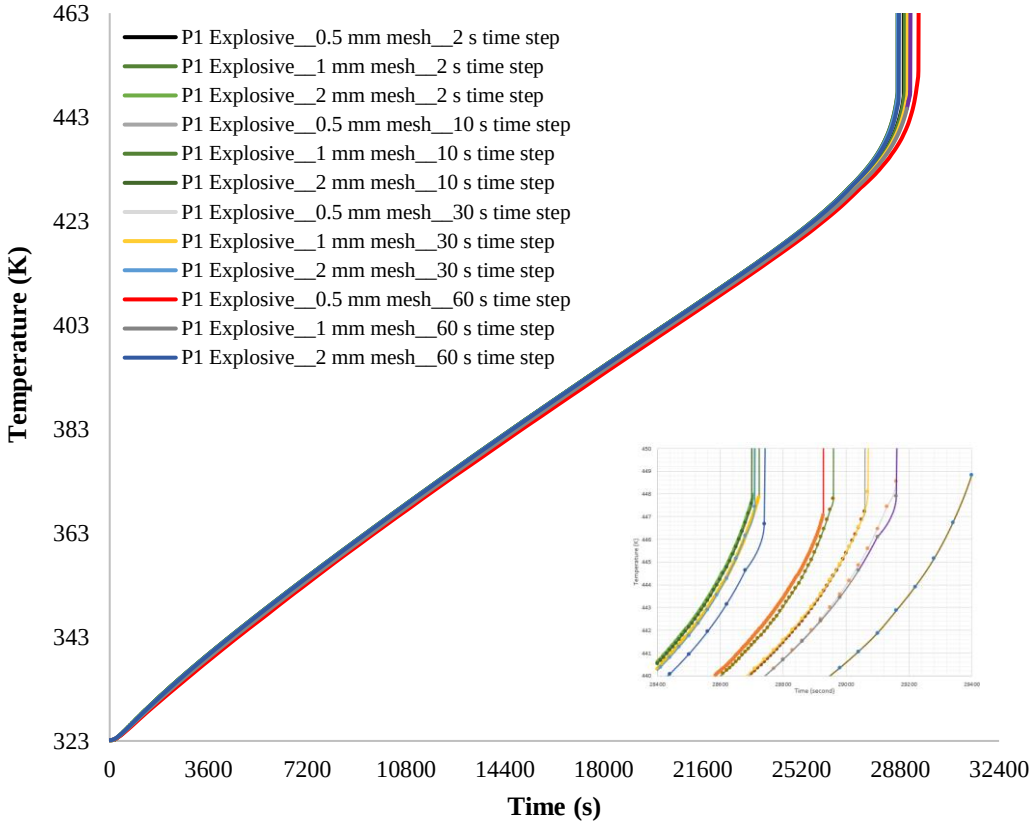

Figure 4.5. Sensitivity Analysis of Small-Scale Test Item with P1 Explosive (Forced Convection Conditions, 15°C/h heating rate)

4.2.3 Small-Scale Simulations

Simulations for small-scale test item were performed by Ansys Fluent 19.2 software. Before starting simulations, some prerequisites should be met for both geometries. Firstly, physical properties of materials were imported to the software by a material database as shown in Appendix C. These properties are density, thermal conductivity, and specific heat. For thermal conductivity and specific heat temperature dependent values were measured and compiled for simulations.

Thermal decomposition parameters that were used for source term calculation, air temperature profile for chamber and convective heat transfer coefficient equations were introduced to software with a user defined file (UDF) in “C” programming

language. UDF file considered for small-scale and large-scale simulations are given in Appendix D. Melting of PETN in igniter and evaporation of isodecyl pelargonate (IDP) in P2 and P3 explosives were also included in calculations. In addition to this, temperature profiles of air inside chamber for the experiments were involved in the calculations by fitting temperature profile to a time dependent polynomial equation. According to UDF file given in Appendix D; convective heat transfer coefficient, source term, temperature of air inside chamber, film temperature and temperature dependent air properties (density, specific heat, thermal conductivity, and dynamic viscosity) were calculated for each time step. Elevation at TUBITAK SAGE that affected air properties was also considered in calculations. Air properties for small-scale slow heating (cook-off) tests at TUBITAK SAGE-ANKARA (1118 m altitude) (P_{atm}=88.21 kPa) is given in Table 4.2. Average air velocity is constant for small-scale simulations and Pr, Re, Nu numbers and convective heat transfer coefficient (h) values was calculated in table below for evaluating the effect of temperature to these parameters. In transient simulations, these parameters were calculated instantaneously considering the film temperature according to UDF file given in Appendix D.

4.3 Large-Scale Simulation Model

Transient large-scale simulations were conducted with Ansys Fluent 19.2 software that uses finite volume method (FVM) for simulations similar to small-scale test set-up.

4.3.1 Solid Geometry Preparation

Solid model was prepared with Ansys SpaceClaim software with the same consideration used for small-scale test set-up. Model is illustrated in Figure 2.3 in section 2.1.2.

Table 4.2 Air Properties for Constant Average Air Velocity in Small-Scale Slow Heating (Cook-Off) Tests

Temp (K)	**ρ (kg/m^3)**	**Cp (J/kg.K)**	**λ (W/m.K)**	**μ (N/m^{2}s)**	**ν (m^2/s)**	**r (m)**	**V (m/s)**	**Pr Number (Cp*μ/λ)**	**Re Number (ρ*v*2*r/μ)**	**Pr*Re**	**Nusselt Number (h*D/k)**	**h (w/m^{2}K)**
323.0	**0.947**	1007.9	2.80E-02	1.95E-05	2.06E-05				853.0	600.1	14.7	**9.4**
350.0	**0.874**	1009.0	3.00E-02	2.08E-05	2.38E-05				739.0	517.5	13.7	**9.3**
400.0	**0.765**	1014.0	3.38E-02	2.30E-05	3.01E-05	0.022	**0.4**	0.7	585.1	403.9	12.1	**9.3**
450.0	**0.680**	1021.0	3.73E-02	2.51E-05	3.69E-05				477.4	327.6	10.9	**9.3**
475.0	**0.644**	1025.5	3.90E-02	2.60E-05	4.04E-05				435.4	298.1	10.4	**9.2**

4.3.2 Meshing and Determination of Heat Transfer Boundaries

Meshing was performed with Ansys Meshing software as illustrated in Figure 4.6. To select optimum mesh size and time step for large-scale simulation sensitivity analysis was conducted for large-scale geometry with P1 explosive. It took 6 h to 479 h to simulate the transient analysis that contains 19 to 28 million elements for the 32 out of 48 threads of a 2 socket 12 core/socket Intel Xeon Gold 3136 3.6 GHz processor equipped with 64 GB RAM. 3 mm element size was used for large-scale test item as bitumen liner has 3 mm thickness. 1.2 mm element size was used for deflector plates. Skewness value which has a 0.90 maximum limit value for effective analysis would exceed the limit value if munition or deflector element size was increased. Also, liner which constitutes a thermomechanical barrier between steel munition case and explosive, has 3 mm thickness and 3 mm element size in analysis element size cannot be further increased. On the other hand, decreasing element size below 3 mm leads to more than $40*10^6$ total element size, which would extend the analysis duration from weeks to months. Patch conforming was also considered between contact faces and adaptive meshing was applied for air. 4, 6 and 8 mm mesh size were implemented to air inside large-scale test chamber and these mesh sizes corresponded to $9.4*10^6$, $7.0*10^6$ and $6.1*10^6$ elements respectively.

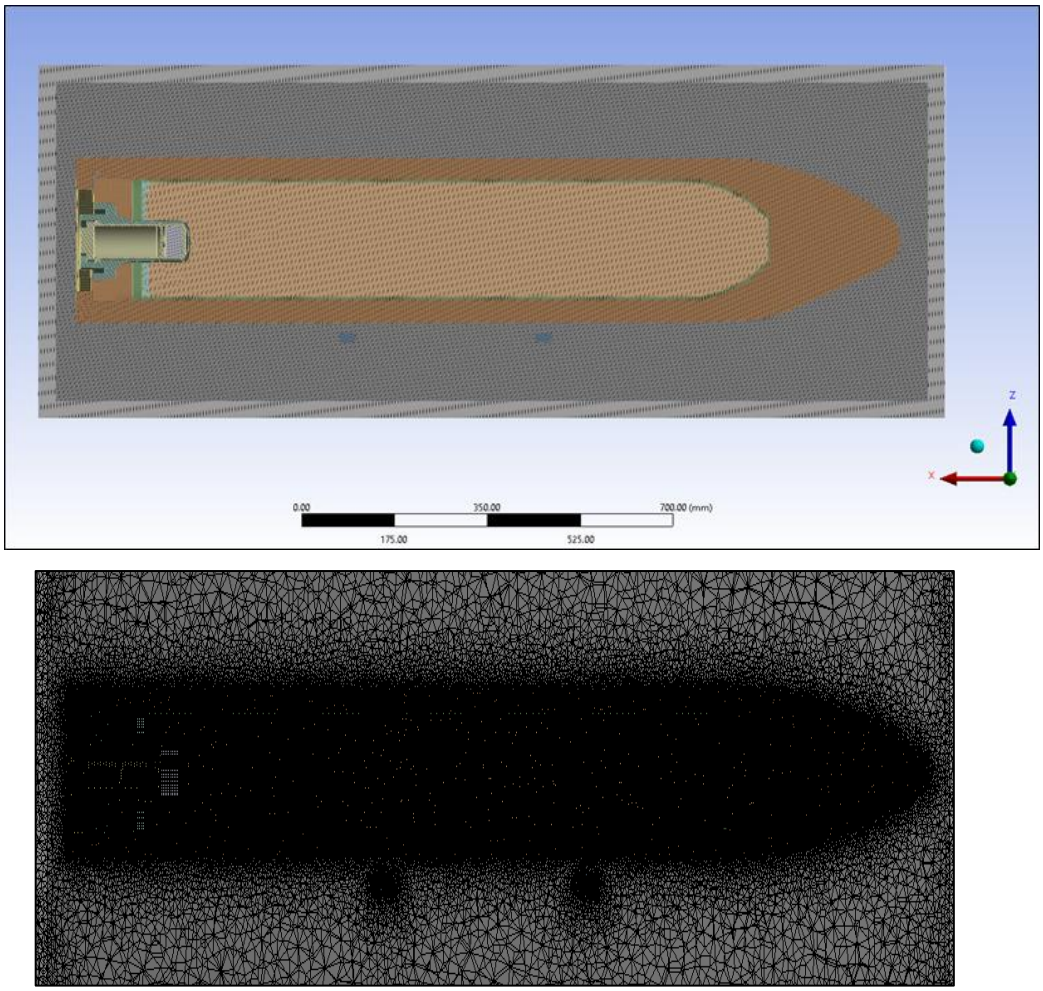

Figure 4.6. 3D Model of Large-Scale Test Set-Up

Sensitivity analysis for large-scale slow heating and simulations were performed with 4, 6 and 8 mm mesh size for 2, 10 and 60 seconds time steps respectively with large-scale test set-up. Munition element size was considered as 3 mm for all trials due to 3 mm liner thickness between the munition casing and explosive. Results of the sensitivity analysis are tabulated in Table 4.3.

All the trials corresponded to less than 4.5 % time and temperature error compared to experimental results. As can be expected, 2 and 10 second time step configurations led to less computational error compared to 60 s time step. Selection of the mesh size and time step was carried out by considering the total absolute error (error in ignition

time + ignition temperature). Absolute error for temperature or time was calculated by taking absolute value of (100*[Experimental Value-Calculated Value]/Experimental Value). 4 mm element size and 10 second time step resulted in least total absolute (time + temperature) error (4.1%).

Temperature profile of analysis were illustrated in Figure 4.7 along with experimental value. All the analyses performed for the sensitivity investigations led to similar temperature profile with the experiment up to 41000 second where thermal decomposition began. In sensitivity analysis, 4 mm mesh size with 10 second time step led to least absolute error (3.0% temperature + 1.1% time=4.1%) at cook-off instant. However, 4 mm mesh size with 2 second time step is selected for final mesh and time step in order to solve the air flow inside chamber accurately during heating until cook-off although these parameters led to slightly higher absolute error (2.7% temperature + 2.2% time=4.9% compared to 4.1%) at cook-off instant. Figure 5.47 in section 5.5 shows the simulation and experimental data comparison of the large-scale slow heating test.

Table 4.3 Sensitivity Analysis of Large-Scale Test Item with P1 Explosive

Analysis Type	**3D**								
Munition Element Size (mm)	3			3			3		
Air Element Size (mm)	4			6			8		
Air Element (#)	$9.4*10^6$			$7.0*10^6$			$6.1*10^6$		
Element (#)	$28*10^6$			$22*10^6$			$19*10^6$		
Node (#)	$4.9*10^6$			$3.7*10^6$			$3.3*10^6$		
Orthogonal Quality	0.11			0.11			0.10		
Skewness	0.89			0.89			0.90		
Time Step Duration (s)	2	10	60	2	10	60	2	10	60
Calculation Time (h)	479	49	22	206	35	14	131	26	6
Ignition Time (s)	42902	42460	43380	42872	43830	43500	43240	43320	43560
Ignition Temperature (°C)	178.1	178.6	179.4	178.3	178.6	181.2	178.3	178.6	180.9
Error-Time (%)	2.2	1.1	3.3	2.1	4.4	3.6	3.0	3.2	3.8
Error-Temperature (%)	2.7	3.0	3.5	2.8	3.0	4.5	2.8	3.0	4.3
Total Absolute Error (Temperature + Time Errors)	4.9	4.1	6.8	4.9	7.4	8.1	5.8	6.2	8.1

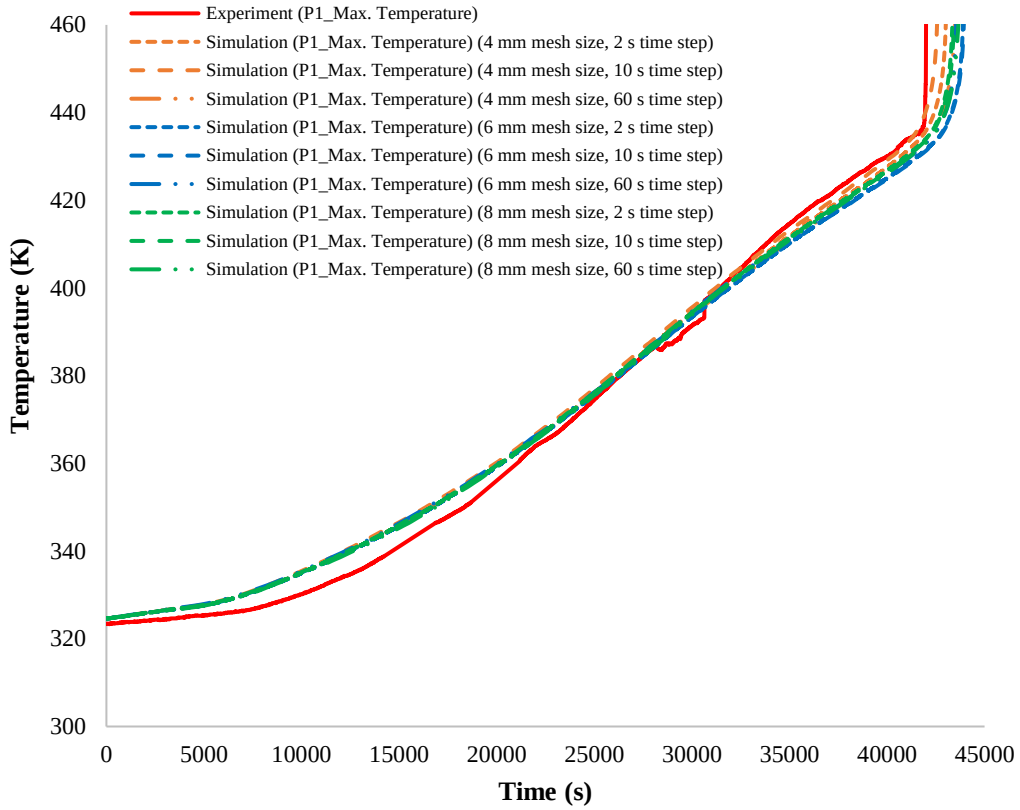

Figure 4.7. Sensitivity Analysis of Large-Scale Slow Heating Test (P1 Explosive-Without Igniter) (15°C/h heating rate)

4.3.3 Large-Scale Simulations

Simulations for large-scale test item were performed by Ansys Fluent 19.2 software. Material database (given in Appendix C) that consists of density, thermal conductivity, and specific heat of the material and UDF file (given in Appendix D) that contains source term for explosives and experimental heating profile was introduced to software similar to small-scale simulations. Air inlet velocity was measured before experiment as approximately 10 m/s with Kestrel 4000 anemometer.

Since large-scale experiment was conducted including the fuze that contains booster pellets (95 % HMX and 5% polymer) the source term of the booster pellet was also

simulated considering literature data [68] which is given in Appendix D (E:220.5 kJ/mol, A:5x10^{19} s^{-1}, Q:2092 J/g, ρ:1810 kg/m3).

CHAPTER 5

RESULTS AND DISCUSSION

Results of investigations of slow heating (cook-off) characteristics of energetic materials are summarized in this chapter. In section 5.1, characterization of energetic materials (physical properties and decomposition parameters) is given. In addition, sensitivity characteristics such as autoignition temperature and impact/friction sensitivity of igniter and energetic materials are presented, which clarifies whether the selected igniter can be used for initiation of explosives from P1 to P4 (P1: optimum blast and heat effect, P2: high blast for fragment and shaped charge, P3: enhanced blast for closed and confined volumes, P4: oxygen rich composition for underwater applications). Characterization of energetic materials is backbone of this study, since numerical simulations are dependent on measured and/or calculated parameters and any deviation or error on those parameters leads to incorrect simulation results.

Small scale slow heating (cook-off) tests results are presented in section 5.2 for igniter and explosives from P1 to P4. Small scale slow heating (cook-off) tests were performed under forced convection conditions for different heating rates (5, 15, 25°C/hour). Igniter and four different explosive compositions (from P1 to P4) and the three different heating rates (5, 15, 25°C/hour) led to fifteen different configurations for investigation. Considering the repeatability requirement to be met, at least two replicate tests for each configuration were conducted that comprised of at least thirty tests, each of which took 24 to 48 hour and includes serious deflagration or detonation risk.

Small-scale slow heating (cook-off) simulation results that were performed simultaneously with the experiments are given in section 5.3. Using the physical

properties and decomposition parameters obtained in section 5.2, numerical simulations were carried out for 3D geometry for different mesh and time step sizes that constituted sensitivity analyses of simulations. After validation of the model in small-scale, full-scale test and simulations were carried out which are summarized in sections 5.4 and 5.5, respectively.

5.1 Characterization of Energetic Materials

Characterization of energetic materials is required to obtain the physical parameters (thermal conductivity, specific heat, density) and decomposition parameters (activation energy, pre-exponential factor) for numerical simulations. Material Database and User Defined Functions (UDF), which Ansys Fluent FVM solver uses for calculations, were generated and are given in Appendix C and Appendix D by using the data tabulated in section 5.1.1 (physical and thermal properties with respect to temperature) and using the data tabulated in sections 5.1.1 to 5.1.4 (thermal decomposition parameters and source term of energetic materials). Furthermore, impact and friction response of energetic materials were measured for handling purposes and autoignition temperature of the materials were evaluated to estimate the cook-off test conditions.

5.1.1 Physical and Thermal Properties of Energetic Materials

Density of energetic materials was measured with AccuPyc II 1340 gas pycnometer at room temperature. Density of the energetic materials were measured as 1505.9±1.5 kg/m^3 for igniter, 1665.0±0.7 kg/m^3 for P1, 1658.3±0.6 kg/m^3 for P2, 1721.5±0.4 kg/m^3 for P3 and 1807.8±0.6 kg/m^3 for P4. Since it is not possible to use gas pycnometer at elevated temperatures, density of the energetic materials was assumed to be constant at elevated temperatures. This assumption was also validated from literature, which shows that density of HMX (used in P2 and P3) decreases less than 3% between 300-500 K [109].

Specific heat of energetic materials given in Figure 5.1 was measured with Perkin Elmer Pyris 1 DSC as a function of temperature. Specific heat of the igniter (42 % PETN by weight) and explosives (P1 [64 % RDX by weight], P2 [87 % HMX by weight] and P3 [45 % HMX by weight]), increases nearly 15-25 % between 50-130 °C. 15-25% increase trend is also reported in literature for energetic constituents of the igniter and explosive formulations from P1 to P3 (RDX, HMX and PETN) [110] and illustrated in Figure 5.1. On the other hand, since for P4 that consists of mainly AP (43% by weight), specific heat rises around 15% similar to literature data of AP shown in the figure [111].

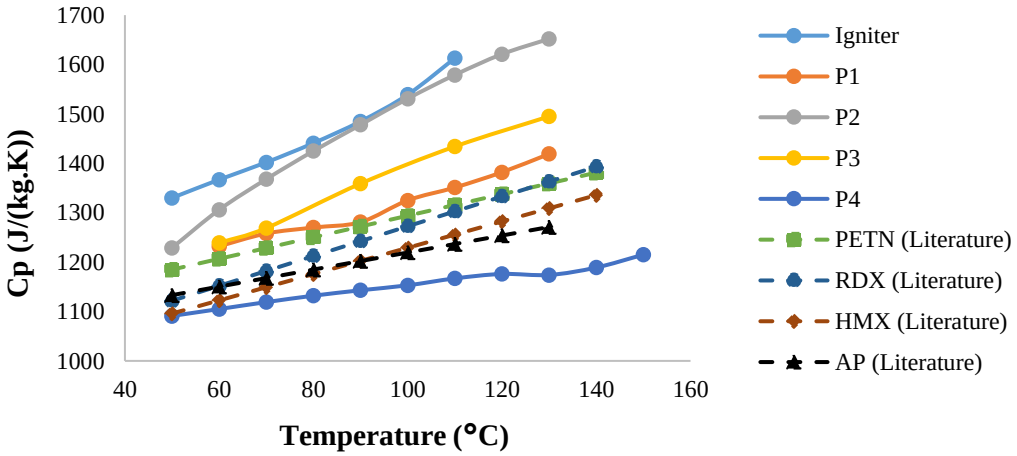

Figure 5.1. Specific Heat Capacity of Energetic Materials w.r.t. Temperature

Thermal conductivity of energetic materials given in Table 5.1 was measured with C-Therm TCI thermal conductivity analyzer as a function of temperature. Since energetic fillers (PETN, RDX, HMX) and Aluminum metal powder are incorporated in polyurethane matrix (13-20%) that has relatively low thermal conductivity, thermal conductivity values were measured to be lower than the energetic fillers reported in the literature [110]. In addition, thermal conductivity of energetic material compositions given in Table 5.1 stays nearly constant with increasing temperature between 25-125°C. It was also noted that thermal conductivity of P1 (0.47 W/(m.K) @30°C) is compatible with the reported literature value (0.454 W/(m.K) @20°C) [49].

Table 5.1 Thermal Conductivity (W/(m.K)) of Energetic Materials

		Igniter			**P1**			
Measurement Temperature (°C)		**20.7**	**48.3**	**99.3**	**29.9**	**50.1**	**90.2**	**100.3**
Measurement #	**1**	0.39	0.46	0.43	0.47	0.47	0.54	0.57
	2	0.40	0.45	0.44	0.48	0.47	0.54	0.56
	3	0.40	0.45	0.42	0.47	0.47	0.52	0.53
	4	0.39	0.45	0.43	0.47	0.48	0.53	0.55
Average		**0.40**	**0.45**	**0.43**	**0.47**	**0.47**	**0.53**	**0.55**
Standard Deviation		0.005	0.004	0.007	0.004	0.004	0.008	0.015
		P2				**P3**		
Measurement Temperature (°C)		26.4	51.3	77.5	98.1	24.6	50.6	99.7
Measurement #	**1**	0.55	0.52	0.51	0.51	0.81	0.79	0.72
	2	0.55	0.52	0.52	0.51	0.83	0.80	0.71
	3	0.55	0.52	0.51	0.51	0.83	0.80	0.72
	4	0.54	0.53	0.52	0.51	0.84	0.80	0.72
Average		0.55	0.52	0.52	0.51	0.83	0.80	0.72
Standard Deviation		0.004	0.004	0.005	0.000	0.011	0.004	0.004
		P4					**HMX**	**PETN**
Measurement Temperature (°C)		20.2	40.6	80.4	100.7	125.0	20	25
Measurement #	**1**	0.75	0.70	0.63	0.60	0.58	Literature Value	Literature Value
	2	0.74	0.70	0.63	0.59	0.63		
	3	0.75	0.70	0.62	0.59	0.62		
	4	0.75	0.70	0.62	0.58	0.64		
Average		0.75	0.70	0.63	0.59	0.61	0.51 [38]	0.25 [42]
Standard Deviation		0.004	0.002	0.005	0.008	0.022	-	-

5.1.2 Decomposition Parameters of Igniter

Decomposition parameters of igniter was calculated by using weight loss data that was measured with thermal analyzer instruments (Q500 TGA). Weight loss and conversion (α, calculated by Eq. 17 in section 2.2 or 1-weight loss %/100) data of

igniter is given in Figure 5.2 and Figure 5.3, respectively. Weight loss data obtained in Figure 5.2 was converted to the conversion as given in Figure 5.3 to obtain reaction model f (α) (Eq. 15 in section 2.2). This figure was also used to obtain the peak decomposition temperature (minimum value of derivative of conversion with respect to temperature (dα/dT)), which was used to calculate decomposition parameters and source term of igniter with different calculation methods summarized in section 2.2. Rapid decomposition of igniter because of PETN content and lack of data point during rapid thermal decomposition can be observed from the figures. Due to rapid decomposition, only several data points could be obtained for reaction model f (α) calculation during the thermal decomposition, even though TGA measurements were conducted with three different TGA devices and the data given in figures were also repeated several times to obtain valid data. Increasing the sample mass for the TGA studies to eliminate the possible concentration gradient in the igniter mixture was also considered. However, relatively high decomposition enthalpy (Figure 5.6) limited the sample size (≤4 mg) for the thermogravimetric analyzer pan.

Rapid decomposition of igniter was observed in Figure 5.2 and Figure 5.3 that was also justified from literature thermogram given in Figure 5.4 (Nitrogen Atmosphere, 20°C/min heating rate) [112]. A slight jump in thermogram for heating rate of 2°C/minute was attributed to relatively slow decomposition of PETN in igniter compared to relatively faster heating rates (5,10,20°C/minute). For relatively faster heating rates, heat released due to exothermic decomposition of PETN in short period (0.5-2 minute) led to decomposition of other materials (RDX and polyurethane) in igniter, however for 2°C/minute, released heat for relatively broader period was dissipated or was not sufficient to ignite the other constituents in igniter.

Rapid decomposition observed in igniter led to only several data points in decomposition process (at the start and at the end of decomposition), which prevented use of reaction model f(α) calculation and model-based modelling of decomposition (explained in section 3.2.2) for igniter. Since model-based

decomposition could not be applied for igniter, isoconversional (model-free) kinetics was used for decomposition. While applying isoconversional (model-free) methods to calculate E_A for igniter, A (pre-exponential) factor could not be calculated without a kinetic assumption. For A calculations, first-order decomposition was considered in isoconversional (model-free) decomposition approach.

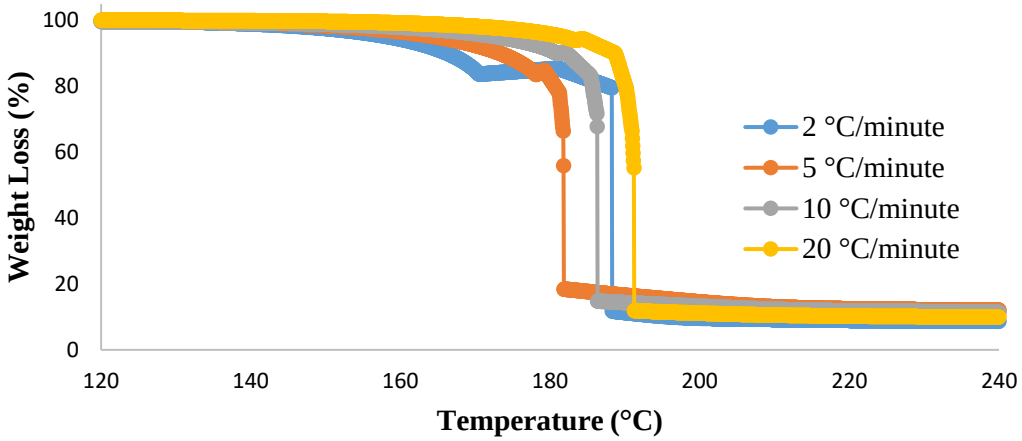

Figure 5.2. TGA Thermograms of Igniter for Different Heating Rates

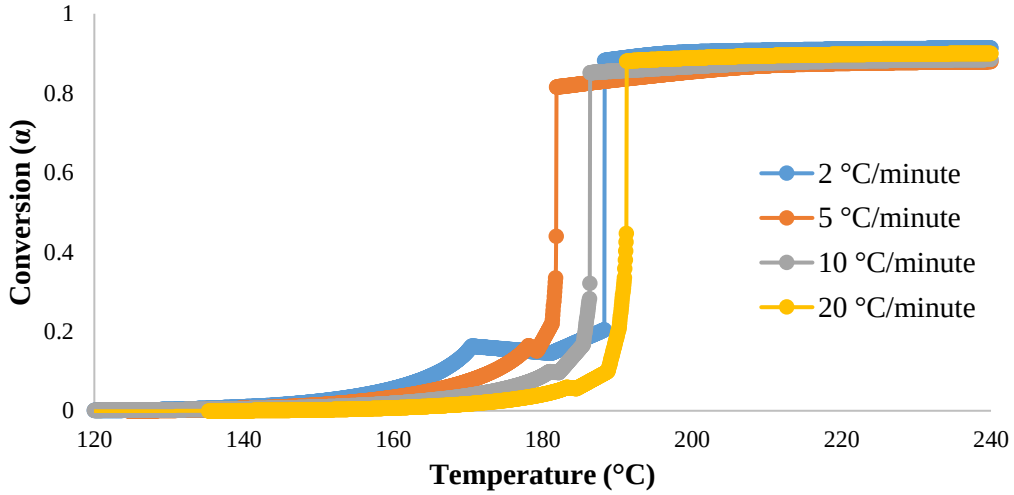

Figure 5.3. Conversion of Igniter for Different Heating Rates

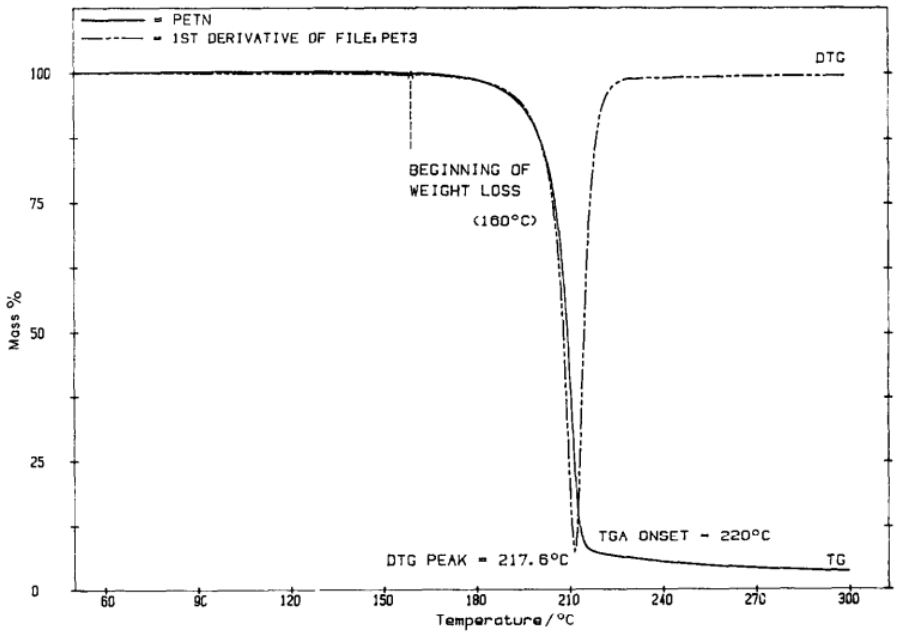

Figure 5.4. TGA Thermogram of PETN from Literature [112]

Using the model-free kinetic decomposition approach, activation energy (E_A) and pre-exponential factor (A) for igniter was calculated based on peak temperatures in TGA thermograms. Two approaches, which are Method 1 (Flynn/Wall/Ozawa (F/W/O) [32], [96], [97], [113]) (Eq. 20 in section 2.2) and Method 2 (Kissinger/Akahira/Sunose (K/A/S) [30], [114]) (Eq. 21 in section 2.2), were utilized for decomposition kinetics [115]. Method 1 adopts peak decomposition temperature (1/T) with respect to heating rate (log(β)) and Method 2 adopts peak decomposition temperature (1/T) with respect to heating rate ($\ln(\beta/T^2)$). While both methods employ model-free kinetics for E_A calculations, first-order decomposition kinetics were assumed for A (pre-exponential factor) calculations. Results of both approaches are shown in Figure 5.5. For both methods, coefficient of determination (r^2) value was calculated as approximately ≈ 0.99 which shows the linear trendline selection is appropriate. Using the values of the slopes of the fitted lines, E_A and A values of the igniter were calculated and tabulated in Table 5.2. Although method 2 is suggested in literature for being more accurate for E_A determination, there is not any significant difference between the results [33]. Both isoconversional (model-free) methods were

employed for slow heating (cook-off) simulations in this study, which are presented in section 5.3.1.

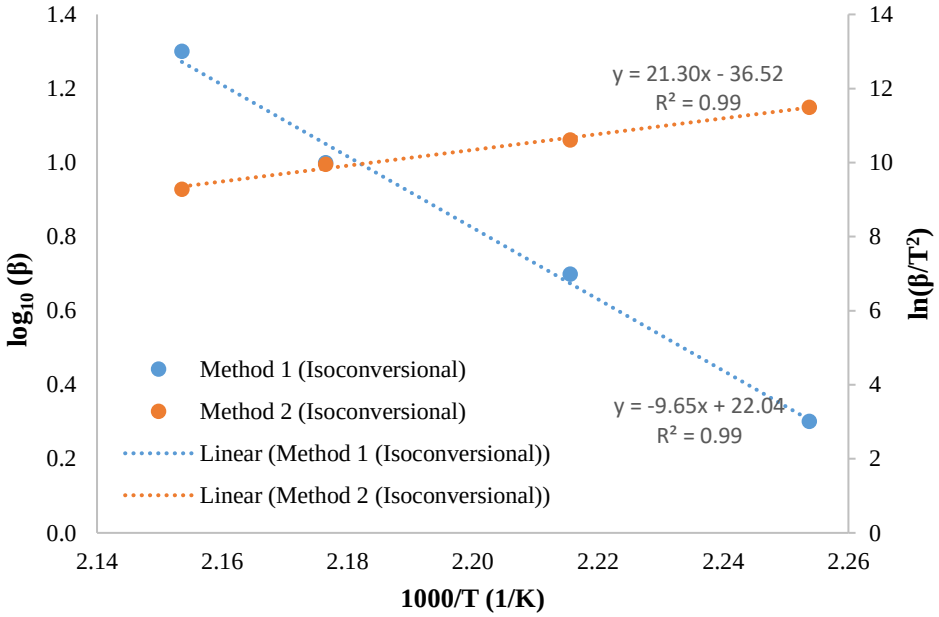

Figure 5.5. Activation Energy (E_A) Calculation of Igniter According to Isoconversional Method 1 and 2

Table 5.2 Activation Energy (E_A) and Pre-exponential Factor (A) of Igniter

Raw Data				Method 1 (Isoconversional)			Method 2 (Isoconversional)		
Heating Rate (β) (°C/min)	**Peak T (°C)**	**Peak T (K)**	**1000/T**	**$\log_{10}(\beta)$**	**E_A (kJ/mol)**	**A (1/s)**	**$\ln(\beta/T^2)$**	**E_A (kJ/mol)**	**A (1/s)**
2	**170.60**	443.65	2.25	0.30	**175.62**	**1.54E+18**	11.50	**177.10**	**2.29E+18**
5	**178.20**	451.35	2.22	0.70			10.62		
10	**186.30**	459.45	2.18	1.00			9.96		
20	**191.20**	464.35	2.15	1.30			9.29		

In addition to thermogravimetric analysis, differential scanning calorimetry (DSC) thermogram shown in Figure 5.6 was also obtained for igniter to calculate the decomposition enthalpy. Melting was reported between 138-141°C for PETN

molecule in literature [116]. Melting enthalpy was also calculated for igniter (42 % PETN by weight) which occurs between 132-136°C in this study.

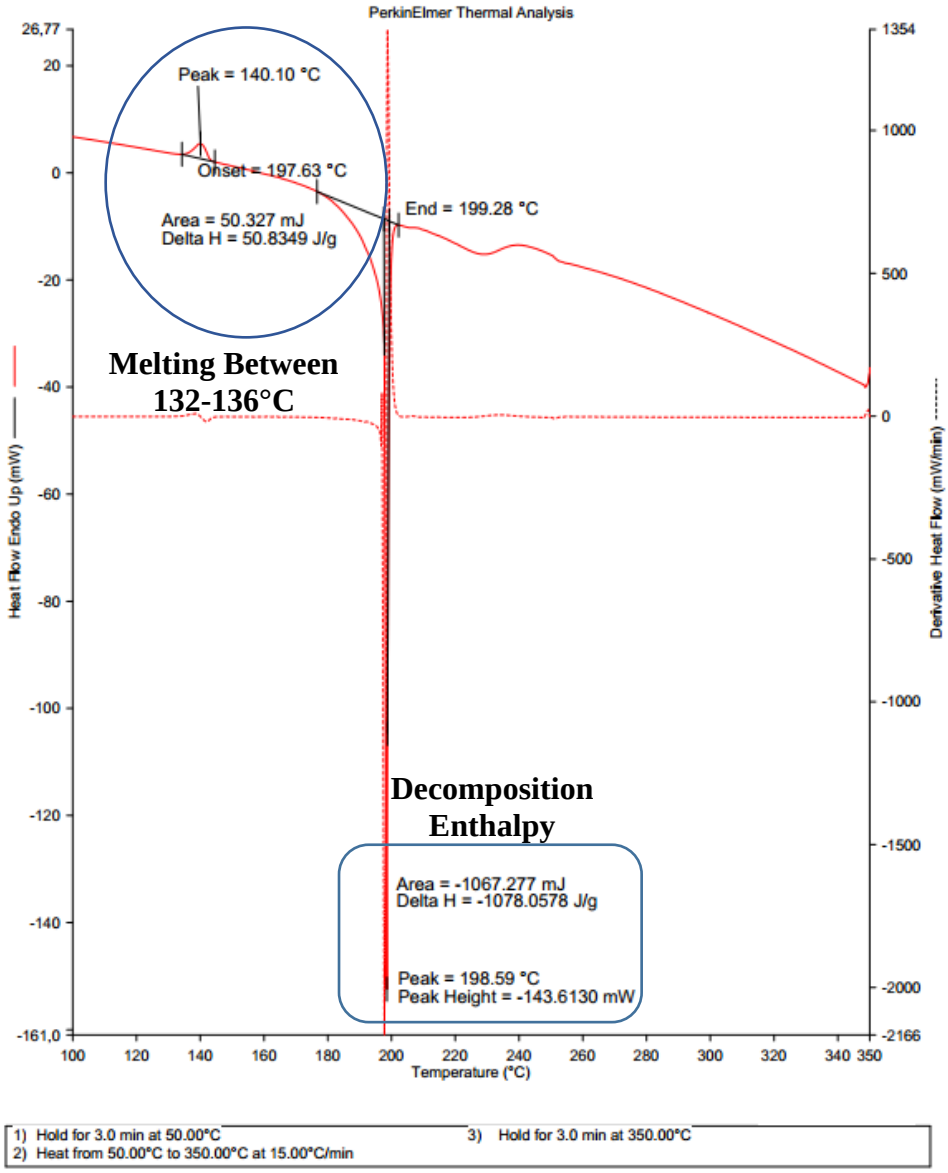

Figure 5.6. Melting and Decomposition Enthalpy of Igniter

Calculated activation energy (E_A) and pre-exponential factor (A) and measured decomposition enthalpy (Q) can be used to calculate the source term of the igniter. The two isoconversional (model-free) calculation methods summarized in previous

paragraphs led to similar results as shown in Figure 5.7. Moreover, considering that igniter contains approximately ≈ 42 % PETN by weight, source term based on only PETN was also calculated using decomposition parameters from literature [68]. This curve, illustrated also in Figure 5.7, shows significantly less heat generation due to decomposition. This trend may result from the fact that exothermic decomposition in igniter may facilitate the decomposition of other constituents in the mixture (RDX and/or polyurethane binder) and can lead to even more heat generation. This implies that instead of modelling each decomposition reaction and interaction between chemical species, which requires more experiment and modelling efforts; an approach that focuses on the modelling of total decomposition enthalpy by using isoconversional (model-free) and/or model-based kinetic models can also lead to accurate source term results as long as calculated data from thermal analysis devices is verified with full-scale experiments.

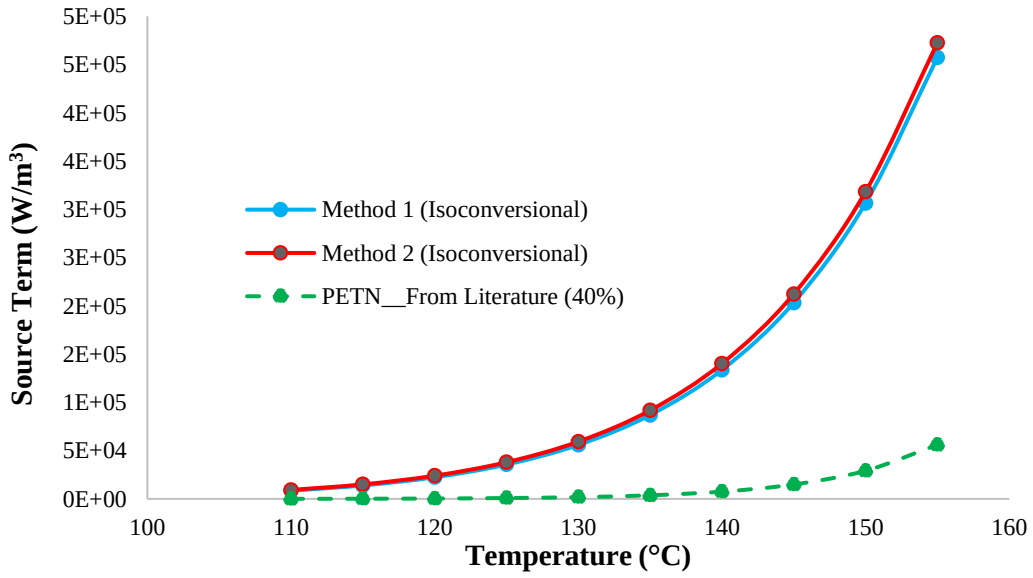

Figure 5.7. Effect of Decomposition Parameters on Source Term of Igniter

5.1.3 Decomposition Parameters of P1 Explosive

Decomposition parameters of P1 explosive (64/20/16 % by weight, RDX/Aluminum/Polyurethane) was also calculated by using similar approach that was followed for igniter as explained in section 5.1.2. Weight loss data was obtained by Hitachi 6300 TG/DTA in nitrogen atmosphere for different heating rates (1, 2, 5, 10, 20 °C/min). Weight loss and conversion calculations are illustrated in Figure 5.8 and Figure 5.9. Contrary to rapid decomposition of igniter in a narrow temperature range (<2°C), P1 explosive that is composed of 64 % RDX by weight, decomposes in broader temperature range (10-20°C). This facilitated collecting more data during decomposition and enabled implementation of model-based methods as well as the isoconversional (model-free) decomposition methods. Broader temperature range (10-20°C) in decomposition of RDX was also noted in literature as shown in Figure 5.10 [112].

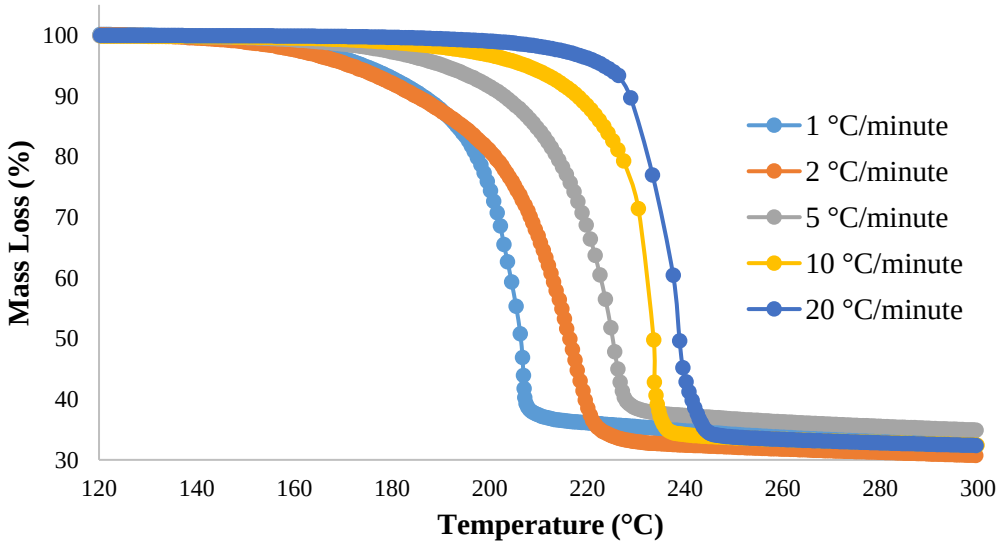

Figure 5.8. TGA Thermograms of P1 Explosive for Different Heating Rates

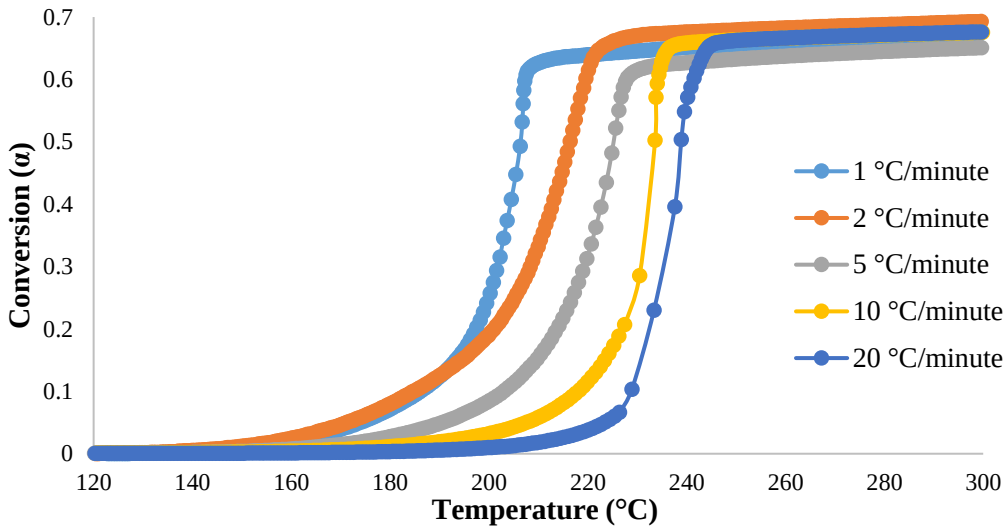

Figure 5.9. Conversion of P1 Explosive at Different Heating Rates

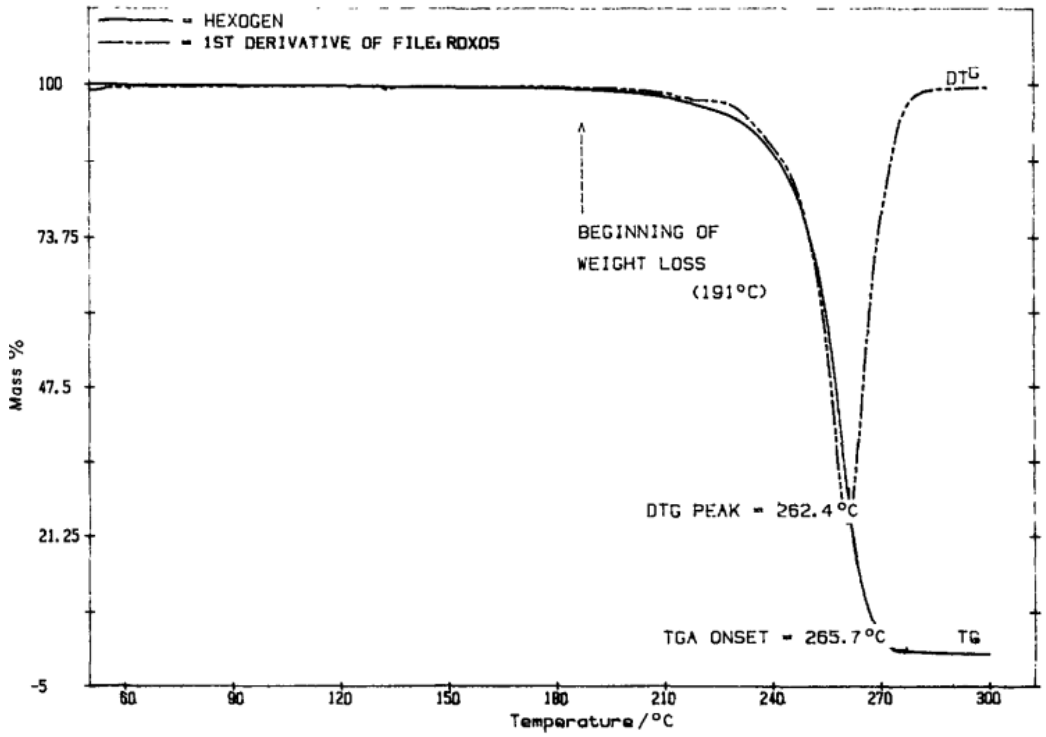

Figure 5.10. TGA Thermogram of RDX from Literature [112]

Decomposition parameters of P1 explosive was calculated for both isoconversional (model-free) and model-based methods. For model-free methods similar calculation

procedures that was followed for igniter in section 5.1.2 was followed. Peak temperatures for different heating rates and calculated E_A and A values are summarized in Figure 5.11 and Table 5.3. For both calculation methods coefficient of determination (r^2) value was obtained approximately as 0.98.

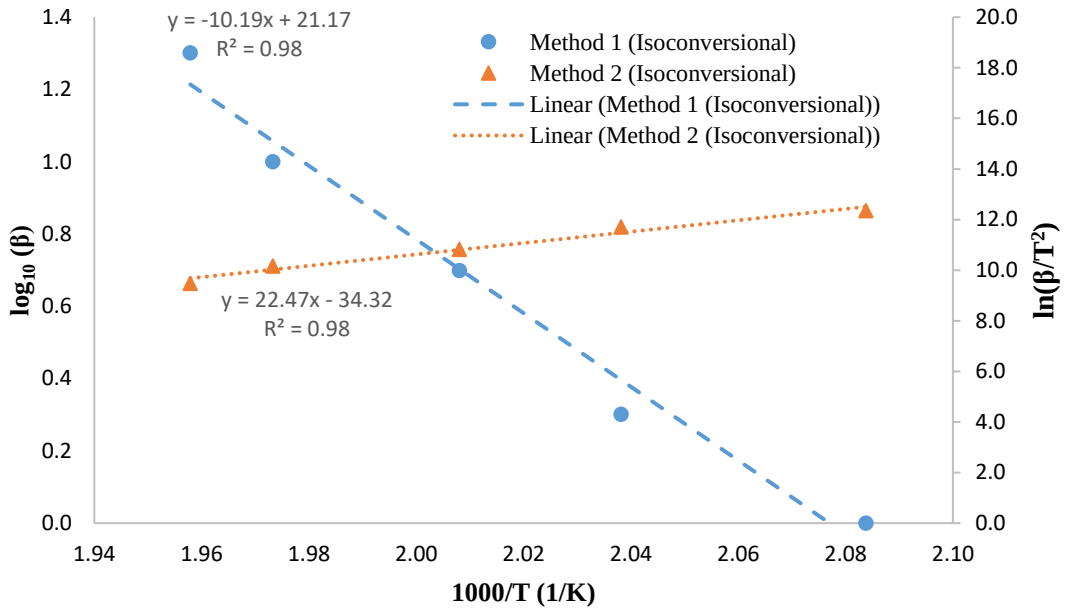

Figure 5.11. Activation Energy (E_A) Calculation of P1 Explosive According to Isoconversional Method 1 and 2

Table 5.3 Activation Energy (E_A) and Pre-exponential Factor (A) of P1 Explosive (Model-Free Methods)

Raw Data				**Method 1 (Isoconversional)**			**Method 2 (Isoconversional)**		
Heating Rate (β) (°C/min)	**Peak T (°C)**	**Peak T (K)**	**1000/ T**	**$\log_{10}$ (β)**	**E_A (kJ/mol)**	**A (1/s)**	**$\ln(\beta/T^2)$**	**E_A (kJ/mol)**	**A (1/s)**
1	**206.74**	479.89	2.08	0.00			12.35		
2	**217.49**	490.64	2.04	0.30			11.70		
5	**224.80**	498.00	2.01	0.70	**185.54**	**1.93E+17**	10.81	**186.85**	**2.65E+17**
10	**233.62**	506.77	1.97	1.00			10.15		
20	**237.60**	510.75	1.96	1.30			9.48		

In addition to isoconversional (model-free) methods, thermal decomposition of RDX based P1 explosive was also investigated with model-based methods. Decomposition kinetics of RDX and RDX based compositions such as P1 explosive was reported to be unimolecular and first order in the literature [101], [117]. Considering this finding, reaction order was calculated by assuming 1^{st}, 2^{nd} and n^{th} order kinetics as given in Table 5.4. Before comparing the effect of model-free and model-based methods in thermal decomposition of P1 explosive and source term, decomposition enthalpy that affects source term was also measured using Perkin Elmer Diamond DSC as shown in Figure 5.12. 1352 J/g value for decomposition enthalpy of P1 explosive is compatible with the 1300 J/g average value of three measurements obtained from DSC in literature [118].

Table 5.4 Activation Energy (E_A) and Pre-exponential Factor (A) of P1 Explosive (Model-Based Methods)

	E_A (kJ/mol)	**A (1/s)**	**n**	**r^2**
N^{th} order	199.54	1.04E+19	0.656	0.99
1^{st} Order	203.59	3.35E+19	1	0.99
2^{nd} Order	229.83	3.66E+22	2	0.99

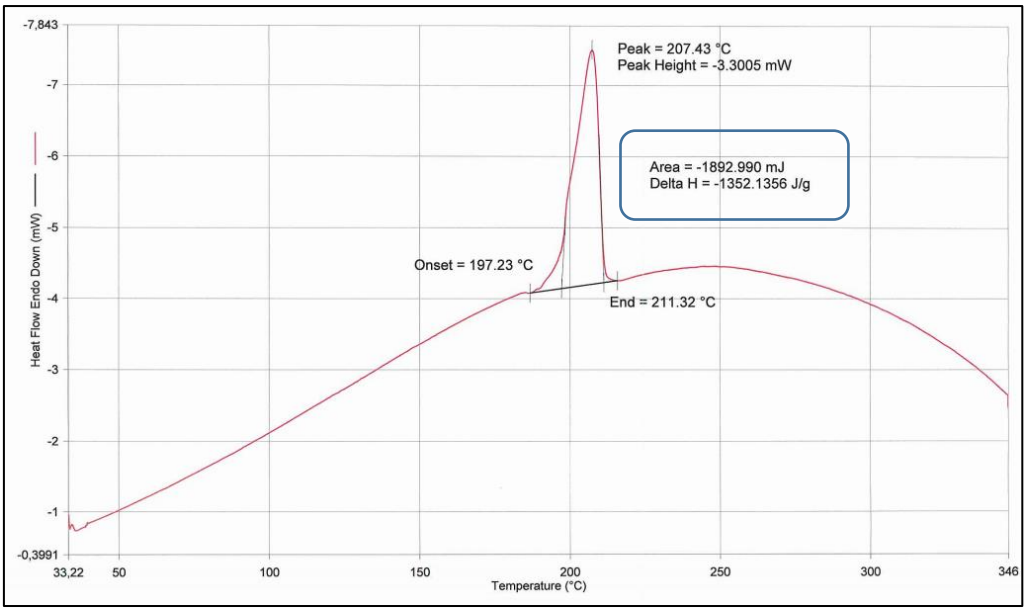

Figure 5.12. Decomposition Enthalpy of P1 Explosive

Using the decomposition parameters (E_A, A, Q) calculated and/or obtained from literature, source term (S) for thermal decomposition of P1 explosive was calculated and summarized in Figure 5.13. Isoconversional (model-free) and model-based (1^{st}, 2^{nd} and n^{th} order) calculation methods resulted in similar values between 140-180°C. After 180°C, model-based methods decompose more rapidly due to the effect of weight loss and reaction order included in the calculation.

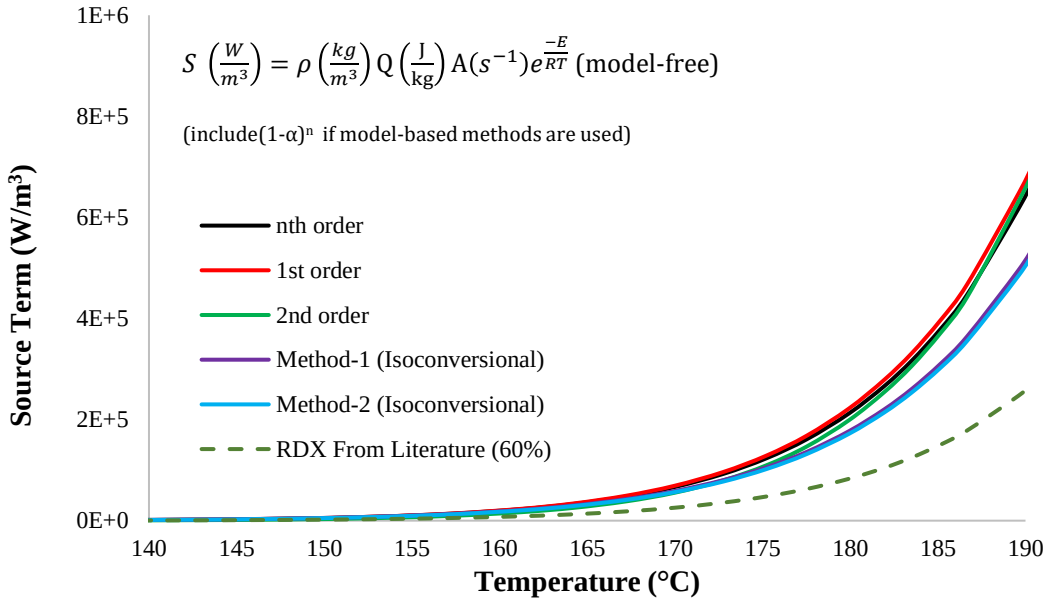

Figure 5.13. Effect of Decomposition Parameters on Source Term of P1 Explosive

5.1.4 Decomposition Parameters of P2, P3 and P4 Explosive

P2, P3 and P4 explosives decomposition parameters were calculated according to similar approaches conducted for igniter (section 5.1.2) and P1 explosive (section 5.1.3). P2 and P3 are HMX based energetic materials compositions containing 40-45% and 87 % HMX by weight. P4 explosive, on the other hand, contains 20 % RDX and 43% AP. For P2 and P3 it is known that HMX decomposes rapidly [112] similar to PETN in Igniter (section 5.1.2) and only model-based decomposition approach was applicable for these formulations. Rapid decomposition of HMX in a narrow temperature band (<2°C) is demonstrated in Figure 5.14.

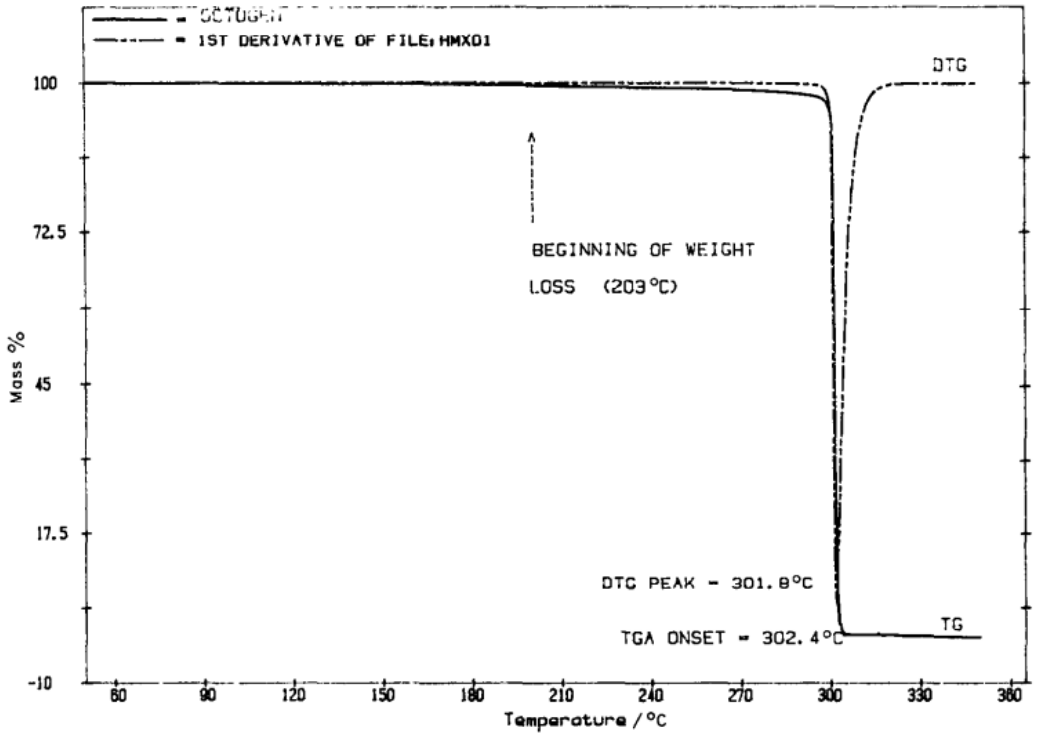

Figure 5.14. TGA Thermogram of HMX from Literature [112]

Decomposition parameters of P2 explosive was obtained using weight loss data in Figure 5.15 for different heating rates (2, 5, 10, 15°C/min). Approximately ≈5% weight loss was observed between 140-160 °C from the figure, before the decomposition of energetic material. ≈5% weight loss before the decomposition of energetic materials was attributed to evaporation of isodecyl pelargonate (IDP) plasticizer which constitutes ≈6% of P2 composition. Similar weight loss was also noted in literature as a result of plasticizer [118]. From trendlines drawn in Figure 5.16, isoconversional (model-free) decomposition parameters for P2 explosive were calculated and are given in Table 5.5. It was noted that source term values (215.56 kJ/mol and 2.49×10^{18} s^{-1}) from literature [119] are compatible with the experimental value when data in Table 5.5 (obtained by non-isothermal TGA measurements) is compared with the literature values (obtained by isothermal TGA measurements). Moreover, considering the lack of data point during decomposition of P2 explosive as shown in Figure 5.15, a model-based approach that employs decomposition

kinetics not to fastest area (T_{peak}) but to initial decomposition area (α=5% or 10 %) was applied to P2 for α=10% [37]. Table 5.6 shows the E_A and A values calculated using this method. α=10% was chosen because between α=0-5%, IDP plasticizer evaporated from the P2 explosive composition.

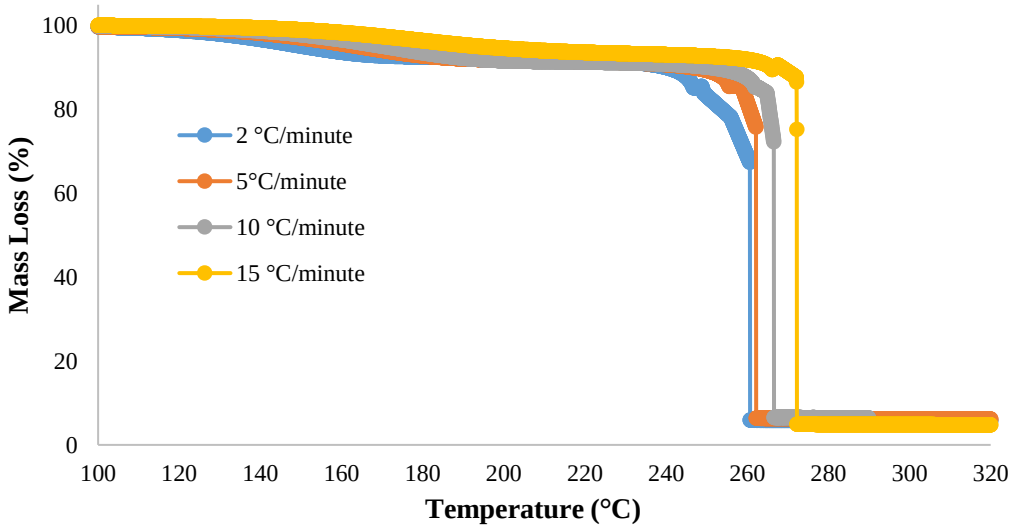

Figure 5.15. TGA Thermograms of P2 Explosive for Different Heating Rates

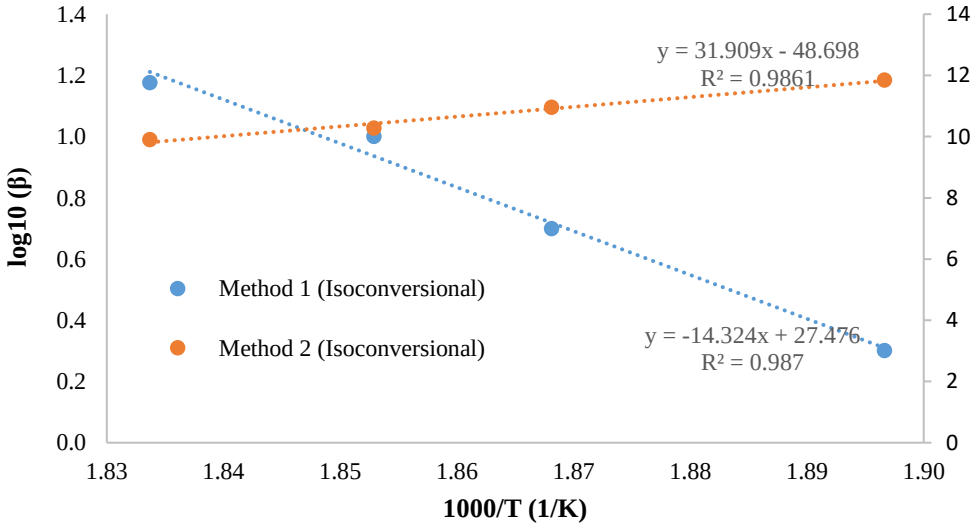

Figure 5.16. Activation Energy (E_A) Calculation of P2 Explosive According to Isoconversional Method 1 and 2

Table 5.5 Activation Energy (E_A) and Pre-exponential Factor (A) of P2 Explosive (Model Free Methods)

Raw Data				Method 1 (Isoconversional)			Method 2 (Isoconversional)		
Heating Rate (β) (°C/min)	**Peak T (°C)**	**Peak T (K)**	**1000/T**	**$\log_{10}$ (β)**	**E_A (kJ/mol)**	**A (1/s)**	**$\ln(\beta/T^2)$**	**E_A (kJ/mol)**	**A (1/s)**
2	254.10	527.20	1.90	0.30	**260.81**	**3.14E+23**	11.84	**265.29**	**4.61E+23**
5	262.15	535.30	1.87	0.70			10.96		
10	266.55	539.70	1.85	1.00			10.28		
15	272.20	545.35	1.83	1.18			9.90		

Table 5.6 Activation Energy (E_A) and Pre-exponential Factor (A) of P2 Explosive (α=10%, first order assumption)

Raw Data				Method 3 (α=10%)		
Heating Rate (β) (°C/min)	**Peak T (°C)**	**Peak T (K)**	**1000/T**	**$\log_{10}$ (β)**	**E_A (kJ/mol)**	**A (1/s)**
3	253.70	526.80	1.90	0.477	**221.19**	**4.48E+19**
5	257.40	530.55	1.88	0.699		
10	265.08	538.23	1.86	1.000		
20	272.78	545.93	1.83	1.301		

Additionally, for P3 explosive, similar procedure was applied and weight loss data from Figure 5.17 for different heating rates (2, 5, 8, 10, 15 °C/min) lead to data in Figure 5.18 for model-free kinetics. E_A and A values are summarized in Table 5.7. Similar to P2 explosive, P3 also contains isodecyl pelargonate (IDP) plasticizer (≈9% by weight) and showed an initial weight loss (7-8 %) between 140-160 °C. Weight loss of IDP plasticizer was also encountered in literature [118]. Similar to P2, a model-based approach that employs decomposition kinetics not to fastest area (T_{peak}) but to initial decomposition area (α=5% or 10 %) was applied to P3 for α=12% [37]. Table 5.8 shows the E_A and A value calculated using this method. α=12% is

chosen because between α=0-7% IDP plasticizer evaporated from the P3 explosive composition.

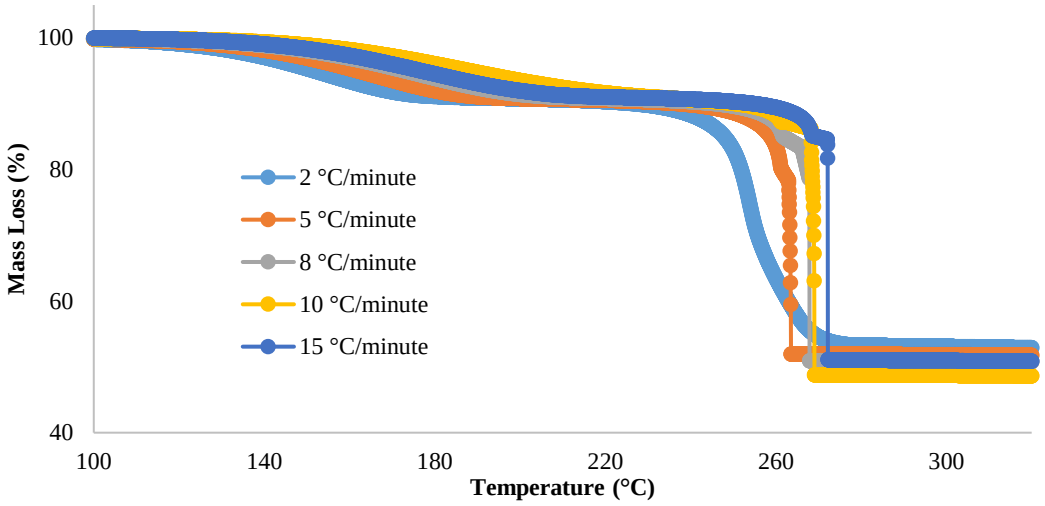

Figure 5.17. TGA Thermograms of P3 Explosive for Different Heating Rates

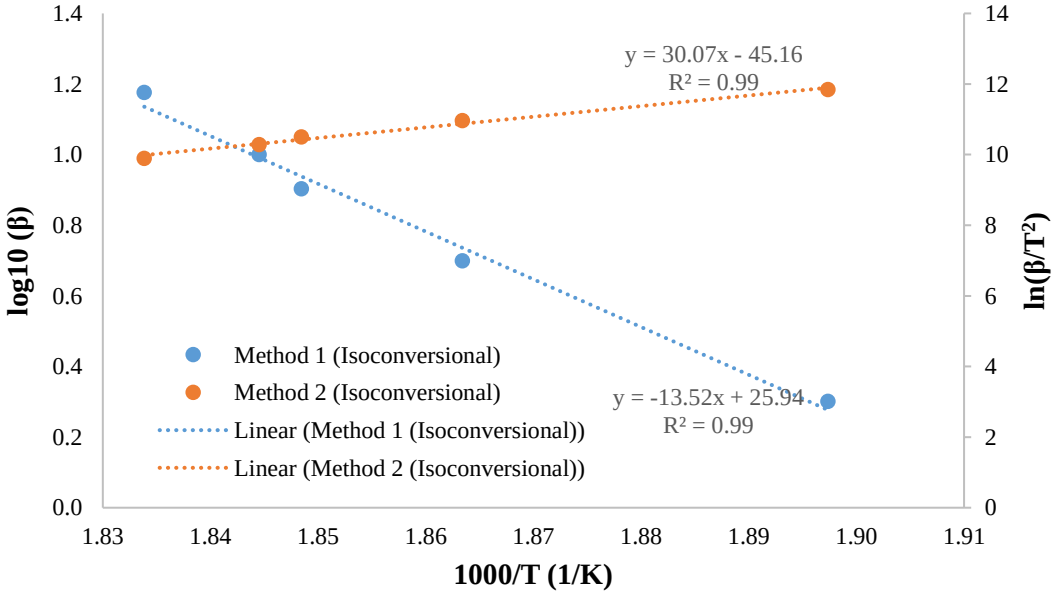

Figure 5.18. Activation Energy (E_A) Calculation of P3 Explosive According to Isoconversional Method 1 and 2

Table 5.7 Activation Energy (E_A) and Pre-exponential Factor (A) of P3 Explosive (Model Free Methods)

Raw Data				ASTM E698 Method 1			ASTM E698 Method 2		
Heating Rate (β) (°C/min)	**Peak T (°C)**	**Peak T (K)**	**1000/T**	**$\log_{10}$ (β)**	**E_A (kJ/mol)**	**A (1/s)**	**$\ln(\beta/T^2)$ [K]**	**E_A (kJ/mol)**	**A (1/s)**
2	253.90	527.00	1.90	0.30	**246.24**	**8.92E+21**	11.80	**249.99**	**2.08E+22**
5	263.50	536.65	1.86	0.70			10.96		
8	267.85	541.00	1.85	0.90			10.51		
10	269.00	542.15	1.84	1.00			10.29		
15	272.15	545.30	1.83	1.18			9.90		

Table 5.8 Activation Energy (E_A) and Pre-exponential Factor (A) of P3 Explosive (α=12%, first order assumption)

Raw Data				Method 3 (α=12%)		
Heating Rate (β) (°C/min)	**Peak T (°C)**	**Peak T (K)**	**1000/T**	**$\log_{10}$ (β)**	**E_A (kJ/mol)**	**A (1/s)**
2	241.55	514.65	1.94	0.30	**183.78**	**1.26E+16**
5	253.10	526.25	1.90	0.70		
8	258.25	531.40	1.88	0.90		
10	260.50	533.65	1.87	1.00		
20	265.90	539.05	1.86	1.18		

Decomposition parameters for P4 explosive was conducted with Perkin Elmer Pyris 1 TGA. P4 explosive contains 20 % RDX, 43% AP, 25 % Aluminum and 12% polyurethane. Presence of three (RDX, AP, Al) energetic materials led to the possibility of unmixed microstructures in composition and oxygen rich AP resulted in elevated heat of decomposition that was detrimental to thermal analysis device. Despite this risk, more than fifteen TGA thermograms were obtained for P4 and only data shown in Figure 5.19 was considered as meaningful. However, data summarized

in figure does not have an increasing peak temperature trend with increasing heating rate. This fluctuation can be attributed to fact that 0.5-2 mg specimen was used for TGA measurements and the composition is not uniform for the specimens with different heating rates. In order to prevent possible damage to TGA, literature values for decomposition parameters were used for P4 explosive (E_A: 180 kJ/mol, A:5.9x115 s^{-1} and Q:1510 J/g) [73].

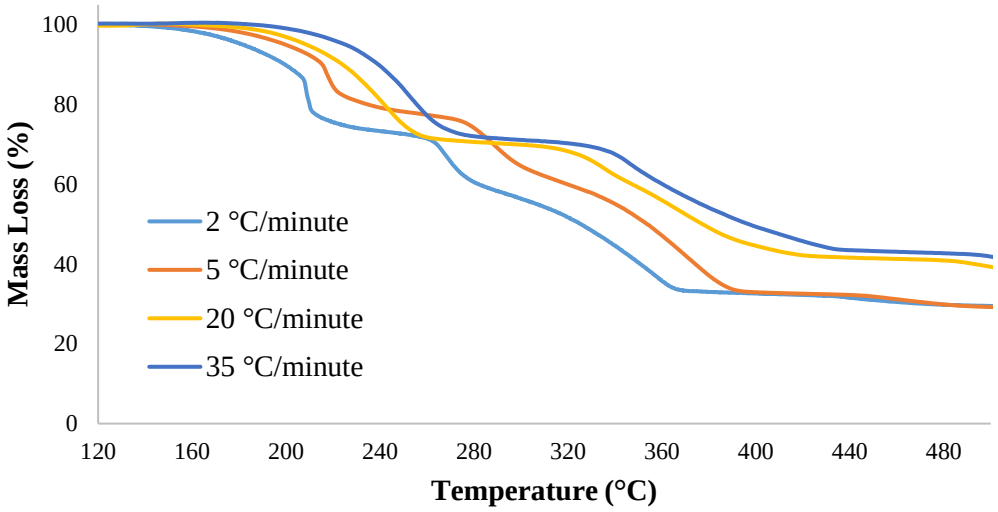

Figure 5.19. TGA Thermograms of P4 Explosive for Different Heating Rates

Source term of igniter and explosives from P1 to P4 was calculated by Eq. 23 from section 2.2 ($\dot{q} = \rho Q A e^{-E_A/RT}$) using the measured density (ρ), decomposition enthalpy (Q) and calculated pre-exponential factor (A) and activation energy (E_A). Comparison of the calculated source term values are shown in Figure 5.20. From figure it was understood that for a given temperature value > 100°C, source term of order is igniter>P1>P4>P3≈P2. Source term magnitude shows that for a given temperature igniter is thermally least stable material and P2 is the most stable material. This comparison implies that igniter can be used for burning of explosives from P1 to P4.

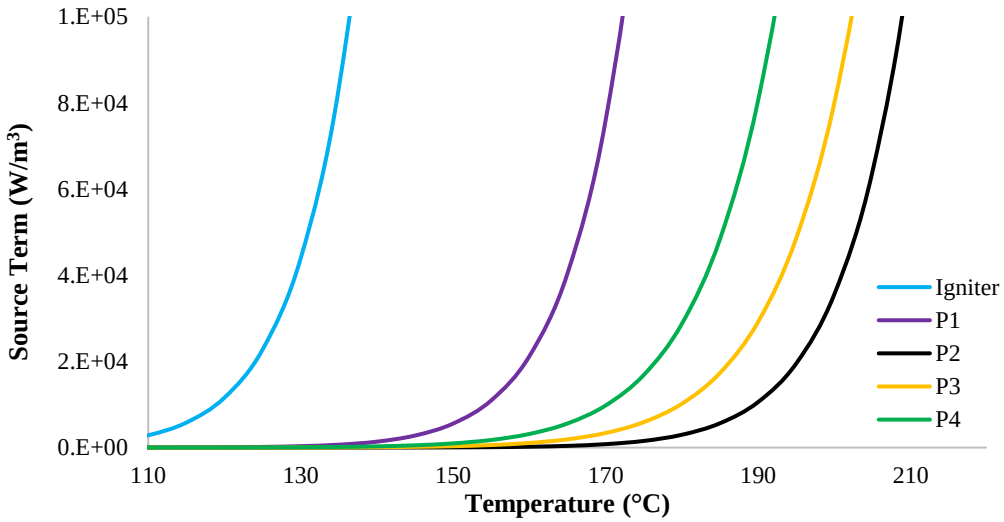

Figure 5.20. Source Term Comparison of Igniter and Explosives from P1 to P4

5.1.5 Sensitivity of Energetic Materials

Autoignition temperature, friction sensitivity and impact sensitivity are the main parameters for qualification of an energetic material composition along with electrostatic discharge and shock sensitivity tests. For the igniter composition and P1 to P4 explosive compositions, autoignition temperature, friction sensitivity and impact sensitivity tests were performed according to standards from literature [106]–[108].

The aim of the measurement of autoignition temperature in this study is to compare the ignition properties of an unconfined energetic material with the confined configuration. Since autoignition temperature measurements are conducted in test tubes open to air, this temperature is expected to be greater than the confined slow heating tests explained in section 5.2. Autoignition temperature of igniter and P1-P4 explosives are summarized in Table 5.9. The difference between igniter autoignition temperature and explosives from P1-P4 implies that igniter can be used to initiate the burning of explosives from P1-P4 in slow heating tests before self-ignition of

explosives. Measured values for P1, P2 and P4 values are found to be similar to the literature values.

Table 5.9 Autoignition Temperature (°C) of Energetic Materials

Measurement #	**Igniter**	**P1**	**P2**	**P3**	**P4**
1	164.8	207.9	236.2	235.0	212.2
2	166.1	209.9	235.1	235.0	212.9
3	173.5	206.9	241.9	243.2	213.9
4	171.8	212.6	238.0	243.0	214.5
Std. Dev.	3.7	2.2	2.6	4.1	0.9
Average	**169.1**	**209.3**	**237.8**	**239.1**	**213.4**
Literature Value [118]	**-**	**207**	**231**	**-**	**209**

Impact and friction sensitivities of the developed igniter composition were also investigated considering the suggested test methods from literature [107], [106]. The aim of the measurement of impact and friction sensitivity was to investigate whether the use of igniter would reduce the sensitivity of coupled explosive formulations from P1 to P4, which would reduce the total sensitivity of missile and munition systems. Impact sensitivity was measured as 9.2±0.2 J and friction sensitivity was measured as 301.2±0.2 N. Measured values of igniter (PETN + RDX + Polymer Matrix) for impact and friction sensitivity lies between the pure energetic materials (RDX/HMX) and explosive compositions (energetic material (RDX/HMX) + polymer matrix) which shows that igniter can be coupled with explosive compositions without reducing the sensitivity level of the pure energetic material. Impact sensitivity of pure energetic materials were measured as 1.5, 5.6, 6.5 J for PETN, RDX, HMX. The corresponding values reported in the literature are 17.6, 14.4, 16.7 J for P1, P2 and P4, respectively [118], [120] . Friction sensitivity of pure energetic materials were measured as 60,120, 120 N for PETN, RDX, HMX. The corresponding values reported in the literature are >360 N, >360N, 150.6 N for P1, P2 and P4, respectively [118].

5.2 Small-Scale Slow Heating Tests

Small-scale slow heating tests were conducted with small test items defined in section 3.3.1. The aim of the small-scale tests was to obtain repeatable heating rate, cook-off temperature and cook-off time data and use obtained data for validation of the small-scale numerical simulations. Temperature and time data was collected with 1 Hz frequency and collected data was analyzed with Origin 9.0 software. Heating chamber was set to 50°C to ensure uniform temperature distribution in the test set-up before the heating ramp started and the instant that temperature of the explosive reaches 50°C was regarded as t=0 in all small-scale experiments.

Small-scale slow heating tests in forced convection conditions were performed by turning on the heating fan that leads to constant cross air flow in heating chambers with a constant velocity of 0.4 m/s. 30 tests were conducted to test five different test items at three different heating rates (5,15,25°C/h) in three different chambers. At least two replicate tests were conducted for each configuration. Five test item configurations were igniter coupled with P1 explosive and bare P1 to P4 explosives. Igniter was only coupled with P1 explosive. Since igniter initiates at a lower temperature compared to main explosive as desired, changing the explosive type that is coupled with igniter would not change the igniter initiation temperature/time or any other test parameter.

Test items, details of which were explained in section 3.3.1, are comprised of an Aluminum casing that has 34.2/42.2 mm ID/OD and 85 mm length, and explosive test item with Teflon plugs in one side. Tested explosive (P1 to P4) volume is 64±2 cm^3 and igniter mass (if used) is 1.5±0.3 g (20 mm diameter and 3±0.5 mm thickness). The set and measured heating rates in the chambers in the small-scale experiments are compared in Table 5.10. The results show that measured and set heating rates agree with each other.

Table 5.10 Set and Measured Heating Rates in Experiments Conducted in Forced Convection Conditions

Configuration	Experiment #	Heating Rate (°C/h) (Set)	Heating Rate (°C/h) (Measured)
Igniter Coupled with P1 Explosive	1	15	14.9
	2	15	15.0
	3	5	5.1
	4	5	5.1
	5	25	24.3
	6	25	24.4
Only P1 Explosive	7	15	15.3
	8	15	15.4
	9	15	15.4
	10	5	4.8
	11	5	4.9
	12	25	25.4
	13	25	25.5
	14	25	24.9
Only P2 Explosive	15	15	14.6
	16	15	14.6
	17	25	26.4
	18	25	25.8
Only P3 Explosive	19	5	4.8
	20	5	4.8
	21	15	14.5
	22	15	14.5
	23	25	25.8
	24	25	25.8

Table 5.10 (continued)

Configuration	Experiment #	Heating Rate (°C/h) (Set)	Heating Rate (°C/h) (Measured)
Only P4 Explosive	25	5	5.2
	26	5	5.2
	27	15	15.0
	28	15	14.6
	29	25	25.6
	30	25	25.6

5.2.1 Igniter Coupled with P1 Explosive

Heating profile of the small-scale slow heating tests for igniter coupled with P1 explosive is shown in Figure 5.21 for different heating rates. As summarized in previous chapters, the aim of implementation of igniter in tests are to show that igniter can burn the P1 or any other explosive (P2 to P4) at a predefined temperature before the cook-off and violent behavior of these explosives. Two tests were conducted for each heating rate for igniter coupled with P1 explosive configuration. As can be seen in Table 5.11, cook-off temperature and time was reproducible for each configuration. Cook-off temperatures were found to rise with increasing heating rate. Cook-off temperature and cook-off time were found to deviate within only ± 1.9°C and ± 4.7 minutes respectively. The values corresponded to only 1.3% maximum temperature difference and 0.5% maximum time difference. % differences were calculated by considering the ratio of deviated values to average measured value (for instance 1.9°C deviation for 146.9°C average temperature for 15°C/h heating rate). Relatively small cook-off temperature and time shows that PETN energetic material that initiates igniter is distributed relatively homogenously in polyurethane matrix that includes five other ingredient and can be used for burning other energetic materials reliably. In addition, it was noted that cook-off temperature

increased with increased heating rate as shown in table due to elevated temperature gradient inside igniter and heat dissipation with increasing heating rate. It was also observed that temperature difference between chamber air temperature and center of P1 explosive increased as ≈3.5 °C, ≈6°C and ≈11.5°C for the 5, 15 and 25°C/h heating rates respectively as temperature gradient increases with increasing heating rate. Moreover, heating rate of the igniter slowed down between 130 to 136°C for all tests conducted with igniter due to melting of PETN in igniter composition. Repeatability of replicate tests in which igniter is coupled with P1 Explosive are presented in Appendix E. Maximum temperature difference between start of heating and cook-off of igniter was calculated as only 2.0°C, 0.9°C and 1.8°C between two replicate tests shown in Appendix E for 5, 15 and 25°C/h heating rates respectively.

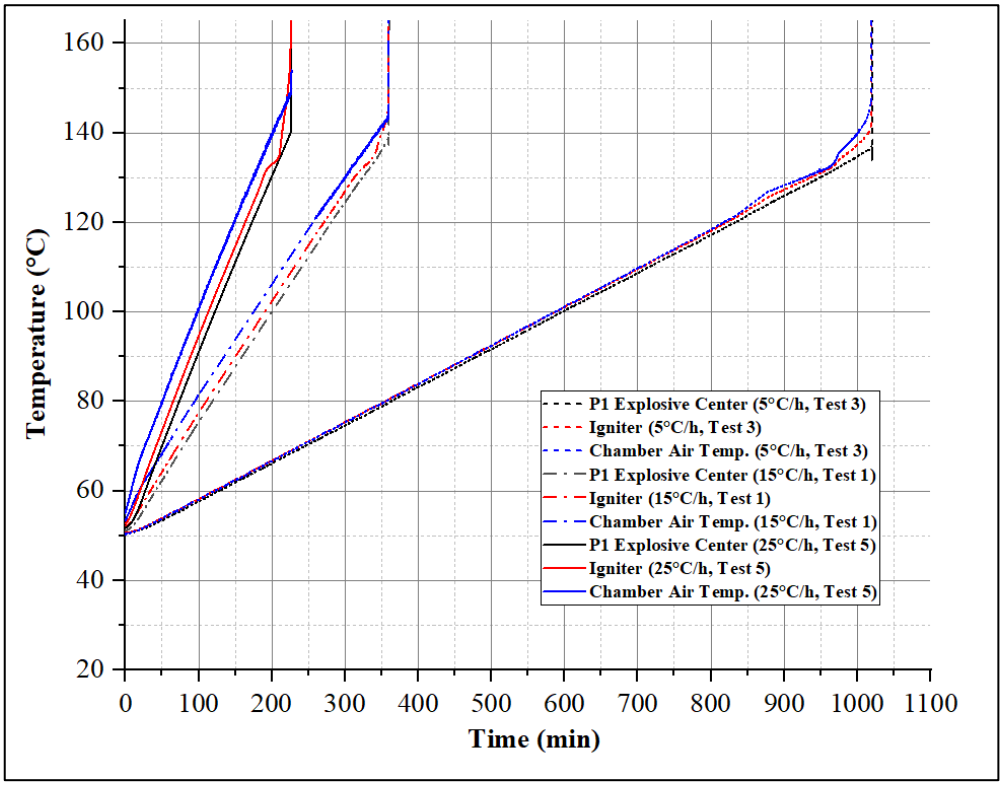

Figure 5.21. Comparison of Tests Conducted with Igniter Coupled with P1 Explosive (5, 15, 25°C/h heating rate)

Table 5.11 Summary of Experiments Conducted with Igniter Coupled with P1 Explosive (5, 15, 25°C/h heating rate)

Heating Rate (°C)	Test #	Cook-Off Temperature (°C)	Cook-Off Time (minute)	Average Cook-Off Temperature (°C)	Average Cook-Off Time (minute)
5	3	140.7	1019.5	**142.5 ± 1.8**	**1014.8 ± 4.7**
	4	144.3	1010.2		
15	1	145.0	359.6	**146.9 ± 1.9**	**360.9 ± 1.3**
	2	148.7	362.2		
25	5	153.7	225.7	**153.6 ± 0.1**	**226.8 ± 1.1**
	6	153.5	227.9		

After each test, test items were photographed for further evaluation. Figure 5.22 shows the test item that contains P1 explosive coupled with igniter for a 15°C/h heating rate. Illustrated photographs show that igniter and P1 explosive burned completely after the cook-off.

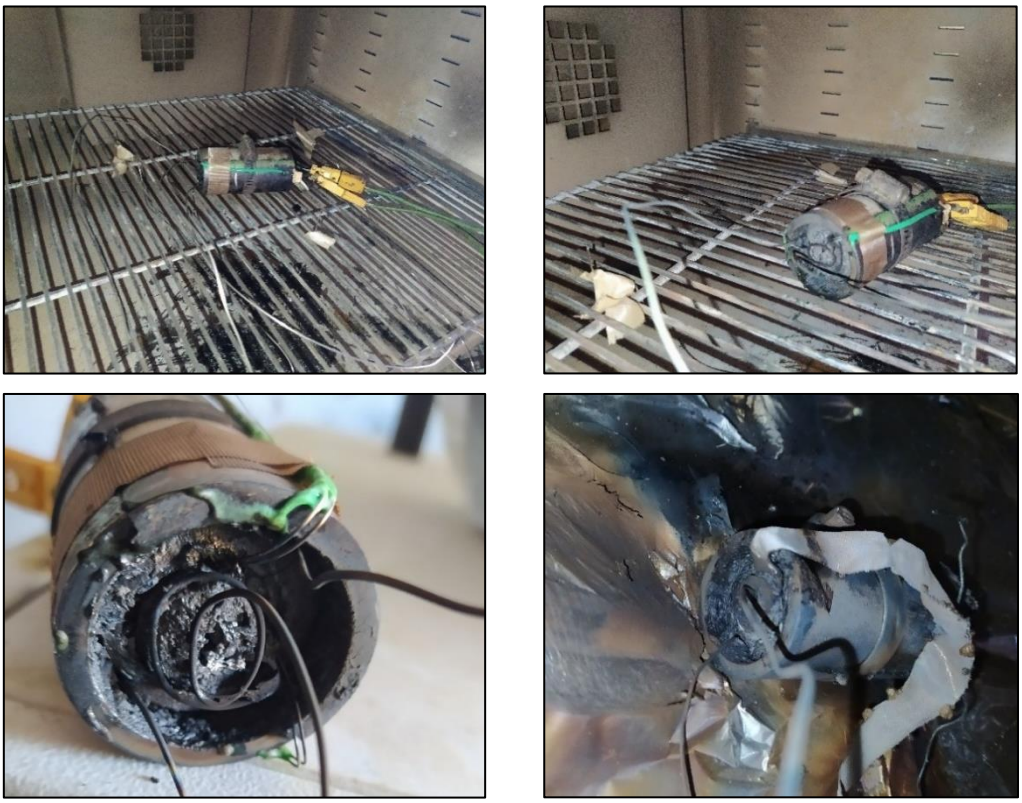

Figure 5.22. Burned Test Samples of Igniter Coupled with P1 Explosive (15°C/h heating rate)

5.2.2 Bare P1, P2, P3 and P4 Explosives

After the determination of igniter cook-off temperature and time for different heating rates, it was intended to show the cook-off temperature, time and violent behavior of bare explosives (without igniter) from P1 to P4 for different heating rates (5, 15 and 25°C/h). As can be seen in Table 5.12 for 24 tests were conducted with bare explosives without the igniter. Maximum temperature difference was observed as 1.7% for P2 explosive at 25°C/h heating rate and maximum time difference was observed as 1.7% for P3 explosive at 15°C/h heating rate. % differences were calculated by considering the ratio of deviated values to average measured value (for instance 3.4°C deviation for 204.8°C average temperature for P2 at 15°C/h heating rate). In addition to this, repeatability of replicate tests in for bare explosives from P1 to P4 are presented in Appendix E. Maximum temperature difference between start of heating and cook-off process of explosive presented in Appendix E was measured between 0.4-2.1°C as shown in Table 5.13.

In some tests (Tests 17, 18 and 24) that were performed with 25°C/h heating rate higher temperature differences between the test item and chamber air temperature were observed, since the center and end of the explosive were exposed to the chamber air. Temperature profile for these tests showed that cook-off started from the surface open to air inside chamber instead of center of explosive. For those tests, air temperature at the ignition instant was considered as cook-off temperature.

Table 5.12 Summary of Experiments Conducted with Bare Explosive Items P1 to P4 (Without Igniter) (5, 15, 25°C/h heating rate)

Test Item	Heating Rate (°C/h)	Test #	Cook-Off Temperature (°C)	Cook-Off Time (minute)	Average Cook-Off Temperature (°C)	Average Cook-Off Time (minute)
P1	5	7	172.0	1409.3	**174.8 ± 2.8**	**1408.9 ± 0.4**
		8	177.6	1408.6		
	15	9	177.2	481.1	**179.6 ± 2.6**	**481.0 ± 2.2**
		10	178.3	478.3		
		11	183.2	483.7		
	25	12	183.6	304.5	**183.7 ± 0.8**	**304.9 ± 2.8**
		13	182.7	301.7		
		14	184.7	308.5		
P2	15	15	198.5	610.6	**200.9 ± 2.4**	**617.5 ± 6.8**
		16	203.3	624.3		
	25	17	208.2 (air temp.) 193.0 (center of P2)	325.7	**204.8 ± 3.4**	**328.7 ± 2.9**
		18	201.3 (air temp.) 191.4 (center of P2)	331.6		
P3	5	19	215.4	1745.2	**217.2 ± 1.8**	**1760.1 ± 14.9**
		20	219.0	1775.0		
	15	21	205.9	614.1	**207.4 ± 1.6**	**624.7 ± 10.6**
		22	209.0	635.2		
	25	23	201.1	335.2	**200.1 ± 0.9**	**337.1 ± 2.0**
		24	199.2 (air temp.) 195.8 (center of P3)	339.1		
P4	5	25	198.6	1470.6	**198.1 ± 0.5**	**1464.2 ± 6.4**
		26	197.6	1457.7		
	15	27	198.5	538.4	**196.6 ± 1.9**	**543.8 ± 5.4**
		28	194.7	549.3		
	25	29	188.8	319.5	**188.0 ± 0.8**	**316.5 ± 3.0**
		30	187.2	313.5		

Table 5.13 Summary of Maximum Temperature Difference for Replicate Experiments Conducted with Bare Explosive Items P1 to P4 (Without Igniter) (5, 15, 25°C/h heating rate)

Heating Rate (°C/h)	**Maximum Temperature Difference for Replicate Tests (°C)**			
	P1	**P2**	**P3**	**P4**
5	0.7	-	1.3	1.5
15	0.8	1.0	2.0	1.8
25	1.3	2.1	0.4	1.9

Temperature profiles of bare explosives illustrated from Figure 5.23 to Figure 5.26 . Effect of heating rate on the cook-off temperatures of the materials are summarized in Figure 5.27. It was observed that cook-off temperature changes with following order: P2≈P3>P4>P1>Igniter. This trend was expected in the slow heating test since source term (volumetric heat generation) due to exothermic thermal decomposition was calculated in Figure 5.20 (in section 5.1.4) had the nearly same trend (P2≈ P3>P4>P1>Igniter).

It was initially observed that cook-off temperature could increase or decrease depending on the explosive type with increasing heating rate as shown in Figure 5.27. To explain this phenomena, two factors that affect the cook-off temperature are considered; (i) the temperature gradient inside test item due to heating rate and (ii) ratio of heat generation in explosive formulations due exothermic thermal decomposition to heat dissipation to the air especially after critical temperature. For relatively higher heating rates (25°C/h) first factor dominates and increased temperature gradient inside the test item is expected. Temperature gradient inside test chamber limits the volumetric heat generation inside the test item and leads to higher cook-off temperature for higher heating rates. This trend was observed for igniter coupled with P1 explosive, bare P1 explosive and bare P2 explosive as shown in Figure 5.27 as well as in the literature [28]. For instance, for bare P1 explosive

(without igniter) average cook-off temperature during cook-off was measured as 174.8°C, 179.6°C, 183.7°C for 5, 15, 25°C/h heating rates respectively. In addition to this, approximately 30°C ignition temperature difference was noted in literature for 3.3 and 15°C/h heating rates for same test items [28]. Second factor was also observed for P3 (45±5% HMX by weight) and P4 (20±2% RDX by weight) explosives that have relatively less energetic material content compared to P1 (64±4 % by weight RDX) and P2 (87±3 % by weight HMX) explosives. After the critical temperature which is tabulated in section 5.6, heat generation due to thermal decomposition of explosive surpassed the heat transfer from air inside the chamber to the test item and self-ignition started. For P3 and P4 explosives critical temperature values for 25°C/h heating rate was observed to be higher compared to 15°C and 5°C/h heating rates. It was initially expected to have also higher cook-off temperatures for P3 and P4 due to higher critical temperature at 25°C/h heating rate, however lower weight percent of energetic constituents in P3 and P4 explosive limited the volumetric heat generation due to thermal decomposition of explosive and for 5 and 15°C/h heating rates heat dissipation to the environment (air) delayed the cook-off process and led to higher cook-off temperatures for 5 and 15 °C/h heating rates compared to 25°C/h heating rate as shown in Figure 5.27.

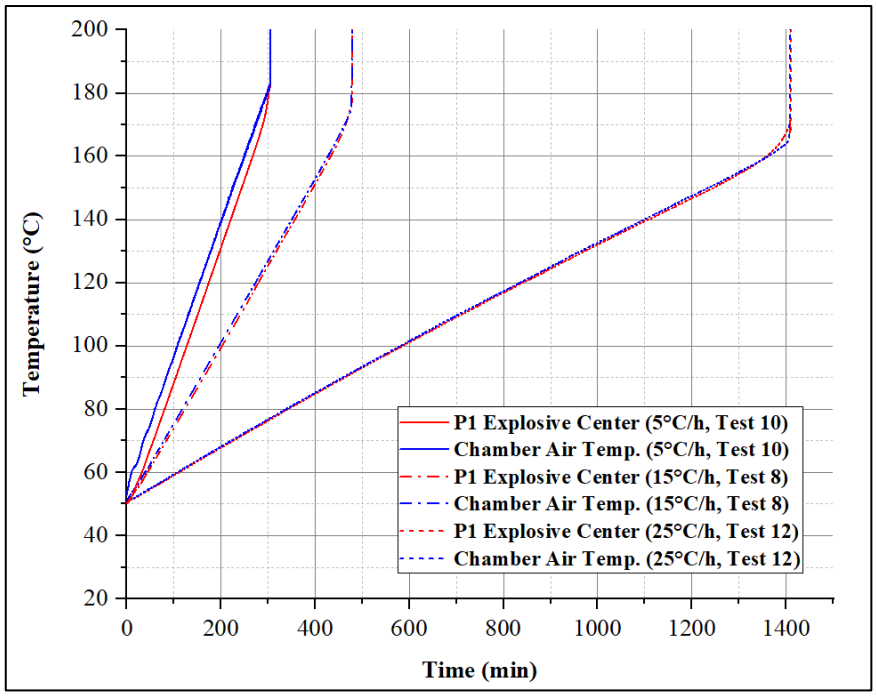

Figure 5.23. Comparison of Bare P1 Explosive Tests (Without Igniter) (5, 15, 25°C/h heating rate)

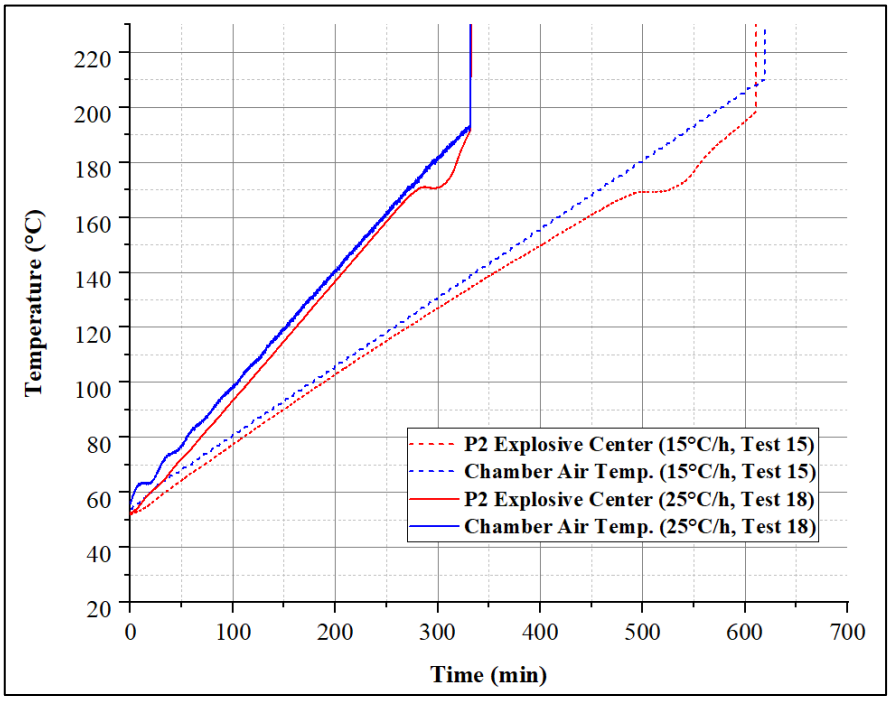

Figure 5.24. Comparison of Bare P2 Explosive Tests (Without Igniter) (15, 25°C/h heating rate)

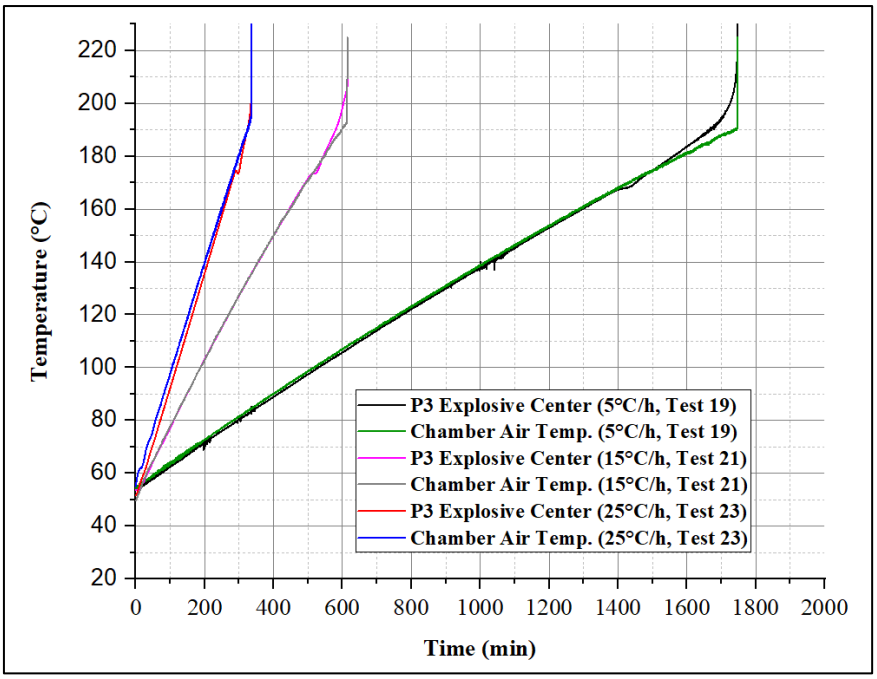

Figure 5.25. Comparison of Bare P3 Explosive Tests (Without Igniter) (5, 15, 25°C/h heating rate)

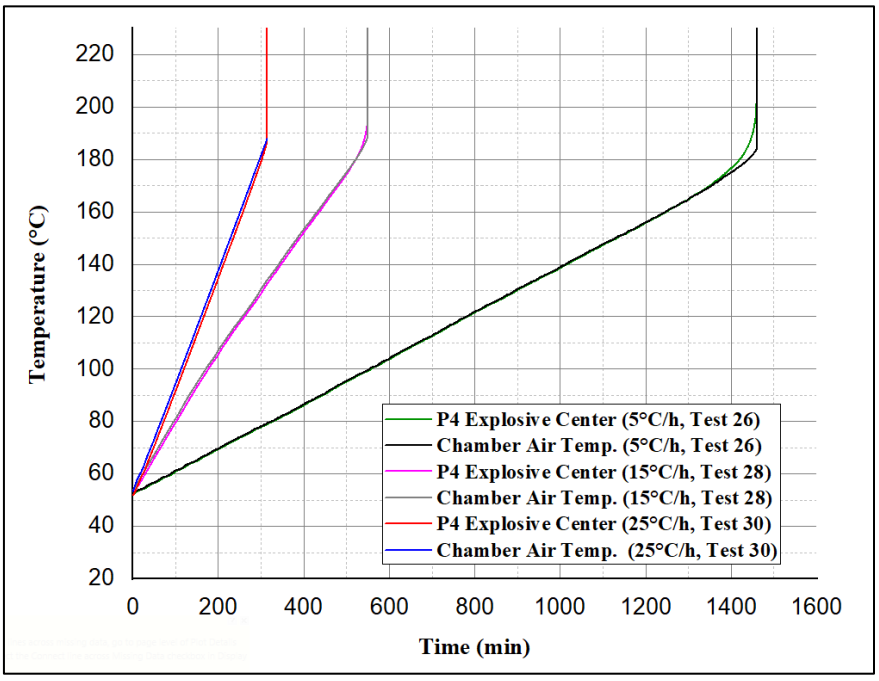

Figure 5.26. Comparison of Bare P4 Explosive Tests (Without Igniter) (5, 15, 25°C/h heating rate)

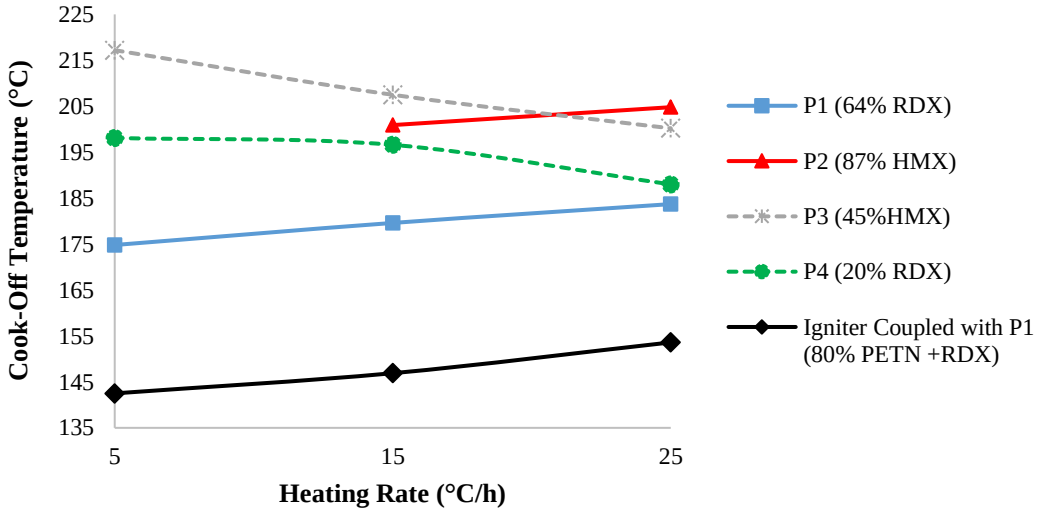

Figure 5.27. Effect of Heating Rate (5, 15, 25°C/h) on Cook-Off Temperature of Bare Explosives (P1 to P4) (Without Igniter)

The cook-off temperature of the igniter is at least 30-60°C lower than the explosive formulations. Therefore, igniter can be used for burning of explosives from P1 to P4 in slow heating tests. The test items and munitions that contains explosive formulations from P1 to P4 can be burned in a controlled manner between 140-155°C with the use of igniter from the vented side of the munition or test item before the violent cook-off of the explosive.

The severity of the ignition of bare explosives were also investigated during small-scale testing. Ignition instant of P1 explosive is shown in Figure 5.28. After the self-ignition, P1 explosive (105 g) severely burned more than 30 seconds. To discharge the burnt products in test item, one end of the test item was left as open and other end of the test item was closed loosely with Teflon plug. If experiment had been conducted with closing both ends with plugs, an explosion due the pressure rise resulting from the burnt products could have been observed. This pressure rise would have demolished the test chamber. In a confined munition or missile system, the pressure rise due to the burnt products could result in deflagration or deflagration to detonation, which shows the importance of controlled burn approach with igniters.

Figure 5.28. Ignition Instant of P1 Explosive (Without Igniter)

Burned test item after the slow heating test is also illustrated in Figure 5.29. Residual of the P1 explosive remained as char. During the cook-off, nearly half of the explosive was divided separated from the main part but did not separate during cook-off. After the experiment, it was noted that the second part was separated from the main part from the center of the explosive. Perimeter of the second part was also remained with the main part that showed that ignition started from the center and propagated outwards.

Figure 5.29. Burned Test Samples of P1 Explosive (Without Igniter)

Although it is theoretically expected that ignition due to thermal decomposition starts from the center of the explosive, practically it was not always observed in the test items. Explosive mixtures summarized in section 3.1 were prepared in a state-of art planetary mixer system to obtain a homogeneous mixture. However, it is practically impossible to have a homogenous explosive mixture regardless of mixing time. As P1 explosive is a heterogeneous mixture of RDX energetic material (64 % by weight) Al metal powder (20 % by weight) in a polyurethane matrix (16 % by weight), RDX rich locations in P1 explosive tends to generate more heat during thermal decomposition that leads to self-ignition. To understand ignition point in the P1 explosive during the small-scale slow heating test, the location of the ignition point was also investigated for three different tests (test 7 to 9). Five thermocouples were inserted to test item (two inner walls, one center, two between center and inner wall) as shown in Appendix G. From tests it was observed that ignition occurred randomly for each test. For test 7, temperature rose near the air thermocouple inside chamber

close to the front of the test item. This showed that ignition occurred from the top or top edge of the test item. For test 8 and 9, ignition occurred near the inner wall and between inner wall-center of the test item, respectively. Random ignition point in the test item was attributed to inadequate mixing in explosion production that may lead to agglomeration or accumulation of energetic materials in the test items. Temperature distribution of the tests from 7-9 are also given in Appendix G.

5.3 Small-Scale Slow Heating Simulations

Small-scale slow heating simulations were conducted with fifteen configurations (5, 15, 25 °C/h for igniter and P1 to P4 explosives). Before these simulations, to determine the mesh size and time step for the simulations, sensitivity analyses were first performed. Then using the parameters obtained from sensitivity analysis small-scale slow heating simulations were completed. Sensitivity analyses for small-scale slow heating simulations were performed with 0.5, 1 and 2 mm mesh size and with 2, 10, 30 and 60 second time steps respectively with P1 explosive. As a result of analyses 1 mm mesh size and 10 second time step was selected which corresponds to least absolute error. Details of the sensitive analyses conducted for small-scale slow heating test set-up is given in section 4.2.2.

5.3.1 Igniter Coupled with P1 Explosive

Simulation and experimental data comparison of igniter coupled with P1 explosive was performed for 5, 15 and 25°C heating rates. Summary of this comparison is shown in Table 5.14. It was shown that error for the cook-off temperature and cook-off time is 4.3 % and 1.5 % respectively. Error in cook-off temperature was calculated as 0.2 % for 15°C/h heating rate which is the recommended heating rate by the test standards from the literature for the slow heating tests. Error values for temperature or time was calculated as (100%*[Experimental Value-Calculated Value]/Experimental Value). These error values seem to be reasonable, since

isoconversional (model-free [F/W/O or K/A/S methods]) decomposition kinetic was used for the calculation of decomposition parameters (E_A and A).

Table 5.14 Comparison of Simulations and Experimental Data for Igniter Coupled with P1 explosive

Heating Rate (°C)	Experimental Average Cook-Off Temperature (°C)	Calculated Cook-Off Temperature (°C)	Error in Cook-Off Temperature (%)	Experimental Average Cook-Off Time (minute)	Calculated Average Cook-Off Time (minute)	Error in Cook-Off Time (%)
5	142.5	145.4	2.1	1014.8	1025.7	1.1
15	146.9	146.5	-0.2	360.9	366.2	1.5
25	153.6	147.0	-4.3	226.8	228.5	0.8

Two isoconversional methods were used for the calculation of decomposition parameters in the simulations. Comparison of experimental data with simulation including the two decomposition models and heating profiles are summarized in Figure 5.30 to Figure 5.32 for 5, 15 and 25°C/h heating rates respectively. In these figures calculated igniter temperatures are given in dashed lines for different models and experimental igniter temperature (orange colored line, measured from the interface with P1 explosive given in Figure 3.4 (section 3.3.1) and experimental average air temperature (blue colored line) in small-scale test chamber is given in continuous lines. Although method 2 (Kissinger/Akahira/Sunose (K/A/S)) (Eq. 21 in section 2.2), is suggested in literature [33] compared to Method 1 (Flynn/Wall/Ozawa (F/W/O) (Eq. 20 in section 2.2), both methods resulted in the same cook-off time and cook-off temperature.

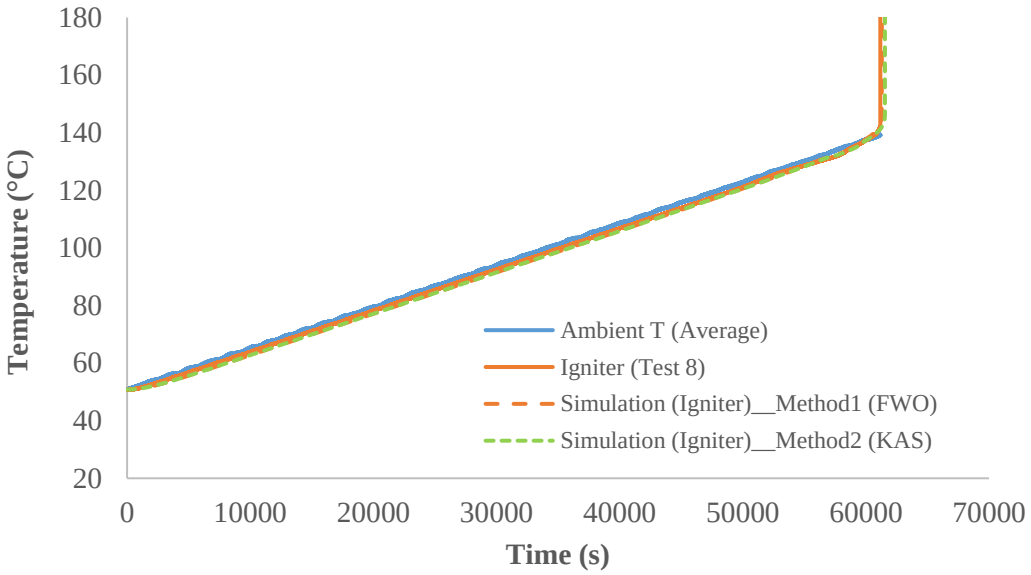

Figure 5.30. Test and Simulation Comparison of Experimental and Simulated Temperature Profiles for Igniter Coupled with P1 Explosive (5°C/h heating rate)

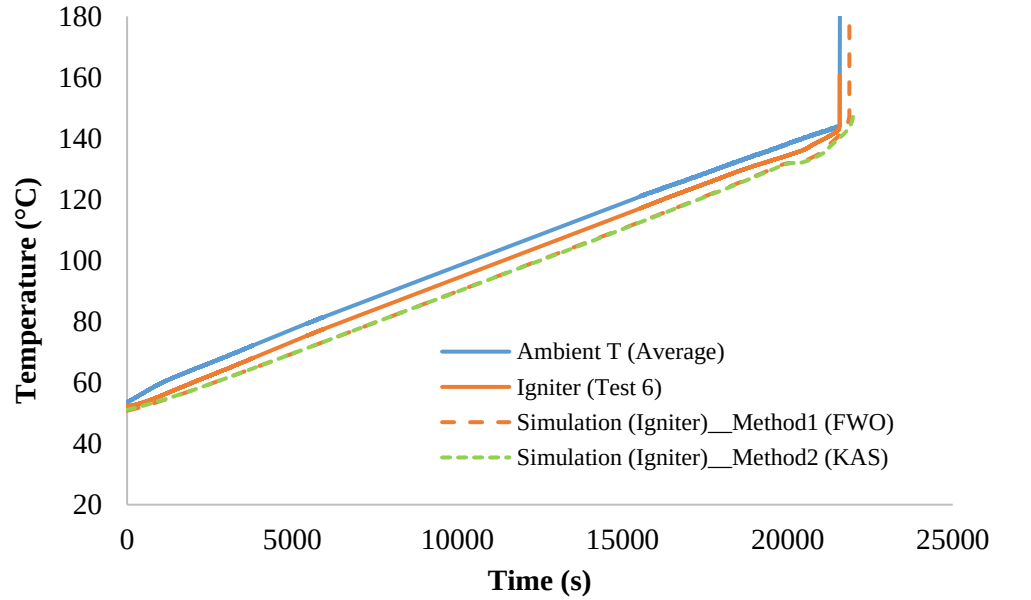

Figure 5.31. Test and Simulation Comparison of Experimental and Simulated Temperature Profiles for Igniter Coupled with P1 Explosive (15°C/h heating rate)

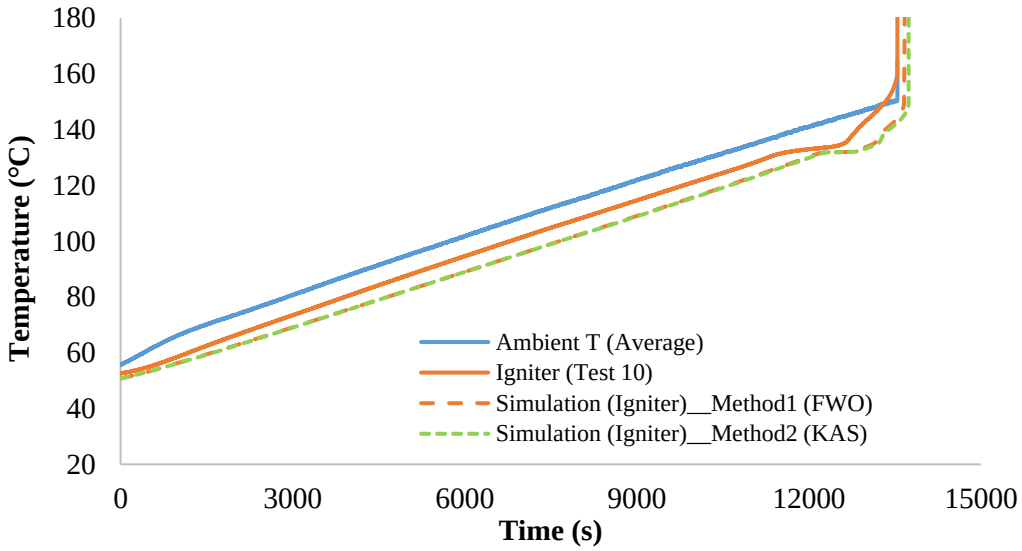

Figure 5.32. Test and Simulation Comparison of Experimental and Simulated Temperature Profiles for Igniter Coupled with P1 Explosive (25°C/h heating rate)

Effect of heating rate on predicted temperature profile between start of heating and cook-off was also investigated in Figure 5.30 to Figure 5.32 for 5, 15 and 25°C/h heating rates Maximum error between measured and predicted temperature was obtained as ≈1.0°C, ≈ 5.0°C and ≈6.0°C for 5, 15 and 25°C/h heating rates respectively. The increase in error value with increasing heating rate can be attributed to: (i) Increasing measurement error of air temperature in small-scale test chamber with respect to increasing heating rate due to elevated temperature gradient, (ii) Calculation errors in convective heat transfer coefficient using Churchill and Bernstein correlation, which is reported to cause up to 20 % error in literature [85] (iii) Measurements errors of physical and thermal properties (λ, ρ, c_p) from the characterization experiments.

First mentioned possible error stems from the fact that for higher heating rates such as 15 and 25°C/h, small-scale test chamber inner wall temperature (due to heating elements inside wall) is much higher than the center of the chamber where test item is located. Temperature gradient between different locations might lead to

measurements error in air temperature inside test chamber that is used for simulations. Air temperature inside the test chamber was measured from three locations in experiments and average of measured temperature data was used in simulations. Second and third mentioned errors can be considered in combination. Measurement errors in physical and thermal properties (λ, ρ, c_p) may lead to errors in correlation for convective heat transfer coefficient. The effect of errors in correlation for convective heat transfer coefficient is investigated in section 5.3.2 for P1 explosive.

Ignition location was also investigated for the igniter. Figure 5.33 shows the ignition location of the igniter pellet between 21870 and 21880 seconds. As expected, ignition starts from the center of the igniter pellet where the volumetric heat generation due to decomposition is higher.

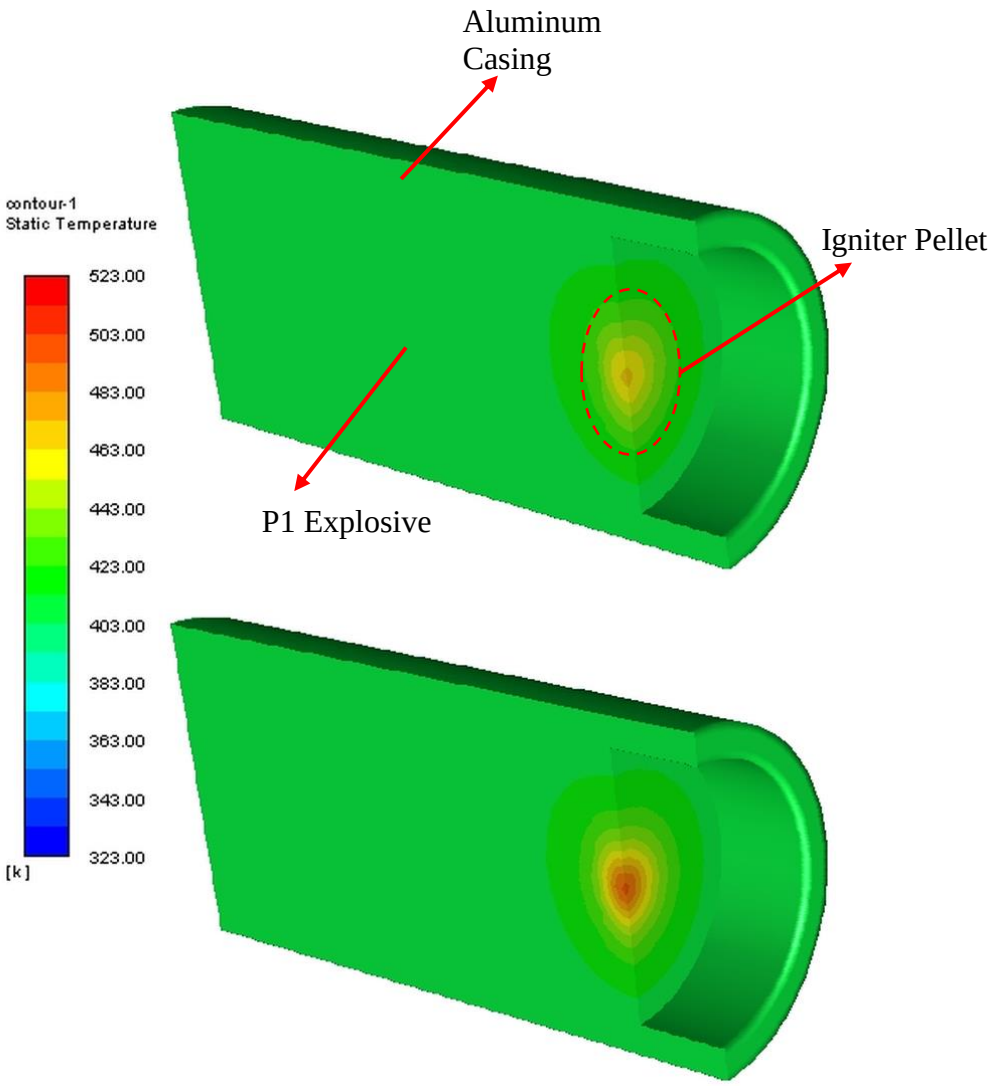

Figure 5.33. Self-Heating and Ignition Location Contour from Simulation for Igniter Coupled with P1 Explosive (15°C/h heating rate) (21870 to 21880 seconds)

5.3.2 Bare P1, P2, P3 and P4 Explosives

Simulation and experimental data comparison of bare P1 to P4 explosive (without igniter) was performed for 5, 15 and 25°C heating rates are summarized in Table 5.15. From the table it can be observed that in majority of the simulations, cook-off temperature of the explosive was calculated with less than 5.0% error. Only P2 explosive led to 7.5 and 5.2 % cook-off temperature error for 15 and 25°C/h heating rates respectively, which may arise from the errors in thermal decomposition

parameters. These error values seem to be reasonable, since isoconversional (model-free [F/W/O or K/A/S methods]) decomposition kinetic was used for the calculation of decomposition parameters (E_A and A) except P1 explosive. 1st order decomposition kinetics were utilized for thermal decomposition of P1 explosive (section 5.1.3). For P2 and P3 decomposition parameters that were calculated at α=10% and α=12% were considered respectively (section 5.1.4) and for P4 decomposition values given in literature was used (section 5.1.4).

Cook-off time error was higher than cook-off temperature due to difference in experimental and calculated temperature profiles in Table 5.15. However, cook-off temperature was not affected from the error in temperature profile as it only depends on the thermal decomposition parameters. Up to 12.9% error (for P2 explosive at 25°C/h hating rate) was observed for cook-off time of bare explosive test items. This relatively higher error percent originates from the difference in experimental and simulation temperature profile.

Comparison of experimental data with simulation including the decomposition models and heating profiles are summarized in Figure 5.34 to Figure 5.36 for bare P1 explosive (without igniter). In these figures, calculated P1 explosive temperatures are given in dashed lines and experimental P1 explosive temperature (red colored line, measured from center of P1 explosive given in Figure 3.4 (section 3.3.1) and experimental average air temperature (blue colored line) in small-scale test chamber is given in continuous lines. The effect of decomposition model (whether isoconversional [model-free] Method 1 (F/W/O) or Method 2 (K/A/S) or model-based [1st order]) was also shown for 15°C/h heating rate in Figure 5.35. It is shown in the figure that simulations results in the same temperature profile and cook-off temperature/time and isoconversional methods can also be applied to P1 explosive for which model-based 1st order decomposition kinetics were considered in section 5.1.3.

Bare P2, P3 and P4 explosives were also simulated and compared with experimental results. Comparison of experimental data with simulation including the decomposition models and heating profiles are summarized in Figure 5.37 to Figure 5.39 for bare P2, P3, P4 explosive (without igniter) at 5, 15 and 25°C/h heating rates respectively.

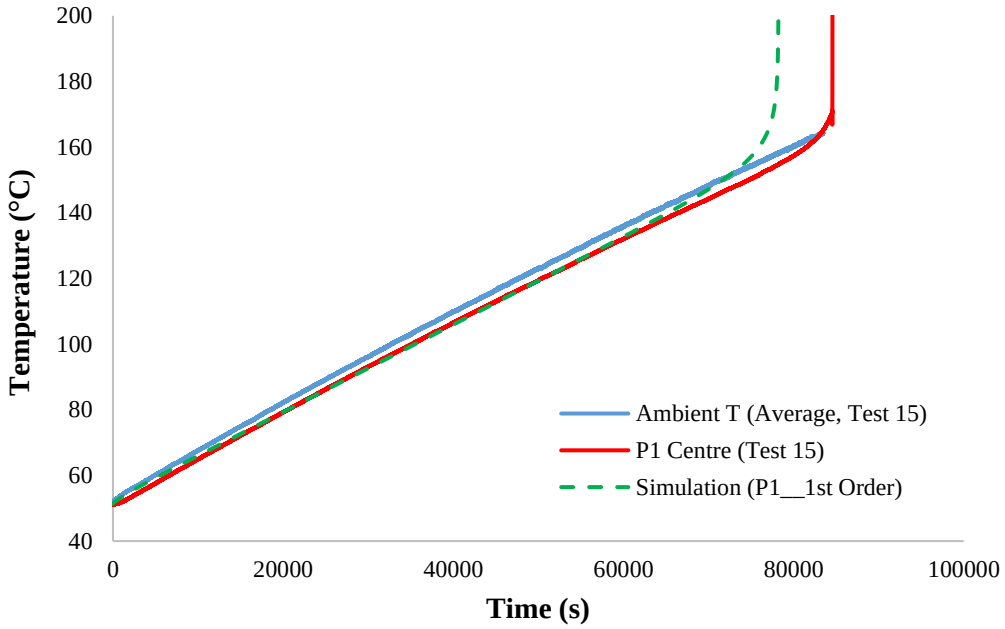

Figure 5.34. Test and Simulation Comparison of Experimental and Simulated Temperature Profiles for Bare P1 Explosive (without Igniter) (5°C/h heating rate)

Table 5.15 Comparison of Simulations and Experimental Data for Bare Explosive from P1 to P4 (Without Igniter) (5, 15, 25 °C/h)

Test Item	Heating Rate (°C)	Experimental Average Cook-Off Temperature (°C)	Calculated Cook-Off Temperature (°C)	Temperature Error (%) (*)	Experimental Average Cook-Off Time (minute)	Calculated Average Cook-Off Time (minute)	Time Error (%) (*)
P1	**5**	174.8	180.8	3.4	1408.9	1301.0	-7.7
	15	179.6	178.8	-0.4	481.0	461.2	-4.1
	25	183.7	178.8	-2.7	304.9	292.3	-4.1
P2	**15**	200.9	215.9	7.5	617.5	624.5	1.1
	25	204.8	215.4	5.2	328.7	371.2	12.9
P3	**5**	217.2	213.2	-1.8	1760.1	1617.8	-8.1
	15	207.4	210.2	1.3	624.7	579.5	-7.2
	25	200.1	209.9	4.9	372.2	408.8	-10.5
P4	**5**	198.1	200.7	1.3	1464.2	1462.5	0.1
	15	196.6	198.9	1.2	543.8	525.0	3.5
	25	188.0	197.3	4.9	316.5	324.2	-2.4

(*) Error values for temperature or time was calculated as (100%*[Experimental Value-Calculated Value]/Experimental Value)

.

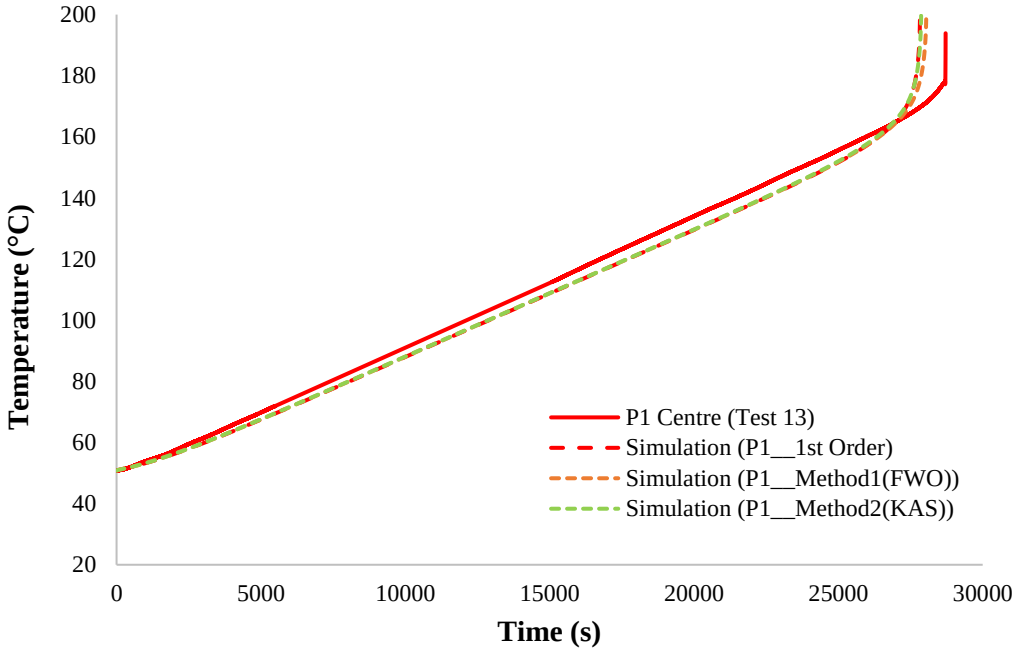

Figure 5.35. Test and Simulation Comparison of Experimental and Simulated Temperature Profiles for Bare P1 Explosive (without Igniter) (15°C/h heating rate)

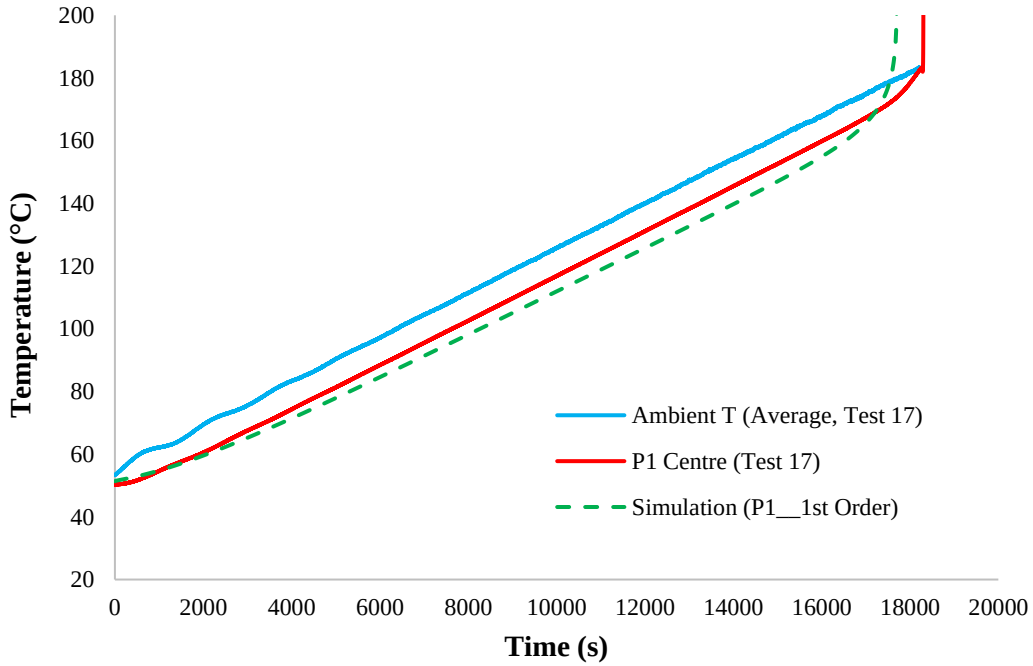

Figure 5.36. Test and Simulation Comparison of Experimental and Simulated Temperature Profiles for Bare P1 Explosive (without Igniter) (25°C/h heating rate)

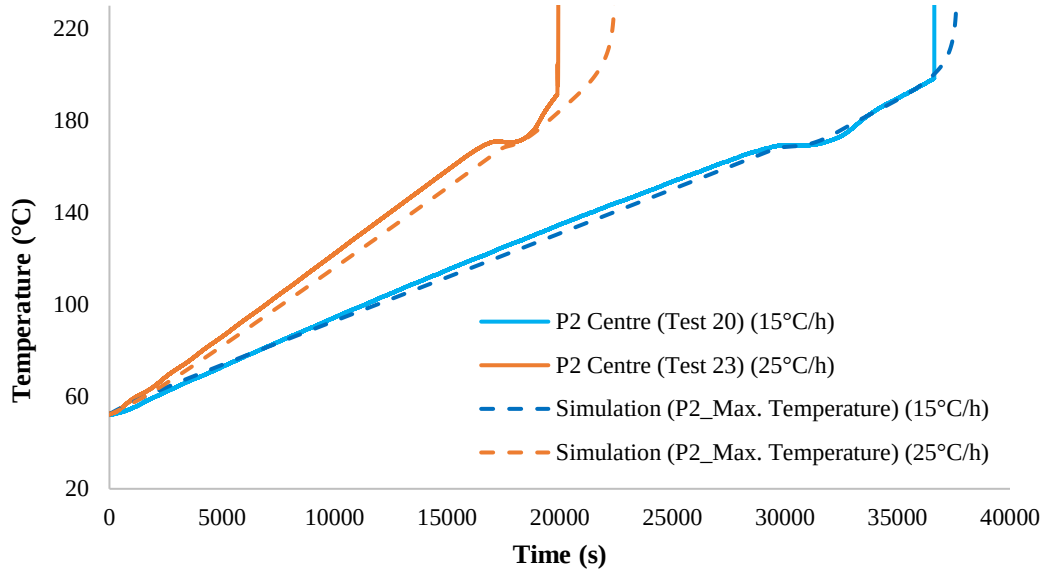

Figure 5.37. Test and Simulation Comparison of Experimental and Simulated Temperature Profiles for Bare P2 Explosive (without Igniter) (15 and 25°C/h heating rate)

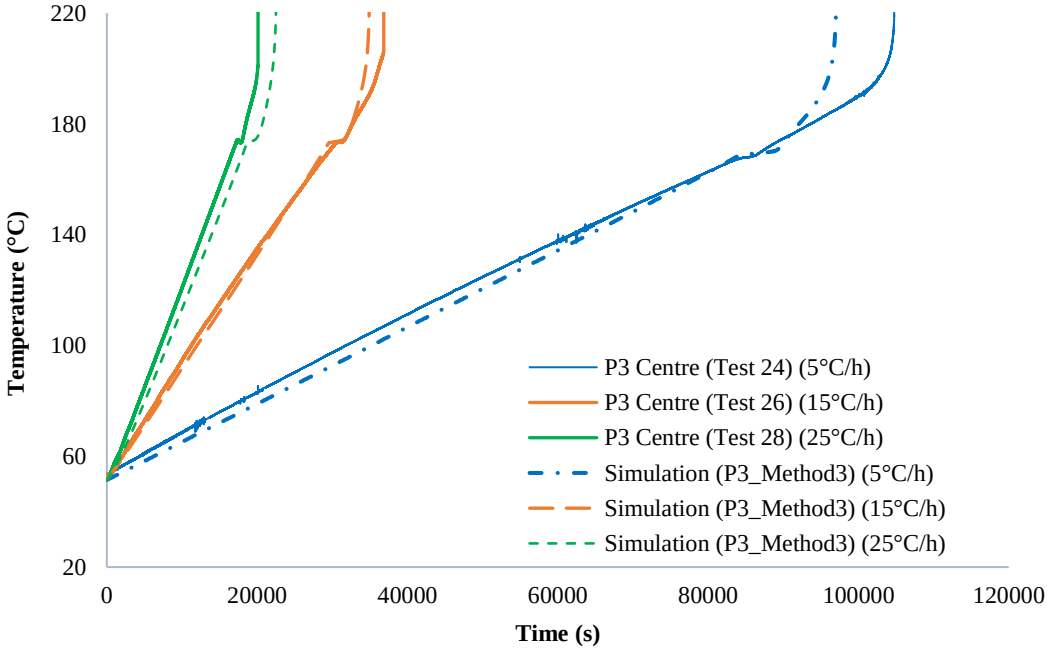

Figure 5.38. Test and Simulation Comparison of Experimental and Simulated Temperature Profiles for Bare P3 Explosive (without Igniter) (5, 15 and 25°C/h heating rate)

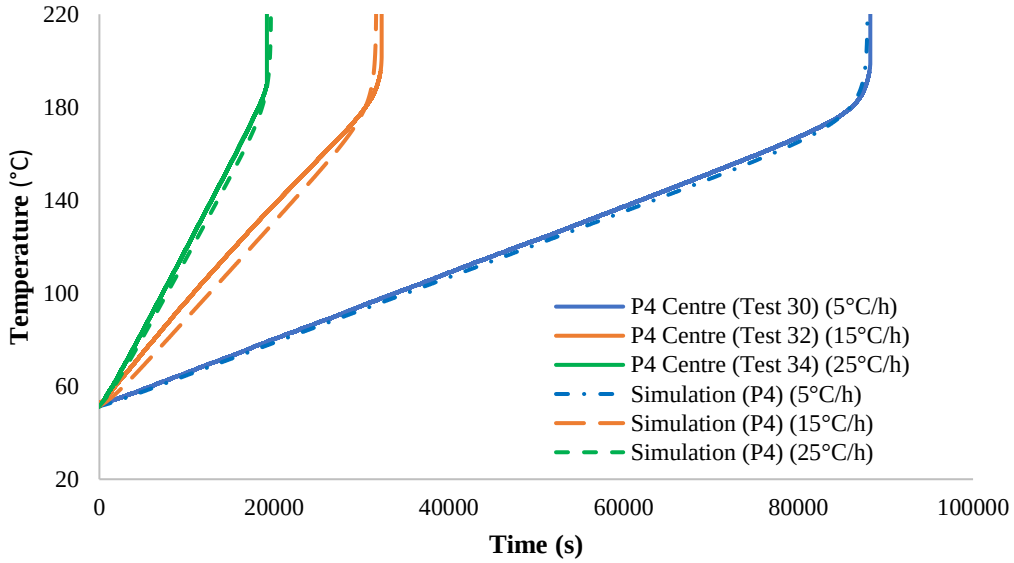

Figure 5.39. Test and Simulation Comparison of Experimental and Simulated Temperature Profiles for Bare P4 Explosive (without Igniter) (5, 15 and 25°C/h heating rate)

Temperature profiles of experiments and simulations given from Figure 5.33 to Figure 5.39 showed temperature difference up to 8.5°C between experimental data and calculated data in simulations. Deviation in experimental and predicted data were discussed in previous section (5.3.1) and this difference was mainly attributed to (i) Higher temperature gradient in air inside test chamber, (ii) Calculation errors in convective heat transfer coefficient correlation, (iii) Measurements errors of physical and thermal properties (λ, ρ, c_p) from the characterization experiments. To investigate the effect of convective heat transfer correlation (Churchill and Bernstein) for cross air flow inside test chamber on temperature profile, additional simulations were conducted by increasing or decreasing the heat transfer coefficient by 20% for bare P1 explosive (without igniter) for 5, 15 and 25°C/h respectively. Deviation magnitude was selected considering ±20% deviation remark from the literature for generalized convection heat transfer coefficient correlations [85]. Comparison of simulation with experimental results as well as ±20% deviated convective heat transfer coefficient is shown in Figure 5.40 for P1 explosive for 5,15

and 25°C/h heating rates. Detailed view of this figure for each heating rate is given in Appendix G. According to figure +20% deviation for Churchill and Bernstein correlation reduced the 5.6°C difference between experimental and simulated data to 2.6°C for 25°C/h heating rate. Similar error reduction (+20% deviation of convective heat transfer coefficient) was also valid for 5 and 15°C/h heating rates in which errors between experiments and simulated data were trivial compared to 25°C/h heating rate. Since Churchill and Bernstein heat transfer coefficient correlation is a generalized correlation that was developed for ideal conditions by considering available experimental data for the correlation, requirement for fine-tuning of correlation for the small-scale set-up was not surprising. In addition to this, fine-tuning requirement for heat transfer coefficient in positive direction from Churchill and Bernstein correlation implied that other correlations (Hilbert, Zukauskas) considered in section 2.1.1 was not needed for this study, since these correlations corresponded to lower heat transfer coefficients (9.03±0.05 and 8.25±0.05 $W/m^2.k$) and compared to Churchill and Bernstein correlation (9.3±0.05 $W/m^2.K$) that required fine tuning in positive direction (+20%) between 50-220°C air temperature and 400-1000 Re_D.

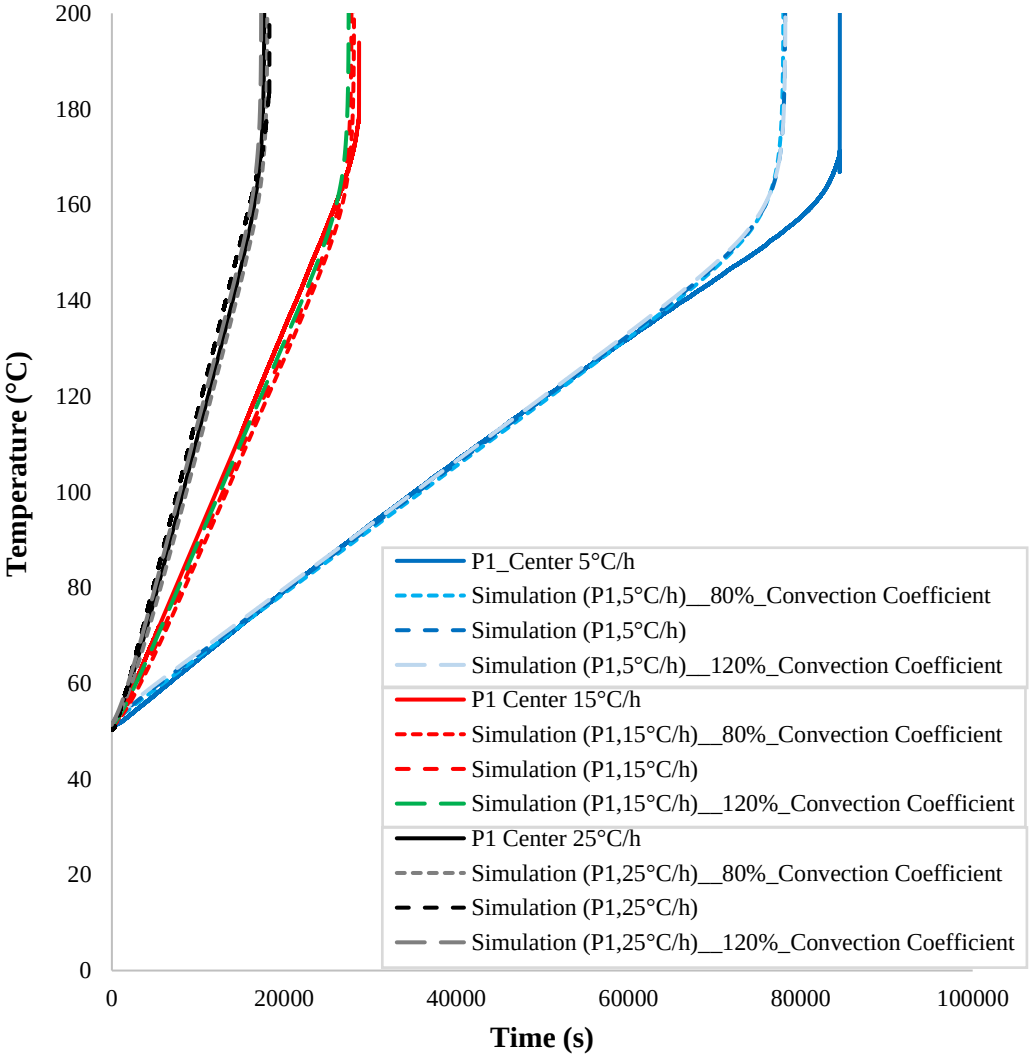

Figure 5.40. Effect of Convection Heat Transfer Coefficient on Temperature Profile for Bare P1 Explosive (Without Igniter): Test and Simulation Comparison (5, 15, 25°C/h heating rate)

Ignition location was also simulated for the bare P1 explosive (without igniter). Figure 5.41 shows the ignition location of the bare P1 explosive between 27739 and 27785 seconds. As expected, ignition starts from the center of the explosive where the volumetric heat generation due to decomposition is higher. This temperature contour clearly shows that for a munition or missile system that contains bare explosive, ignition due to slow cook-off would start from the center. After the ignition starts from the center, burnt products could not be discharged (not before the

burn half of the explosive burns) even if there is a vent at the end of the munition. Ignition of the explosive from the center would increase the pressure inside the munition system which in turn increase the burn rate of the explosive and leads to even more pressure. Increased pressure could result in deflagration or even detonation of the munition. The use of igniter pellet that would ignite at the end of the munition where venting path is available would lead to controlled burn of the explosive without increasing the pressure inside munition.

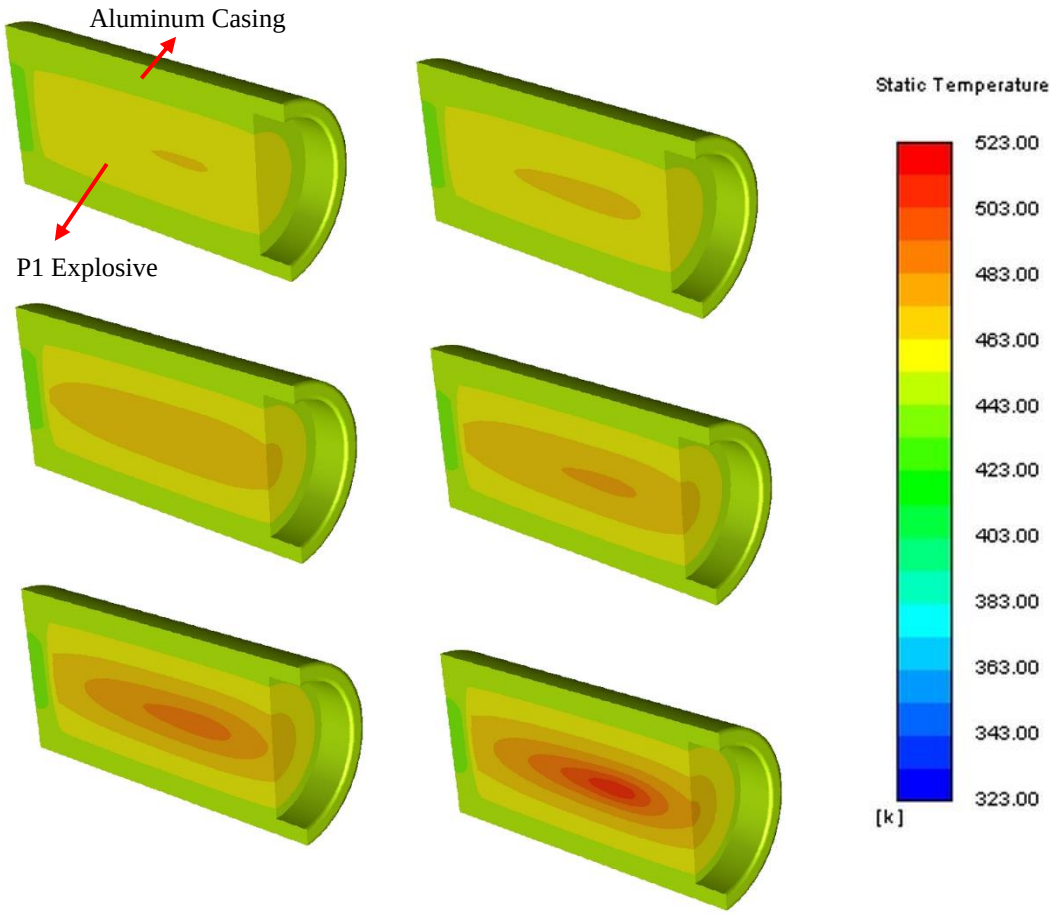

Figure 5.41. Self-Heating and Ignition Location Contour from Simulation for P1 Explosive (Without Igniter) (15°C/h heating rate) (27739 to 27785 seconds)

5.4 Large-Scale Slow Heating Test

Large-scale slow heating test was conducted in a special test area that is far from inhabited buildings and public traffic roads. This test consists of a penetrator munition that contains approximately 25 kg P1 explosive as a test item. Test item was placed in a test chamber that was heated with circulated air. Forced convection configuration and 15°C/h heating rate was used in the test as suggested by the test standard requirement [4]. Other details of set-up are presented in section 3.3.2.

Large-scale slow heating test was performed with a penetrator munition that has steel casing with >20 mm wall thickness. At the beginning of the test, test item was conditioned for nearly 7 hours to eliminate temperature gradient inside and 50°C temperature distribution was attained at the start of the test t_0. Raw temperature-time data for large-scale heating test is shown in Figure 5.42 that was collected from the points presented in Figure 3.8 in section 3.3.2 and processed data is shown in Figure 5.43. For data processing average of ambient temperature thermocouples were calculated and heating time was started from the instant when thermocouple inside the explosive center measured the 50°C temperature. From processed data in Figure 5.43, heating rate was calculated to be 13.03°C/hour between 90°C to ignition point (≈173.4°C) and ignition occurs at 41781st second from the t_0 when P1 explosive temperature is 173.4 °C. Before ignition, it was noted that temperature of the P1 explosive exceeds the surface temperature of the munition due to heat generation in P1 explosive resulting from thermal decomposition.

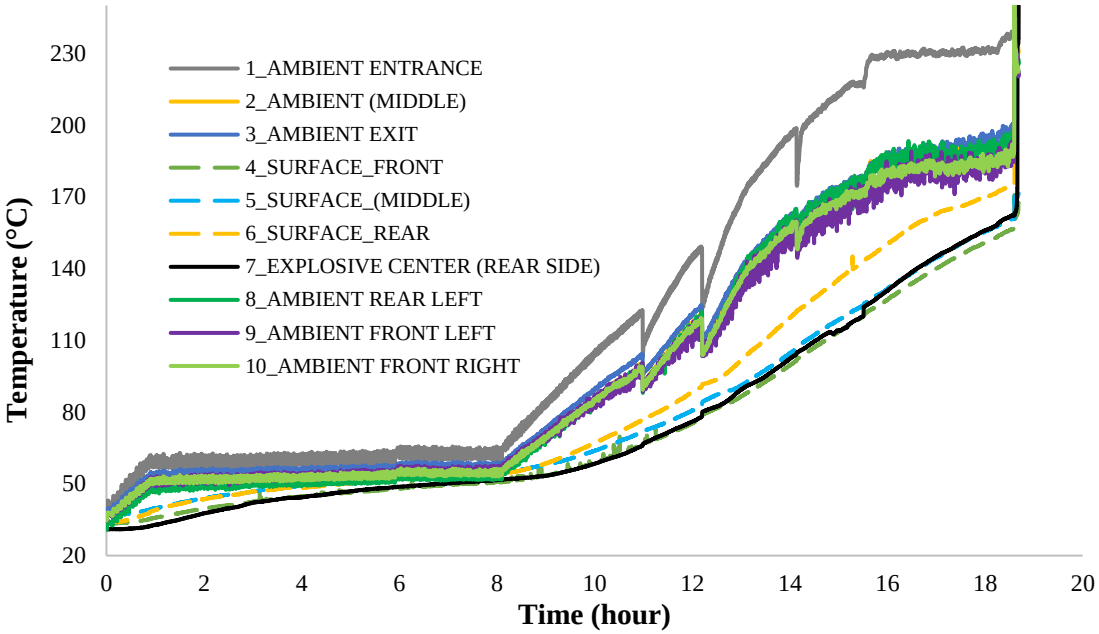

Figure 5.42. Raw Data for Large-Scale Heating Test

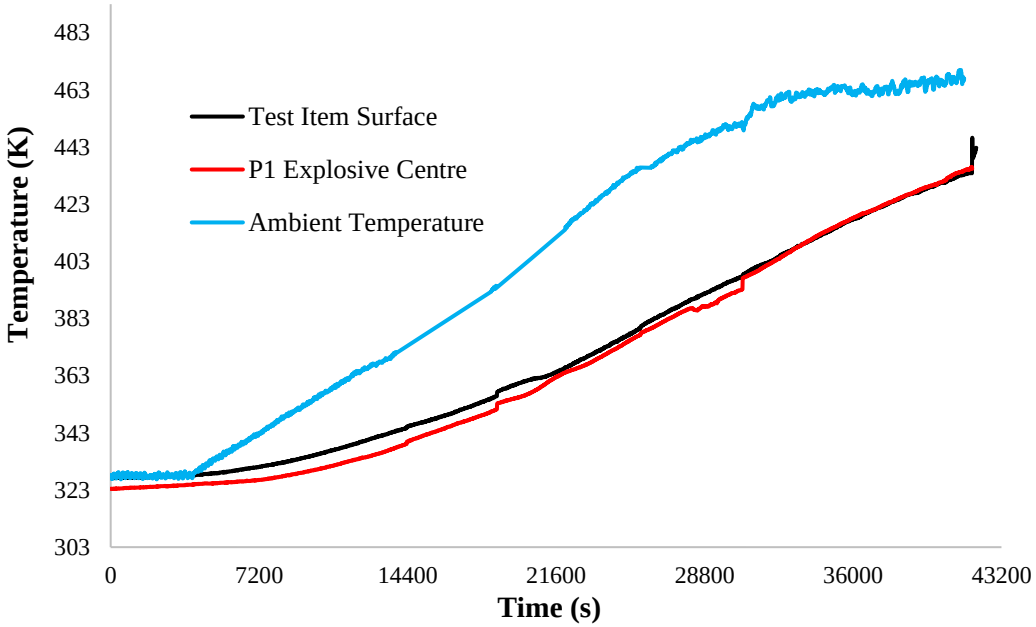

Figure 5.43. Progressed Data for Large-Scale Slow Heating Test

Sequence of incidents after the start of cook-off is summarized in Figure 5.44. Time stamps below the photographs state the instant from the first ignition observed at seconds. For instance, “392 second” indicates the time from the first ignition evidence observed at 41611st second. From Figure 5.44 it can be deduced that:

- At 41765th second, P1 explosive inside the test item started to burn slowly,
- For 392 seconds (between 41611st and 42003rd second), gray smoke had evicted from the chamber slowly due to slow burn of explosive,
- At 392nd (42003rd) second, an instant thrust due to pressure rise inside the munition led to a shattering of chamber at the rear side and more rapid burn of explosive that caused thrust at the rear of test item had been observed for 13 seconds until 405th second,
- At 405th (42016th) second due to elevated thrust at the rear of test item, another instant pressure rise led to shattering of test chamber completely and turned the test item by 90°,
- From 405th second to until 557th second (42016th to 42168th), test item burned with a rapid thrust at the rear (an instant of thrust is shown in Figure 5.44 at 496th second [42107th second]) which was observed for 152 seconds,
- From 557th second to until 591st second (42168th to 42202nd), thrust stopped but test item had burned slowly for 34 seconds.
- At the end of nearly 10 minutes of burning, test chamber was destroyed and all the energetic material (P1) explosive inside the test item was burnt rapidly that which led to a thrust that turned the munition by 90°.

41765th second

41911st second

392nd second (42003rd second)

405th second after first burn (42016th second)

496th second after first burn (42107th second) (Figure 5.44 continued)

591st second after first burn (42202nd second)

Figure 5.44. Response of Test Item during Large-Scale Slow Heating Test

Large scale slow heating test was performed with test item containing only P1 explosive and without the presence of igniter, P1 explosive burned rapidly in an uncontrollable manner that led to rapid thrust. Rapid thrust and numerous instants of pressure rise in test item destroyed the test chamber completely and more importantly caused the munition to turn by 90°. Fortunately, relatively high wall thickness (>20 mm) of the steel case of test item prevented an undesired explosion and limited the high pressure as rapid thrust. However, majority of the munitions used in industry are thin walled (8-12 mm) munitions that have higher explosive charge (80-450 kg instead of 20-25 kg), which leads to undesired explosion due to deflagration or detonation of energetic material. To eliminate uncontrolled burning and risk of detonation in test item, necessity of using igniter pellets were also shown in this test.

Ignition position and time in the large-scale slow heating test can be determined by considering the thermocouples positions after 150°C. To investigate ignition location, temperature distribution of the test item at the first "temperature rise" instant and at the "bulk ignition instant" that means the volumetric ignition of explosive is illustrated in Figure 5.45 and Figure 5.46, respectively. When P1 explosives temperature exceeds 165°C, it is known that thermal decomposition increases exponentially. At 41765th second thermocouple that is located at the rear

center of the explosive (#7) measured higher temperature values compared to surface of the munition. This shows that heat generation due to decomposition surpassed the heat transfer from munition case to P1 explosive. At this instant P1 explosive is on the edge of self-ignition. From Figure 5.45 it was understood that first temperature rise occurred at the rear air thermocouple (#8) at 41765th second (thermocouple locations are shown in Figure 3.8 in section 3.3.2). After two seconds, front air thermocouples (#9 and 10) detected temperature rise. Four seconds after that (at 41772nd second) middle air thermocouple (#2) records temperature increased. Finally, three seconds after that at 41775th second, thermocouple near exit port (#3) measured detected the temperature rise. It was concluded from the caption of the test videos and from Figure 5.44 that, gas pressure due to burnt products was discharged and hot combustion gas was dispersed in the chamber from rear left to front side in couple of seconds. Surface thermocouples recorded (#4-5-6) elevated temperatures shortly after (12 seconds after) the initial temperature rise at air thermocouples at 41777th second. Time lag on the order of 12 seconds can be considered as normal for surface thermocouples as these thermocouples were attached to the munition surface with paper tapes that leads led to time lag. From 41765th to 42002nd second, rear surface thermocouple (#6) on the munition rose to 41°C, while middle surface (#5) and front surface thermocouples temperatures (#4) increased to 9.1°C and 6.4°C, respectively. This observation implied that self-ignition started and propagated between middle and rear end section of the munition. Also, for the same duration, temperature rise of the P1 explosive thermocouple temperature (#7) at the center of the rear fuzewell was recorded as only 10.5°C. This implied that while burnt products were discharging from the rear inner wall heated the rear end surface of the munition (ΔT=41°C), heat transfer to the center of the fuzewell at the rear of the munition was not at this level and temperature rise was only 10.5°C. This observation suggested that ignition location between the middle section and the rear end section of the munition was not close to thermocouple that was located rear center of the munition at the fuzewell (#7).

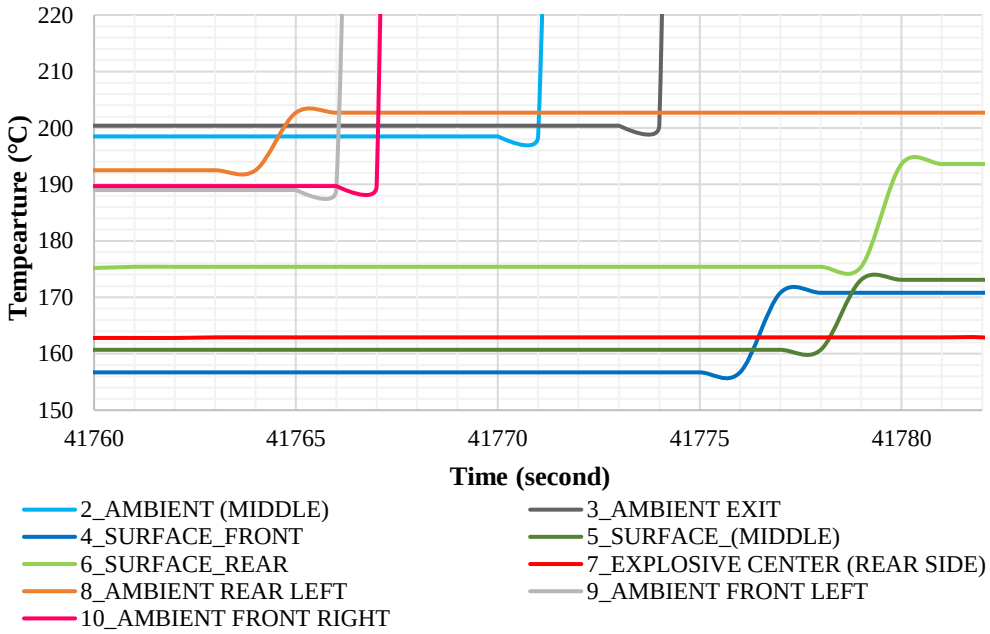

Figure 5.45. Temperature Data at the Instant of Ignition for Large-Scale Slow Heating Test (between 41760th - 41780th second)

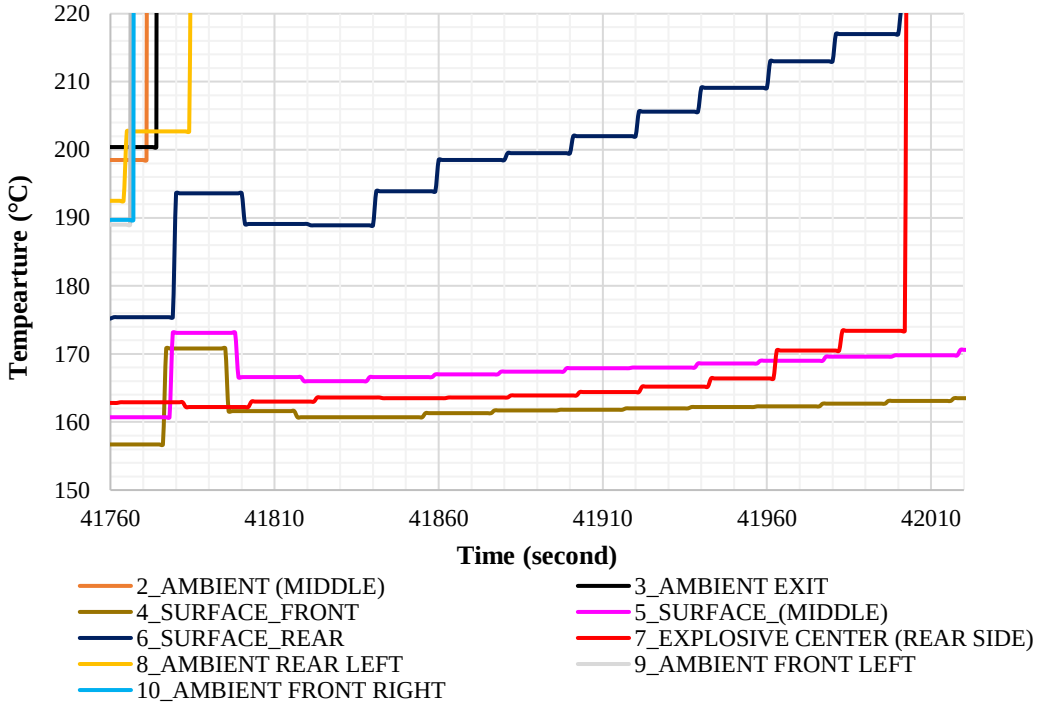

Figure 5.46. Temperature Data at the Bulk Self-Ignition of P1 Explosive for Large-Scale Slow Heating Test (between 41760th - 41780th second)

5.5 Large-Scale Slow Heating Simulation

Large-scale slow heating simulations were conducted with P1 explosive and large-scale penetrator warhead with 15°C/h heating rate. To determine the element size and time step for the simulations, a sensitivity analysis was initially performed with 4, 6 and 8 mm mesh size for 2, 10 and 60 seconds time steps. Details of the sensitivity analysis conducted for large-scale slow heating test set-up is given in section 4.3.2. In sensitivity analysis, 4 mm mesh size with 10 second time step led to least absolute error (3.0% temperature + 1.1% time=4.1%) at cook-off instant. However, 4 mm mesh size with 2 second time step is selected for final mesh and time step in order to solve the air flow inside chamber accurately during heating until cook-off although these parameters led to slightly higher absolute error (2.7% temperature + 2.2% time=4.9% compared to 4.1%) at cook-off instant. Figure 5.47 shows the simulation and experimental data comparison of the large-scale slow heating test.

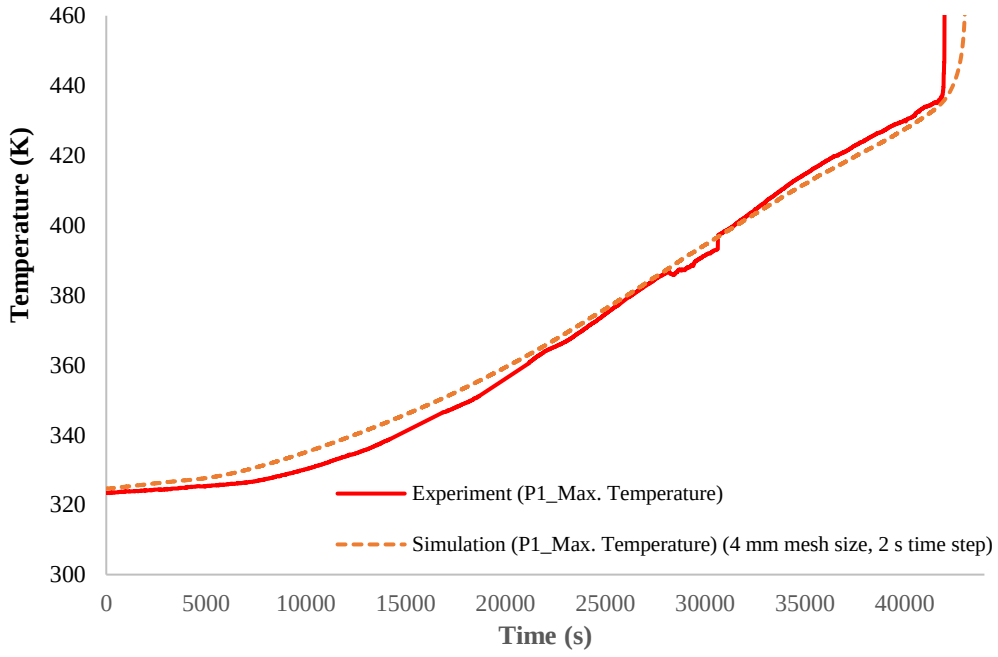

Figure 5.47. Ignition Point Investigation of Large-Scale Slow Heating Test (P1 Explosive-Without Igniter) (15°C/h heating rate)

The predicted temperature distribution and ignition point is given in Figure 5.48 Similar to experimental results, ignition point is located at the rear end of the test item as shown in Figure 5.48. Moreover, at ignition instant temperature distribution of the test item is illustrated in Figure 5.49 showing the ignition location. It was observed that at the ignition instant, temperature of the end of the munition case was greater than the nose of the munition case. This difference was valid from start of the analysis until the self-ignition of the P1 explosive. Although air entered the chamber below the nose of the munition, velocity of the air was quite high (≈1.5 m/s) for the heat transfer to the nose of the munition. Due to high air inlet velocity, more heat was transferred to the rear end of the munition compared to the nose of the munition.

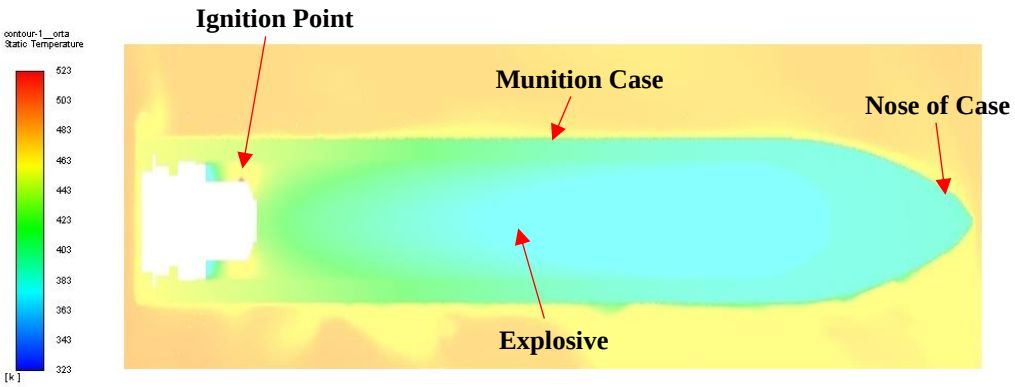

Figure 5.48. Temperature Contour of Large-Scale Slow Cook-Off Simulation at Ignition Instant (15°C/h heating rate) (Ignition Point)

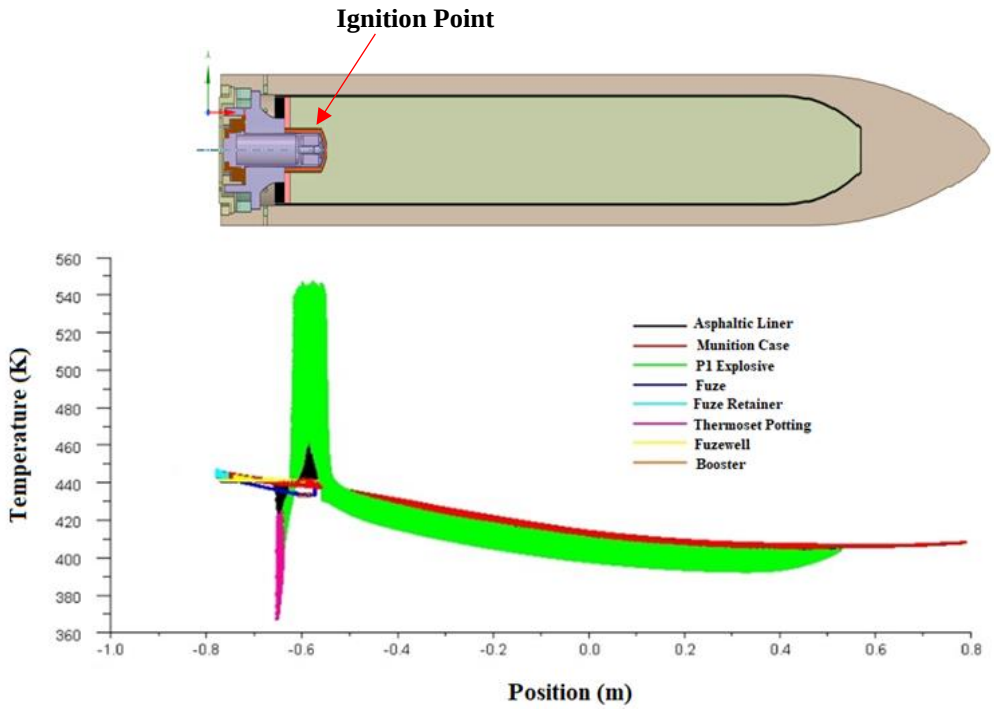

Figure 5.49. Temperature Distribution of Large-Scale Slow Cook-Off Simulation with respect to location at Ignition Instant (15°C/h heating rate) (Ignition Point)

To investigate the velocity profile in the test chamber, velocity contours were calculated from air inlet plane, middle plane, and air outlet plane of test chamber. Velocity profiles of these planes are illustrated with Figure 5.50. In addition, velocity distribution is shown with arrows in Figure 5.51. High velocity profile in air inlet is verified once again from Figure 5.50. Entering air (10 m/s) from inlet flows past the bottom surface of the test chamber (3 m/s) and discharges from outlet (10 m/s) by flowing around the rear end of the munition. Although deflector plates slowed down the air inlet, they were not fully effective for such a high inlet velocity. For the future work, it is intended to change the ventilator with a variable frequency ventilator that can produce the desired volumetric flow rate.

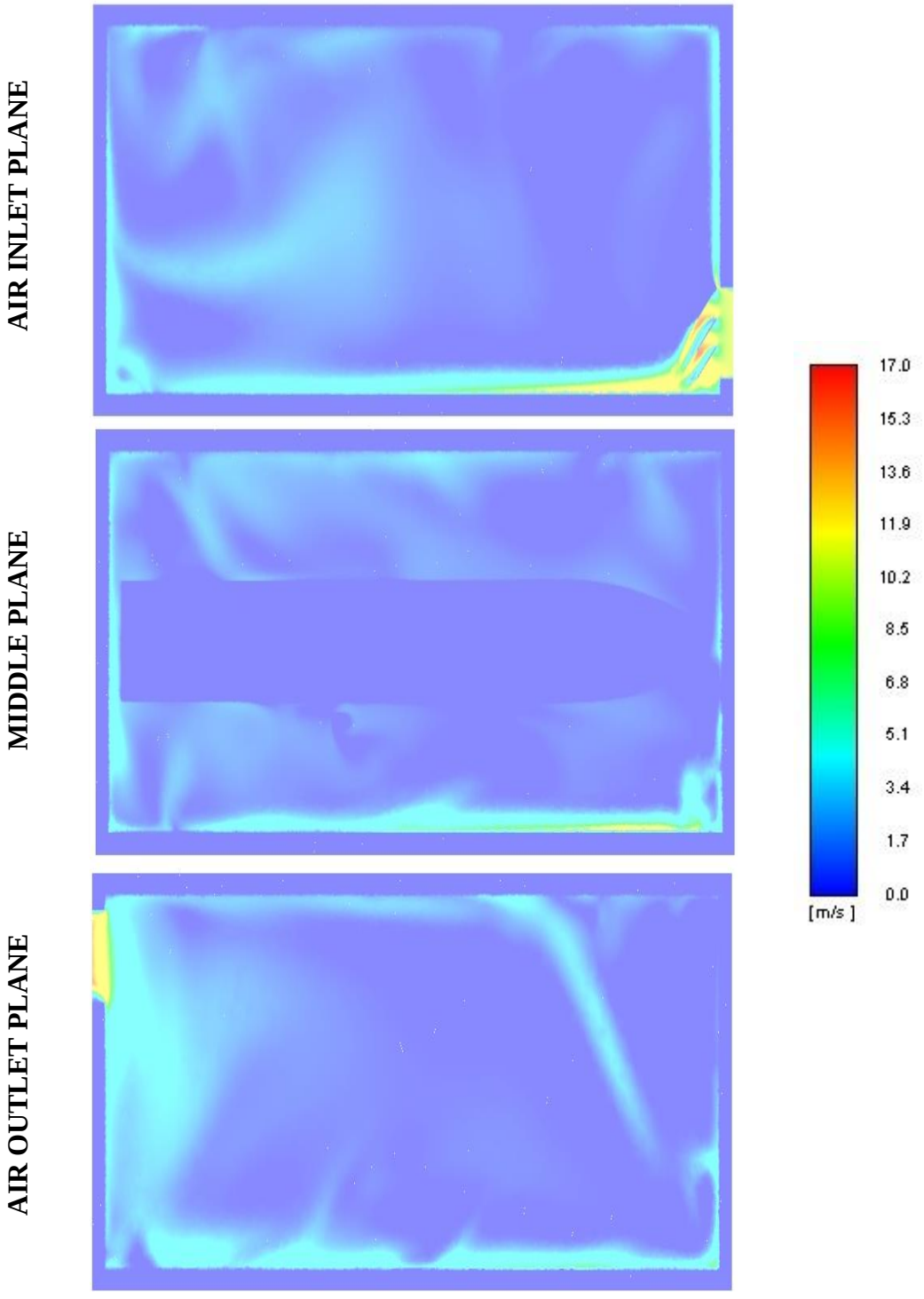

Figure 5.50. Velocity Contour of Large-Scale Slow Cook-Off Simulation (15°C/h heating rate)

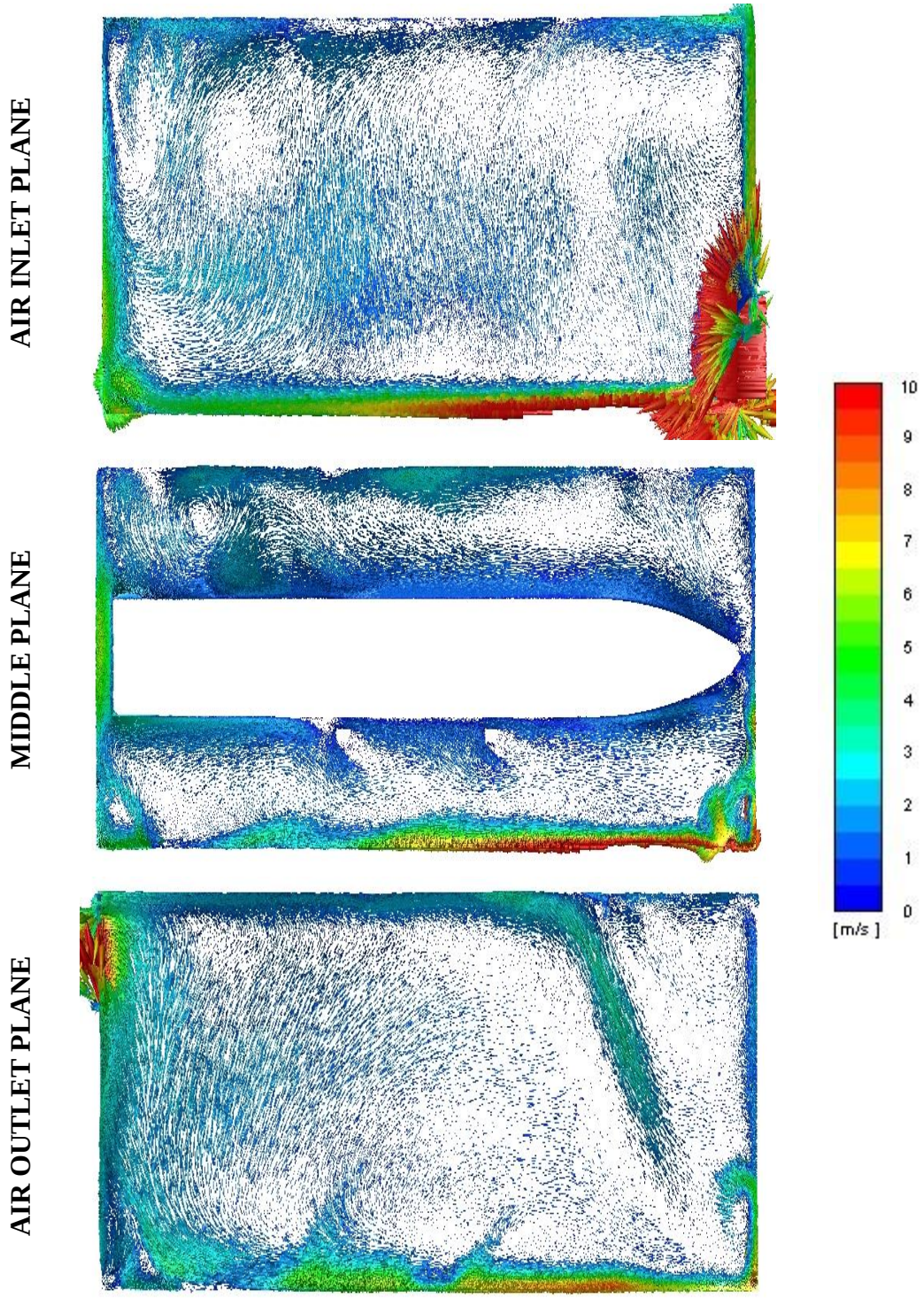

Figure 5.51. Velocity Distribution of Large-Scale Slow Cook-Off (15°C/h heating rate)

To improve the test chamber design and investigate the effect of uniform heat transfer along munition, another hypothetical simulation set-up was created only with munition geometry suppressing test chamber, air inside chamber, and test fixture. As there is not any valid correlation for determination of convective heat transfer coefficient available in literature for this geometry and Reynolds Number observed in test chamber, an average velocity of 0.55 m/s (average of velocity measurements using a Kestrel 4000 anemometer around test item in test chamber) was considered for forced convective heat transfer coefficient calculations. By trial and error convective heat transfer coefficient values of 6 to 10 W/m^2.K; 8 W/m^2.K corresponded the least error in terms of temperature profile as illustrated in Figure 5.52. By performing this hypothetical analysis, it was intended to find out the ignition location in the munition when uniform heat transfer was provided.

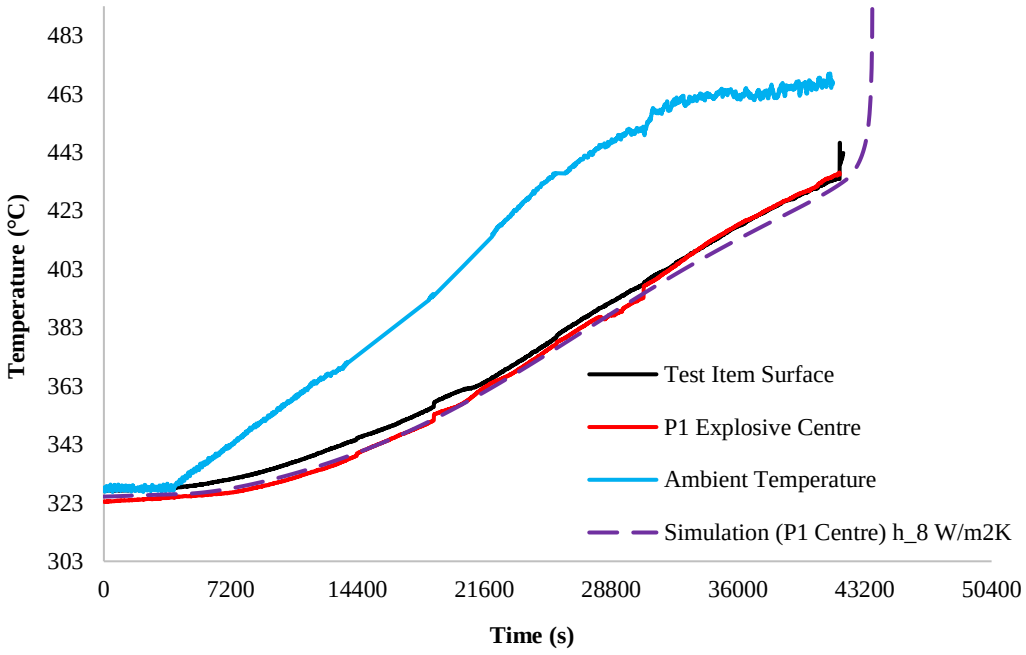

Figure 5.52. Hypothetical Simulation of Large-Scale Slow Cook-Off Simulation (P1 Explosive-Without Igniter) (15°C/h heating rate)

Relative ignition point and temperature distribution with respect to location in the munition at the instant of ignition are also shown in Figure 5.53 and Figure 5.54

respectively. From Figure 5.53 it can be inferred that when uniform heat transfer is provided in a hypothetical simulation, ignition would start from the front of the munition contrary to experiment which results in rear end initiation. Although uniform temperature distribution is desired in a slow heating test, uniform heat transfer also means that after the ignition starts from the front of explosive, burnt products would accumulate at the front of test item which would increase the pressure, temperature and in turn burn rate of the explosive. This would eventually lead to elevated temperature and pressure that could result in undesired deflagration or detonation. To prevent undesired response (deflagration or detonation) in slow heating tests; proposed use of igniter, which enables controlled burning of P1 explosive from the rear of the munition is validated once again from these results.

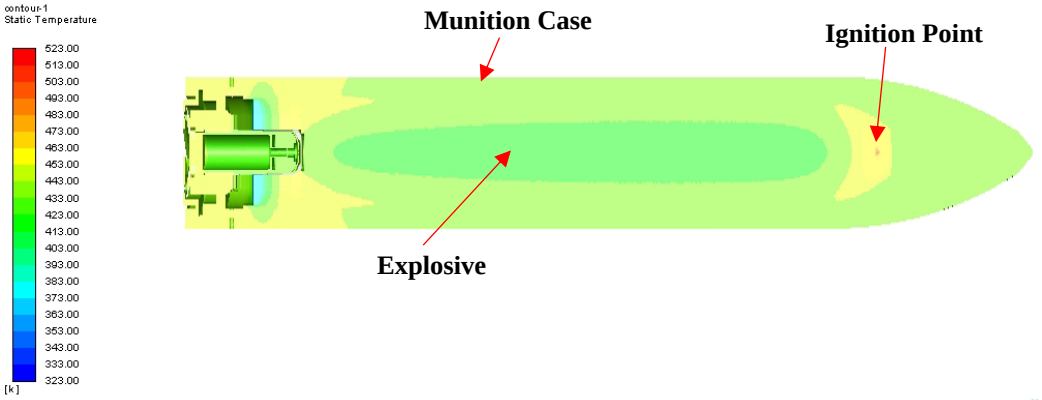

Figure 5.53. Ignition Point of Large-Scale Slow Cook-Off Simulation (P1 Explosive-Without Igniter) (15°C/h heating rate)

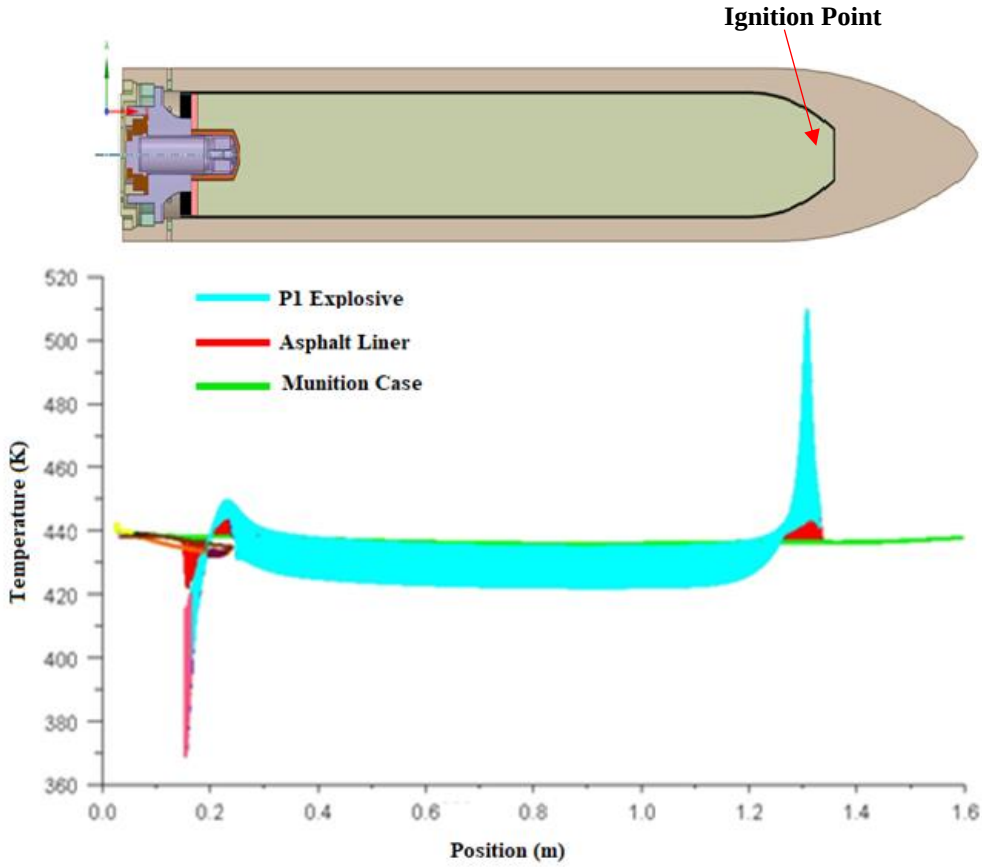

Figure 5.54. Temperature Distribution of Large-Scale Slow Cook-Off Simulation at Ignition Instant (P1 Explosive-Without Igniter) (15°C/h heating rate)

5.6 Comparison of Critical and Ignition Temperatures of Energetic Materials

Critical temperature is vital parameter for self-heating and slow cook-off studies because heat generation due to thermal decomposition rises exponentially after this temperature. Investigating and comparing critical temperature, autoignition temperature and self-ignition temperature in slow cook-off studies would facilitate understanding the decomposition studies of energetic materials. To compare critical temperature and self-ignition temperature, calculation approaches for thermal ignition of energetic materials was investigated from literature. Thermal ignition

theory was studied by Semenov and Frank-Kamenetskii considering uniform temperature distribution and temperature gradient on the surface and center of the energetic materials, respectively [50], [51]. As uniform temperature distribution in slow-heating test is not available, latter approach was employed in literature for ignition studies. To determine the self-ignition temperature, critical temperature (T_c) of the energetic materials should also be calculated. Critical temperature (T_c) is defined as the lowest constant surface temperature above which a given energetic material violently self-heats [57]. To calculate T_c, source term and heat diffusion equation can be expressed as Eq. 24 assuming zero order decomposition and constant thermophysical quantities [53].

$$\rho C_p \frac{\partial T}{\partial t} = \lambda \nabla^2 T + Q.A.e^{\frac{-E}{RT}} \qquad \text{Eq. 24}$$

Eq. 24 can be solved for spheres, infinite cylinders and slabs assuming steady state $\left(\frac{\partial T}{\partial t} = 0\right)$ to determine critical temperature [53], [57], [121], [122]. Critical temperature can be obtained by solving Eq. 25 by trial-error approach for different shapes. Shape factor (δ) is 0.88 for infinite slabs, 2.0 for infinite cylinders, 2.8 for L/D=1 cylinders and 3.32 for spheres [53], [57], [121], [122].

$$T_C = \frac{E_A}{Rln\left(\frac{r^2 \rho Q A E_A}{T_c^2 \lambda \delta R}\right)} \qquad \text{Eq. 25}$$

Autoignition temperature was measured for 0.2 g specimens by 5°C/min heating rate for open air above which ignition was observed (Table 5.9). Critical temperature was calculated from thermal decomposition parameters for different shapes using Eq. 25. Ignition temperature was measured and calculated during small and large-scale slow heating tests and simulations (section 5.2 to 5.5). Comparison of these temperatures are shown in Table 5.16. It is expected that when an energetic material is heated firstly critical temperature is reached (row 2 in table), then ignition (cook-off)

temperature is reached (row 3 in table) (since it is measured in confined test set-up) and finally auto-ignition temperature is reached (row 1 in table) (since it is measured in unconfined method in ambient conditions). For each explosive type shown in Table 5.16 this assumption was validated.

Table 5.16 Autoignition, Critical and Ignition Temperature of Studied Energetic Materials

#	Temperature	Igniter	P1	P2	P3	P4
1	**Autoignition Temperature**	169.1	209.3	237.8	239.1	213.4
2	**Critical Temperature (*)**	127.8	165.2	201.5	198.7	186.2
3	**Ignition (Cook-Off) Temperature @ Slow-Heating Test (**)**	146.9	179.6	203.3	210.2	198.9

(*) Calculated by using Eq. 25 considering L/D=1 for 17.1 mm radius of small-scale test item,

(**) Experimental Result measured for 15°C/h heating rate for 17.1 mm radius of small-scale test item.

As T_C is shape and radius dependent, it was calculated for each explosive type with respect to temperature for L/D=1 cylinder in Figure 5.55. For instance, critical temperature of small-scale-test item (radius 17.1 mm) that contains P1 explosive was calculated as 165.2 °C. Whereas it was calculated as 138.3°C for large-scale-test item (radius approximately 100 mm) that contains P1 explosive. In literature it was reported that critical temperature of a 225 mm diameter munition should be at least 82°C [57]. This shows that all the explosive compositions shown in Figure 5.55 can be safely used in these munitions. Moreover, even though igniter is only used at the rear of the munitions with much smaller diameters, its critical temperature is at safe levels.

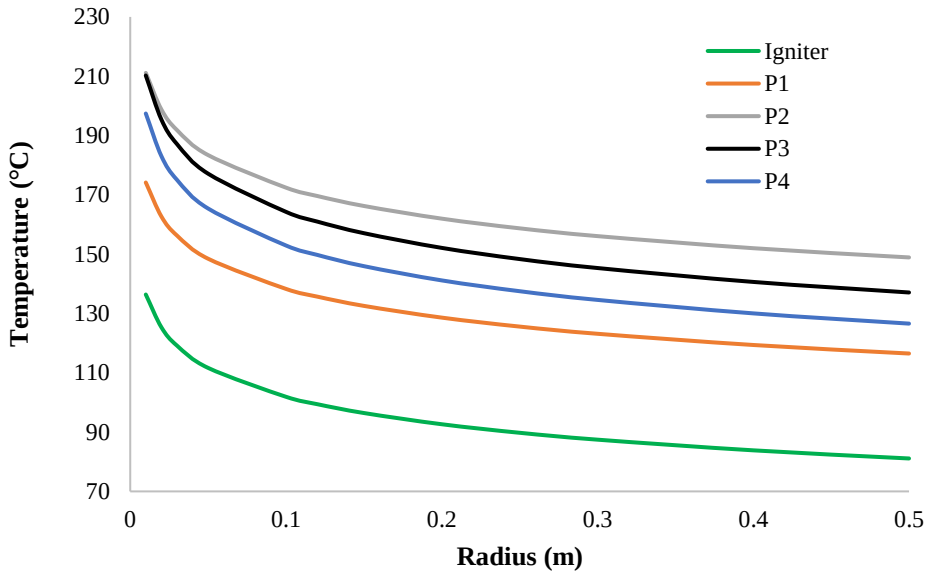

Figure 5.55. Critical Temperature Relation of Studied Energetic Material with respect to Radius

CHAPTER 6

CONCLUSIONS AND FUTURE WORK

6.1 Conclusions

Self-ignition behavior of four castable polymer bonded explosive formulations (P1: optimum blast and heat effect, P2: high blast for fragment and shaped charge, P3: enhanced blast for closed and confined volumes, P4: oxygen rich composition for underwater applications) due to thermal decomposition in slow heating test was successfully determined and simulated in this study. Firstly, an igniter composition based on pentaerythritol tetranitrate (PETN) that has a predetermined critical temperature was developed to burn munitions systems that consist of explosives from P1 to P4 in a controlled manner before undesired deflagration or detonation. Then a small-scale heating chamber was designed according to slow heating test standard requirements to determine the ignition temperature and ignition time of the test items for different heating rates) in forced convection conditions. 30 small-scale slow heating tests were performed in forced configuration conditions for 15 different configurations (5 formulations [igniter and P1 to P4]*3 heating rates [5, 15, 25°C/h]).

Ignition temperature, ignition time, ignition location and repeatability of the tests were investigated in small-scale tests. Small-scale tests showed that igniter cook-off temperature is at least 30-60°C (142.5-153.6°C) lower than the explosive formulations and igniter can be used for burning of explosives from P1 to P4 in slow heating tests. For explosive formulations from P1 to P4, cook-off temperature was measured between 174.8-217.2°C with maximum 1.7% temperature error and 1.7% time error at cook-off instant. In addition to this, it was shown that replicate tests could be performed with designed small-scale heating chamber with only 0.4-2.1°C temperature variance between start of the heating and cook-off instant. Effect of heating rate was also investigated and for igniter, P1 and P2 explosive formulations

that contained more energetic material (64-87% by weight), cook-off temperature was found to rose with increasing heating rate similar to literature because of higher heat generation due to thermal decomposition in explosive formulations to heat dissipation ratio. For the explosive formulations of P3 and P4 that contained relatively less energetic material (20-45% by weight) cook-off temperature was found to decrease with increasing heating rate due to low heat generation to heat dissipation ratio.

Validation of slow heating experiments were performed by cook-off simulation studies by ANSYS Fluent software for both slow and large-scale test set-ups. Slow heating simulations were conducted with convective heat transfer around the test item as boundary condition for different heating rates and led to only 2.6±1.5% temperature and 2.7±1.6% time error for igniter coupled with P1 explosive at cook-off instant. Temperature and time errors for bare explosives P1 to P4 (without igniter) were calculated as 3.1±2.1% and 5.6±3.8% respectively at cook-off instant.

Large-scale slow heating tests with full-scale munition (penetrator warhead) that contained only P1 explosive led to 173.4 °C ignition temperature and 41781 second ignition time. Validation of the large-scale test with numerical simulation was conducted considering axial asymmetric air flow in test chamber and around munition. Numerical simulation resulted in only 2.7% temperature and 2.1% time error as well as correct ignition location in munition.

Relatively low error values encountered in small and large-scale simulations resulted from the correct prediction of source term (heat generation due to thermal decomposition) and thermal decomposition parameters (activation energy, pre-exponential factor, decomposition enthalpy) of igniter and explosives by non-isothermal thermogravimetric analysis and differential scanning calorimetry. It was shown that model-based and model-free (isoconversional) methods (F/W/O or

K/A/S models) predicted the thermal decomposition kinetics of studied igniter and explosive formulations accurately.

As a result of this study, starting from small-scale test items and simulations, slow-cook-off phenomena of self-igniting energetic materials have been tested and verified for large-scale munitions which enhances the ability of designing insensitive munitions against slow cook-off threat and predict munition response in terms of temperature profile, ignition time and ignition location as well as reducing the test risks and costs for developed munitions at TUBITAK SAGE and defense industry.

6.2 Future Work

Using small-scale test set-up along with non-isothermal TGA studies, slow cook-off characteristic of other energetic materials such as pyrotechnics, composite and/or double base propellants can be determined and simulated as a future work. Moreover, with new TGA data sets, thermal decomposition of P4 explosive can be verified from literature for further comparison. The following studies are intended to be carried out in the future with the knowledge and expertise gained in this study:

- By using the successful models developed in this study, slow cook off behavior of other munitions and missile systems containing these energetic materials can be determined without further costly large-scale testing.

- By implementing developed igniter composition in this study to stockpiled munitions systems, slow cook off behavior of those items can be controlled and test response can be shifted to insensitive direction that would diminish the accident risks considerably even if those items were not designed as insensitive in development phase decades ago.

- Test chamber design for the large-scale slow heating test can be improved by variable frequency ventilator to provide uniform heat transfer to the test munition.

- Simulations can be extended after ignition phase by implementing multiphysics software that would simulate heat transfer and combustion reactions for propellants and explosives to calculate pressure in munitions and missile system in slow heating (cook-off) tests if complex heterogeneous reactions of propellants and explosives after ignition can be modeled in detail.

REFERENCES

[1] K. J. Graham, “Insensitive Munitions-Industry Problems and Solutions, NATO STO-EN-AVT-214,” 2013.

[2] K. J. Graham, “Insensitive Munitions-US Problems and Solutions, Insensitive Munitions Technology and its Application, NATO STO-EN-AVT-214,” 2013.

[3] NATO Standardization Office, “AOP-39: POLICY FOR INTRODUCTION AND ASSESSMENT OF INSENSITIVE MUNITIONS (IM),” 2018.

[4] NATO Standardization Office, “AOP 4382, SLOW HEATING TEST PROCEDURES FOR MUNITIONS,” 2020.

[5] NATO Standardization Office, “AOP 4240, FAST HEATING MUNITION TEST PROCEDURES,” 2018.

[6] NATO Standardization Office, “AOP 4241, BULLET IMPACT MUNITION TEST PROCEDURES,” 2018.

[7] NATO Standardization Office, “AOP 4396, SYMPATHETIC REACTION TEST PROCEDURES FOR MUNITIONS,” 2020.

[8] NATO Standardization Office, “AOP 4496, FRAGMENT IMPACT TEST PROCEDURES FOR MUNITIONS,” 2019.

[9] NATO Standardization Office, “AOP 4526, SHAPED CHARGE JET MUNITION TEST PROCEDURES,” 2018.

[10] W. P. W. Jonas A. Zukas, *Explosive Effects and Applications*. New York, NY: Springer New York, 1998.

[11] NATO Standardization Agency, “STANAG 4439 Edition 3 Policy for Introduction and Assessment of Insensitive Munitions (IM),” 2010.

[12] United Nations, “ADR, Agreement concerning the International Carriage of Dangerous Goods by Road Vol 2,” 2021.

[13] “Accident Photographs from Carious US Aircraft Carriers from 1960s, USS Forrestal.” [Online]. Available: http://www.insensitivemunitions.org/history/the-uss-forrestal-cva-59-fire-and-munition-explosions/. [Accessed: 19-Dec-2020].

[14] “Accident Photographs from Carious US Aircraft Carriers from 1960s, USS Enterprise.” [Online]. Available: http://www.insensitivemunitions.org/history/the-uss-enterprise-cvan-65-fire-and-munition-explosions/. [Accessed: 19-Dec-2020].

[15] “Accident Photographs of Conventional TNT Casting Facility in Kırıkkale, 1997.” [Online]. Available: https://www.anadoluimages.com/p/kirikkalede-patlama/43879. [Accessed: 19-Dec-2020].

[16] M. J. Kaneshige, A. M. Renlund, R. G. Schmitt, and W. W. Erikson, “Cook-

Off experiments for model validation at Sandia National Laboratories," *Albuquerque, NM*, vol. 87185, p. 10, 2002, doi: 10.1.1.566.214.

[17] P. P. C. Dubuis, "Multiphysics Modelling of Variable Confinement Cook-off Test (VCCT)," in *Insensitive Munitions & Energetic Materials Technology Symposium (IMEMTS)*, 2013.

[18] H. W. Sandusky and G. P. Chambers, "Instrumentation of Slow Cook-Off Events," in *AIP Conference Proceedings*, 2002.

[19] K. Alexander, K. Gibson, and B. Baudler, "Development of the Variable Confinement Cook-Off Test," 1996.

[20] J. J. Yoh, M. A. Mcclelland, J. L. Maienschein, L. Nichols, and J. F. Wardell, "Towards An Ideal Slow Cookoff Model For PBXN-109," in *JANNAF Conference*, 2003.

[21] A. B. Dodd and M. J. Kaneshige, "Cook-off model development and analysis of energetic materials using Sandia instrumented thermal ignition (SITI) experimental data," in *13th International Detonation Symposium, Norfolk, VA*, 2006.

[22] E. L. Baker *et al.*, "Warhead Venting Technology Development for Cook-off Mitigation," in *Insensitive Munitions & Energetic Materials Technology Symposium (IMEMTS)*, 2006.

[23] H. F. Hayden, E. A. Lustig, and B. G. Lawrence, "Development of a Small-Scale SCO test protocol for granular gun propellants," in *Insensitive Munitions & Energetic Materials Technology Symposium (IMEMTS)*, 2015.

[24] M. Graswald, R. Gutser, and M. Schweizer, "Extended multi-physics model for slow-cook off events of warheads," in *Insensitive Munitions & Energetic Materials Technology Symposium (IMEMTS)*, 2019.

[25] M. GRASWALD, "Modeling of Thermal Reactions and Associated Events," in *30th International Symposium on Ballistics*, 2017, doi: 10.12783/ballistics2017/16954.

[26] D. J. Pudlak and K. Miers, "Structural Analysis of Commonly Used Materials for Slow Heating Ovens (per AOP-4382) and Their Effects on the Projection of Hazardous Debris," in *Insensitive Munitions & Energetic Materials Technology Symposium (IMEMTS)*, 2019.

[27] E. Baker and D. Hubble, "Slow Heating Test Thermal Equilibrium and Maximum Reaction Temperature," in *Insensitive Munitions & Energetic Materials Technology Symposium (IMEMTS)*, 2019.

[28] D. Hubble, "Analysis of the Ramifications of Increasing the Slow Cook-off Test Heating Rate," in *Insensitive Munitions & Energetic Materials Technology Symposium (IMEMTS)*, 2019.

[29] S. Arrhenius, "Über die Dissociationswärme und den Einfluss der Temperatur auf den Dissociationsgrad der Elektrolyte," *Zeitschrift für Phys. Chemie*, vol.

4U, no. 1, pp. 96–116, Jul. 1889, doi: 10.1515/zpch-1889-0408.

[30] H. E. Kissinger, “Reaction Kinetics in Differential Thermal Analysis,” *Anal. Chem.*, vol. 29, no. 11, pp. 1702–1706, 1957, doi: 10.1021/ac60131a045.

[31] H. L. Friedman, “Kinetics of thermal degradation of char-forming plastics from thermogravimetry. Application to a phenolic plastic,” *J. Polym. Sci. Part C Polym. Symp.*, vol. 6, no. 1, pp. 183–195, Mar. 1964, doi: 10.1002/polc.5070060121.

[32] ASTM International, “ASTM E698-18 Standard Test Method for Arrhenius Kinetic Constants for Thermally Unstable Materials Using Differential Scanning Calorimetry and the Flynn / Wall / Ozawa Method,” 2012.

[33] S. Vyazovkin, A. K. Burnham, J. M. Criado, L. A. Pérez-Maqueda, C. Popescu, and N. Sbirrazzuoli, “ICTAC Kinetics Committee recommendations for performing kinetic computations on thermal analysis data,” *Thermochim. Acta*, vol. 520, no. 1–2, pp. 1–19, 2011, doi: 10.1016/j.tca.2011.03.034.

[34] S. Vyazovkin *et al.*, “ICTAC Kinetics Committee recommendations for analysis of multi-step kinetics,” *Thermochim. Acta*, vol. 689, no. May, p. 178597, 2020, doi: 10.1016/j.tca.2020.178597.

[35] E. Moukhina, “Comparison of isothermal predictions based on model-free and model-based kinetic methods,” *J. Test. Eval.*, vol. 42, no. 6, pp. 1–10, 2014, doi: 10.1520/JTE20140145.

[36] NATO Standardization Office, “STANAG 4515 Explosives: Thermal Analysis Using Differential Thermal Analysis (DTA), Differential Scanning Calorimetry (DSC), Heat Flow Calorimetry (HFC) and Thermogravimetric Analysis (TGA) (Edition 2),” 2015.

[37] ASTM International, “ASTM E1641 - 12 Standard Test Method for Decomposition Kinetics by Thermogravimetry,” 2012.

[38] R. R. McGuire and C. M. Tarver, “Chemical-decomposition models for the thermal explosion of confined HMX, TATB, RDX, and TNT explosives,” in *7th Symposium on Detonation*, 1981.

[39] A. Singh, T. C. Sharma, M. Kumar, J. K. Narang, P. Kishore, and A. Srivastava, “Thermal decomposition and kinetics of plastic bonded explosives based on mixture of HMX and TATB with polymer matrices,” *Def. Technol.*, vol. 13, no. 1, pp. 22–32, 2017, doi: 10.1016/j.dt.2016.11.005.

[40] J. S. Lee, C. K. Hsu, and C. L. Chang, “A study on the thermal decomposition behaviors of PETN, RDX, HNS and HMX,” *Thermochim. Acta*, vol. 392, no. 393, pp. 173–176, 2002, doi: 10.1016/S0040-6031(02)00099-0.

[41] C. M. Tarver and T. D. Tran, “Thermal decomposition models for HMX-based plastic bonded explosives,” *Combust. Flame*, vol. 137, no. 1–2, pp. 50–62, Apr. 2004, doi: 10.1016/j.combustflame.2004.01.002.

[42] C. M. Tarver, T. D. Tran, and R. E. Whipple, “Thermal Decomposition of

Pentaerythritol Tetranitrate," *Propellants, Explos. Pyrotech.*, vol. 28, no. 4, pp. 189–193, Aug. 2003, doi: https://doi.org/10.1002/prep.200300004.

[43] C. M. Tarver and J. G. Koerner, "Effects of endothermic binders on times to explosion of HMX- and TATB-based plastic bonded explosives," *J. Energ. Mater.*, vol. 26, no. 1, pp. 1–28, 2008, doi: 10.1080/07370650701719170.

[44] J. F. Wardell and J. L. Maienschein, "The scaled thermal explosion experiment," *Proc. 12th Int. Symp. Detonation, San Diego, CA, Aug 11-16, 2002*, p. 384, 2002.

[45] J. L. Maienschein *et al.*, "Thermal Explosion Violence for Several Explosives—Measurements and Interpretation," in *Proceedings of the Thirteenth International Symposium on Detonation*, 2006.

[46] A. P. Wemhoff, A. K. Burnham, A. L. Nichols, and J. Knap, "Calibration methods for the extended prout-tompkins chemical kinetics model and derived cookoff parameters for RDX, HMX, LX-10 and PBXN-109," in *2007 Proceedings of the ASME/JSME Thermal Engineering Summer Heat Transfer Conference - HT 2007*, 2007, vol. 3, pp. 625–632, doi: 10.1115/HT2007-32279.

[47] A. K. Burnham, R. K. Weese, A. P. Wemhoff, and J. L. Maienschein, "A historical and current perspective on predicting thermal cookoff behavior," *J. Therm. Anal. Calorim.*, vol. 89, no. 2, pp. 407–415, 2007, doi: 10.1007/s10973-006-8161-6.

[48] Q.-L. Yan, S. Zeman, P. E. Sánchez Jiménez, F.-Q. Zhao, L. A. Pérez-Maqueda, and J. Málek, "The effect of polymer matrices on the thermal hazard properties of RDX-based PBXs by using model-free and combined kinetic analysis," *J. Hazard. Mater.*, vol. 271, pp. 185–195, Apr. 2014, doi: 10.1016/j.jhazmat.2014.02.019.

[49] J. J. Yoh, M. A. McClelland, J. L. Maienschein, J. F. Wardell, and C. M. Tarver, "Simulating thermal explosion of cyclotrimethylenetrinitramine-based explosives: Model comparison with experiment," *J. Appl. Phys.*, vol. 97, no. 8, 2005, doi: 10.1063/1.1863429.

[50] N. N. Semenov, "The calculation of critical temperatures of thermal explosion," *Z Phys Chem*, vol. 48, p. 571, 1928.

[51] D. A. Frank-Kamenetskii, "Calculation of thermal explosion limits," *Acta. Phys.-Chim USSR*, vol. 10, p. 365, 1939.

[52] P. Gray and M. J. Harper, "Thermal explosions. Part 1.—Induction periods and temperature changes before spontaneous ignition," *Trans. Faraday Soc.*, vol. 55, pp. 581–590, 1959, doi: 10.1039/TF9595500581.

[53] J. Zinn and C. L. Mader, "Thermal initiation of explosives," *J. Appl. Phys.*, vol. 31, no. 2, pp. 323–328, 1960, doi: 10.1063/1.1735565.

[54] T. Boddington, P. Gray, and G. C. Wake, "Criteria for Thermal Explosions With and Without Reactant Consumption.," *Proc R Soc London Ser A*, vol.

357, no. 1691, pp. 403–422, 1977, doi: 10.1098/rspa.1977.0176.

[55] A. G. Merzhanov and V. G. Abramov, “Thermal Explosion of Explosives and Propellants. A review,” *Propellants, Explos. Pyrotech.*, vol. 6, no. 5, pp. 130–148, 1981, doi: 10.1002/prep.19810060504.

[56] J. M. Pickard, “Critical Ignition Temperature,” *Thermochim. Acta*, vol. 392–393, pp. 37–40, Sep. 2002, doi: 10.1016/S0040-6031(02)00068-0.

[57] US Department of Defense, “MIL-STD-1751A Test Method Standard Safety and Performance Tests for The Qualification of Explosives (High Explosives, Propellants , and Pyrotechnics),” 2001.

[58] D. O. Asante, S. Kim, J. Chae, H. Kim, and M. Oh, “CFD Cook-Off Simulation and Thermal Decomposition of Confined High Energetic Material,” *Propellants, Explos. Pyrotech.*, vol. 40, no. 5, pp. 699–705, 2015, doi: 10.1002/prep.201400296.

[59] E. Aydemir, “Study of Ignition Characteristics of a Plastic Bonded Explosive,” Middle East Technical University, 2008.

[60] H. Sahin, “Investigation of a Generic Warhead Containing Plastic Bonded Explosive under Liquid Fuel Fire by Numerical and Test Methods,” Middle East Technical University, 2015.

[61] M. Graswald and R. Gutser, “Thermal modeling of fast cook-offs,” in *Insensitive Munitions & Energetic Materials Technology Symposium*, 2018.

[62] M. A. McClelland, J. L. Maienschein, A. L. Nichols, J. F. Wardell, A. I. Atwood, and P. O. Curran, “ALE3D model predictions and materials characterization for the cookoff response of PBXN-109,” in *20th JANNAF Propulsion Systems Hazards Subcommittee Meeting, 2002, Volume 1*, 2002, vol. 714, no. 20th JANNAF Propuls. Syst. Hazards Subcomm. Meet. 2002, Vol. 1, pp. 221–235.

[63] E. B. N. Al-Shehab, “Modeling Methodology for Predicting SCO Performance of the Excalibur Warhead,” in *Insensitive Munitions & Energetic Materials Technology Symposium (IMEMTS)*, 2009.

[64] N. Al-Shehab, D. Pfau, E. L. Baker, and A. Daniels, “Venting of Anti-Armor Warheads to Mitigate Cook-Off Threats,” in *Insensitive Munitions & Energetic Materials Technology Symposium (IMEMTS)*, 2010.

[65] E. Aydemir and A. Ulas, “A numerical study on the thermal initiation of a confined explosive in 2-D geometry,” *J. Hazard. Mater.*, vol. 186, no. 1, pp. 396–400, Feb. 2011, doi: 10.1016/j.jhazmat.2010.11.015.

[66] C. A. Anderson, “TEPLO: A Heat Conduction Code for Studying Thermal Explosions in Lamibar Composites,” 1970.

[67] D. L. Popolato, A; Ruminer, J J; Vigil, A S; Kernodle, N K; Jaeger, “Thermal response of explosives subjected to external heating. [TNT, Comp. B, HMX, TATB, DATB, and NQ],” 1979.

[68] A. C. Victor, “Simple Calculation Methods for Munitions Cookoff times and temperatures,” *Propellants, Explos. Pyrotech.*, vol. 20, no. 5, pp. 252–259, Oct. 1995, doi: 10.1002/prep.19950200506.

[69] M. Sućeska, “A computer program based on finite difference method for studying thermal initiation of explosives,” *J. Therm. Anal. Calorim.*, vol. 68, no. 3, pp. 865–875, 2002, doi: 10.1023/A:1016178119729.

[70] Y. Kim, J. J. Yoh, and J. Park, “Isoconversional Method for Extracting Reaction Kinetics of Aluminized Cyclotrimethylene-Trinitramine for Propulsion,” *J. Propuls. Power*, vol. 32, no. 3, pp. 777–784, 2016, doi: 10.2514/1.B35885.

[71] D. D. – Y. G. – B. B. – P. B. – D. Houdusse, “Numerical Simulation of Reaction Violence To Cook-Off Experiments,” in *Advances in Rocket Performance Life and Disposal Meeting NATO RTO-MP-091*, 2002.

[72] S. Defisher *et al.*, “Background Focus Venting Concept Testing Experimental Results Modeling Conclusions,” in *Insensitive Munitions & Energetic Materials Technology Symposium (IMEMTS)*, 2007.

[73] R. G. Fernando Echeverría, Pablo Bernárdez, “Use of CFD Modelling in The Design of an IM Warhead to Cook-Off Stimuli,” in *Insensitive Munitions & Energetic Materials Technology Symposium*, 2015.

[74] P. Gillard and B. Longuet, “Investigation of heat transfer and heterogeneous reactions during the slow cook off of a composite propellant,” *J. Loss Prev. Process Ind.*, vol. 26, no. 6, pp. 1506–1514, 2013, doi: 10.1016/j.jlp.2013.09.005.

[75] N. Al-Shehab and E. L. Baker, “Thermal Modeling the SCO Response of a TOW2B EFP,” in *Insensitive Munitions & Energetic Materials Technology Symposium (IMEMTS)*, 2015.

[76] W. H. M. Amos J. Diede, “US5466537A Intermetallic thermal sensor,” 1995.

[77] A. Elements, “Bismuth Tin Alloy Bi-40% Sn-60% Product Data Sheet,” 2019. [Online]. Available: https://www.americanelements.com/bismuth-tin-alloy-12010-55-8.

[78] M. Gill, I. Avnon, Y. Katz, and T. Yarom, “US5786544A Warhead Protection Device During Slow Cook-Off Test,” 5,786,544, 1998.

[79] M. Gill and I. Avnon, “US5813219A Rocket Motor Protection Device During Slow Cook-off Test,” 1998.

[80] A. Bonnel, D. Houdusse, B. Nouguez, and A. Tinet, “US6615737B2 Safety Igniter for a Pyrotechnic Munition Component Capable of Being Subjected to Slow Cook Off,” US 6,615,737 B2, 2003.

[81] Y. Guengant, M. Rat, and B. Mahe, “Munitions Vulnerability,” in *Insensitive Munitions & Energetic Materials Technology Symposium (IMEMTS)*, 2006.

[82] B. Nouguez, B. Mahé, and P. O. Vignaud, “Cast PBX related technologies for

im shells and warheads," *Sci. Technol. Energ. Mater.*, vol. 70, no. 5–6, pp. 135–139, 2009.

[83] R.Fougeyollas, D.Courrillaud, L.Chaffois, and P. Chabin, "Heavyweight Torpedo warhead IM assessment," in *Insensitive Munitions & Energetic Materials Technology Symposium (IMEMTS)*, 2018.

[84] S. W. Churchill and M. Bernstein, "A correlating equation for forced convection from gases and liquids to a circular cylinder in crossflow," *J. Heat Transfer*, vol. 99, no. 2, pp. 300–306, 1977, doi: 10.1115/1.3450685.

[85] F. P. Incropera, D. P. DeWitt, and others, *Fundamentals of Heat and Mass Transfer*, vol. 3. John Wiley & Sons, Inc, 1990.

[86] A. Žukauskas, "Heat Transfer from Tubes in Crossflow," in *International Communications in Heat and Mass Transfer*, vol. 19, no. 6, 1972, pp. 93–160.

[87] R. Hilpert, "Wärmeabgabe von geheizten Drähten und Rohren im Luftstrom," *Forsch. auf dem Gebiete des Ingenieurwesens*, vol. 4, no. 5, pp. 215–224, 1933, doi: 10.1007/BF02719754.

[88] R. A. Seban and R. Bond, "Skin-Friction and Heat-Transfer Characteristics of a Laminar Boundary Layer on a Cylinder in Axial Incompressible Flow," *J. Aeronaut. Sci.*, vol. 18, no. 10, pp. 671–675, 1951, doi: 10.2514/8.2076.

[89] V. T. Morgan, "The Overall Convective Heat Transfer from Smooth Circular Cylinders," *Adv. Heat Transf.*, vol. 11, no. C, pp. 199–264, 1975, doi: 10.1016/S0065-2717(08)70075-3.

[90] W. Nowak and A. A. Stachel, "Convective heat transfer in air flow around a cylinder at low Reynolds numbers," *J. Eng. Phys. Thermophys.*, vol. 78, no. 6, pp. 1214–1221, 2005, doi: 10.1007/s10891-006-0055-8.

[91] Y. Hadad and K. Jafarpur, "Modeling of Laminar Forced Convection Heat Transfer in Packed Beds with Pebbles of Arbitrary Geometry," *J. Porous Media*, vol. 16, no. 11, pp. 1049–1061, 2013, doi: 10.1615/JPorMedia.v16.i11.80.

[92] Ansys Inc., "Ansys Fluent Theory Guide," 2013.

[93] Ansys Inc., "Turbulence Modelling in Ansys Fluent 15.0 Release," 2013.

[94] I. V. Arkhangel'skii, A. V. Dunaev, and I. V. Makarenko, *Non-Isothermal Kinetic Methods*. Max Planck Research Library for the History and Development of Knowledge, 2017.

[95] J. L. Maienschein and J. F. Wardell, "Deflagration behavior of PBXN-109 and Composition B at high pressures and temperatures," *CPIA Publ.*, vol. 712, no. 38th JANNAF Combustion Subcommittee Meeting, 2002, pp. 425–433, 2002.

[96] J. H. Flynn and L. A. Wall, "A quick, direct method for the determination of activation energy from thermogravimetric data," *J. Polym. Sci. Part B Polym. Lett.*, vol. 4, no. 5, pp. 323–328, 1966.

[97] T. Ozawa, “A New Method of Analyzing Thermogravimetric Data,” *Bull. Chem. Soc. Jpn.*, vol. 38, no. 11, pp. 1881–1886, 1965, doi: 10.1246/bcsj.38.1881.

[98] T. Ozawa, “Kinetic analysis of derivative curves in thermal analysis,” *J. Therm. Anal.*, vol. 2, no. 3, pp. 301–324, 1970, doi: 10.1007/BF01911411.

[99] T. Akahira and T. Sunose, “Method of determining activation deterioration constant of electrical insulating materials,” *Res Rep Chiba Inst Technol (Sci Technol)*, vol. 16, pp. 22–31, 1971.

[100] M. L. Hobbs, M. Steyskal, and M. J. Kaneshige, “Modeling RDX Ignition,” in *JANNAF 24th Propulsion Systems Hazards Subcommittee*, 2008.

[101] T. B. Brill, P. E. Gongwer, and G. K. Williams, “Thermal decomposition of energetic materials. 66. Kinetic compensation effects in HMX, RDX, and NTO,” *J. Phys. Chem.*, vol. 98, no. 47, pp. 12242–12247, 1994, doi: 10.1021/j100098a020.

[102] Naval Surface Warfare Center, “MIL-E-82886(OS) Military Specification EXPLOSIVE, PLASTIC-BONDED, CAST PBXN-109,” 1993.

[103] Naval Surface Warfare Center, “MIL-DTL-82901A(OS) DETAIL SPECIFICATION EXPLOSIVE, EXPLOSIVE, PLASTIC-BONDED, CAST PBXN-110,” 2002.

[104] Naval Surface Warfare Center, “MIL-E-82902 (OS) MILITARY SPECIFICATION EXPLOSIVE, PLASTIC-BONDED, CAST PBXN-111,” 2004.

[105] S. Vyazovkin *et al.*, “ICTAC Kinetics Committee recommendations for collecting experimental thermal analysis data for kinetic computations,” *Thermochim. Acta*, vol. 590, pp. 1–23, 2014, doi: 10.1016/j.tca.2014.05.036.

[106] NATO Standardization Office, “STANAG 4489 Explosives, Impact Sensitivity Tests (Edition 1),” 1999.

[107] NATO Standardization Office, “STANAG 4487 Explosives, Friction Sensitivity Tests (Edition 2),” 2009.

[108] NATO Standardization Office, “STANAG 4491 Explosives, Thermal Sensitiveness And Explosiveness Tests (Edition 2),” 2015.

[109] P. C. Myint and A. L. Nichols, “Thermodynamics of HMX polymorphs and HMX/RDX mixtures,” *Ind. Eng. Chem. Res.*, vol. 56, no. 1, pp. 387–403, 2017, doi: 10.1021/acs.iecr.6b03697.

[110] B. M. Dobratz and P. C. Crawford, “LLNL Explosives Handbook: Properties of Chemical Explosives and Explosive Simulants,” no. UCRL-5299; Rev.2. Lawrence Livermore National Laboratory (LLNL), 1981.

[111] M. W. Chase Jr, “NIST-JANAF thermochemical tables,” *J. Phys. Chem. Ref. Data, Monogr.*, vol. 9, 1998.

[112] S. Zeman, “Thermogravimetric analysis of some nitramines, nitrosamines and

nitroesters," *Thermochim. Acta*, vol. 230, no. C, pp. 191–206, 1993, doi: 10.1016/0040-6031(93)80360-M.

[113] T. Ozawa, "Estimation of activation energy by isoconversion methods," *Thermochim. Acta*, vol. 203, no. C, pp. 159–165, 1992, doi: 10.1016/0040-6031(92)85192-X.

[114] V. Leroy, D. Cancellieri, E. Leoni, and J. L. Rossi, "Kinetic study of forest fuels by TGA: Model-free kinetic approach for the prediction of phenomena," *Thermochim. Acta*, vol. 497, no. 1–2, pp. 1–6, 2010, doi: 10.1016/j.tca.2009.08.001.

[115] M. J. Starink, "The determination of activation energy from linear heating rate experiments: A comparison of the accuracy of isoconversion methods," *Thermochim. Acta*, vol. 404, no. 1–2, pp. 163–176, 2003, doi: 10.1016/S0040-6031(03)00144-8.

[116] J. C. Oxley, J. L. Smith, J. E. Brady IV, and A. C. Brown, "Characterization and analysis of tetranitrate esters," *Propellants, Explos. Pyrotech.*, vol. 37, no. 1, pp. 24–39, 2012, doi: 10.1002/prep.201100059.

[117] O. V. S. A. I. Maksimov, Yu. Ya1 ; Apal'kova, V. N; Braverman, "Thermal decomposition kinetics of cyclotrimethylene-trinitramine and cyclotetramethylenetetranitramine in the gas phase," *Žurnal fizičeskoj Him.*, vol. 59, no. 2, pp. 342–345, 1985.

[118] R. Castiglia, Massimo; Cabrino, *PBX per colaggio e compressione: caratterizzazione e prestazioni: PBXN-109, PBXN-110, PBXN-111 (Italian)*. Edizioni Accademiche Italiane, 2014.

[119] E. Aydemir, A. Ulas, and N. Serin, "Thermal decomposition and ignition of PBXN-110 plastic-bonded explosive," *Propellants, Explos. Pyrotech.*, vol. 37, no. 3, pp. 308–315, 2012, doi: 10.1002/prep.201100011.

[120] A. Elbeih, S. Zeman, M. Jungova, and Z. Akstein, "Effect of different polymeric matrices on the sensitivity and performance of interesting cyclic nitramines," *Cent. Eur. J. Energ. Mater.*, vol. 9, no. 2, pp. 131–138, 2012.

[121] R. N. Rogers, "Thermochemistry of explosives," *Thermochim. Acta*, vol. 11, no. 2, pp. 131–139, Feb. 1975, doi: 10.1016/0040-6031(75)80016-5.

[122] J. M. Pakulak and C. M. Jr. Anderson, "NWC Standard Methods for Determining Thermal Properties of Propellants and Explosives," 1980.

APPENDICES

A. Initial and Boundary Conditions for Small-Scale Test Item

Table AP.1 Initial and Boundary Conditions for Small-Scale Slow Heating Test Item

Al. Casing and Teflon Plug		**t**	**r**	**z**	**θ**
IC	$T(t,r,\theta,z) = T_0 = 323.15$ K (50°C)	= 0	$r_0 \leq r \leq r_1$	$-B/2 < z < B/2$	$0 \leq \theta \leq 2\pi$
		= 0	$0 \leq r \leq r_1$	$-L/2 \leq z \leq -B/2$ and $B/2 \leq z \leq L/2$	$0 \leq \theta \leq 2\pi$
BC	$q_{conducton}(t,r,\theta,z) = q_{convection}(t,r,\theta,z)$ $q_{conducton}(t,r,\theta,z) = h(T)(T_\infty(t) - T(t,r,\theta,z))$ where $T_\infty = T_0 + heating\ rate * t$ heating rate= 5 or 15 or 25 °C/h	> 0	$r=r_1$ (Al. Casing)	$-L/2 < z < L/2$ (Al. Casing)	$0 \leq \theta \leq 2\pi$ (Al. Casing)
		> 0	$0 \leq r < r_1$ (Plug)	$z=L/2$ (Plug)	$0 \leq \theta \leq 2\pi$ (Plug)
BC	Al. Case is coupled with Energetic Material (EM) $q_{conduction}(Al.Casing) = q_{conduction}(EM)$	> 0	$r=r_0$	$-B/2 \leq z \leq B/2$	$0 \leq \theta \leq 2\pi$
BC	Teflon plug is coupled with Energetic Material (EM) $q_{conduction}(Plug) = q_{conduction}(EM)$	> 0	$0 \leq r < r_0$	$z=B/2$	$0 \leq \theta \leq 2\pi$
Energetic Material		**t**	**r**	**z**	**θ**
IC	$T(t,r,\theta,z) = T_0 = 323.15$ K (50°C)	= 0	$0 \leq r \leq r_0$	$-B/2 \leq z \leq B/2$	$0 \leq \theta \leq 2\pi$
BC	$q_{conducton}(t,r,\theta,z) = q_{convection}(t,r,\theta,z)$ $q_{conducton}(t,r,\theta,z) = h(T)(T_\infty(t) - T(t,r,\theta,z))$ where $T_\infty = T_0 + heating\ rate * t$ heating rate= 5 or 15 or 25 °C/h	> 0	$0 \leq r < r_0$	$z=-L/2$	$0 \leq \theta \leq 2\pi$
BC	Al Case is coupled with Energetic Material (EM) $q_{conduction}(Al.Casing) = q_{conduction}(EM)$	> 0	$r=r_0$	$-B/2 \leq z \leq B/2$	$0 \leq \theta \leq 2\pi$
BC	Teflon plug is coupled with Energetic Material (EM) $q_{conduction}(Plug) = q_{conduction}(EM)$	> 0	$0 \leq r < r_0$	$z=B/2$	$0 \leq \theta \leq 2\pi$

B. Shear Stress Transport (SST) κ- ω Empirical Turbulence Model

To implement turbulence models in Eq. 5 to Eq. 9 (section 2.1.2), instantaneous velocity (u) should be considered as the sum of time average velocity ($\bar{u}$) and the fluctuating velocity (u'). Moreover, other scalar quantities (φ) such as pressure, energy and species concentration should be considered as sum of time average ($\bar{\varphi}$) and fluctuating components (φ'). For instance, equation of continuity (Eq. 5) and equation of motion (Eq. 6) given in section 2.1.2 can be written as Eq. 26 and Eq. 27 using the time average and fluctuating components [92]. These transport equations are denoted as Reynold averaged Navier-Stokes Equations (RANS) in computational fluid dynamics (CFD) literature [92].

$$\frac{\partial \rho}{\partial t} + \frac{\partial (\rho \bar{u}_i)}{\partial x_i} = 0 \qquad \text{Eq. 26}$$

$$\frac{\partial (\rho \bar{u}_i)}{\partial t} + \frac{\partial \left(\rho \bar{u}_i \bar{u}_j\right)}{\partial x_j} = -\frac{\partial \bar{p}}{\partial x_i} + \frac{\partial}{\partial x_j}\left[\mu\left(\frac{\partial \bar{u}_i}{\partial x_j} + \frac{\partial \bar{u}_j}{\partial x_i} - \frac{2}{3}\delta_{ij}\frac{\partial \bar{u}_k}{\partial x_k}\right)\right] + \frac{\partial}{\partial x_j}\left(\rho \bar{u}_i \bar{u}_j - \rho\overline{u_i u_j}\right) \qquad \text{Eq. 27}$$

δ_{ij} in Eq. 27 is Kronecker Delta which is δ_{ij}=0 for i≠j and δ_{ij}=1 for i=j. The crucial expression in the same equation is $\left(-\rho\overline{u_i u_j}\right)$ which is Reynolds Stress Tensor ($\bar{\bar{R}}_{ij}$). Reynolds Stress Tensor can be calculated with eddy viscosity models that depends on Boussinesq hypothesis given in Eq. 28 [92].

$$\bar{\bar{R}}_{ij} = \left(-\rho\overline{u_i u_j}\right) = \mu_T\left(\frac{\partial \bar{u}_i}{\partial x_j} + \frac{\partial \bar{u}_j}{\partial x_i} - \frac{2}{3}\delta_{ij}\frac{\partial \bar{u}_k}{\partial x_k}\right) - \frac{2}{3}\rho\kappa\delta_{ij} \qquad \text{Eq. 28}$$

Eq. 28 introduces arbitrary turbulent (eddy) viscosity μ_T term to equation. Turbulent viscosity is an arbitrary term and can be calculated by using turbulence kinetic energy (κ) and specific rate of dissipation of the turbulence kinetic energy into

thermal energy (ω). Relation of turbulent viscosity with the κ and ω is given with Eq. 29 [92]. κ and ω can be calculated with additional partial differential equations that uses empirical turbulence model constants summarized between Eq. 29 to Eq. 55. Shear Stress Transport (SST) κ-ω empirical turbulence model is the recommended empirical turbulence model for transient region regime in air flow and provides more accurate prediction of flow separation and resolves viscous sublayer better compared to other models [93]. SST κ-ω empirical turbulence model with coupled solution method is used for the large-scale slow heating test set-up considering the model and solver capabilities [92], [93]. In addition, after the air flow in the test chamber becomes steady (after 600 seconds) low Reynolds Number correction is introduced to SST k-ω model for more accurate solution around test item. Moreover, gravity is included in simulations and second order schemes are selected for spatial discretization of pressure, momentum, and energy.

$$\mu_T = constant \frac{\rho\kappa}{\omega} \quad \text{Eq. 29}$$

$$\frac{\partial(\rho\kappa)}{\partial t} + \frac{\partial(\rho\kappa u_i)}{\partial x_i} = \frac{\partial}{\partial x_j}\left(\Gamma_K \frac{\partial\kappa}{\partial x_j}\right) + G_\kappa - Y_\kappa \quad \text{Eq. 30}$$

$$\frac{\partial(\rho\omega)}{\partial t} + \frac{\partial(\rho\omega u_j)}{\partial x_j} = \frac{\partial}{\partial x_j}\left(\Gamma_\omega \frac{\partial\omega}{\partial x_j}\right) + G_\omega - Y_\omega + D_\omega \quad \text{Eq. 31}$$

$$G_\kappa = \mu_t \bar{S}^2 \quad \text{Eq. 32}$$

$$\bar{S} = \sqrt{2S_{ij}S_{ij}} \quad \text{Eq. 33}$$

$$G_\omega = \frac{\alpha}{\nu_t} G_K \quad \text{Eq. 34}$$

$$\alpha = \frac{\alpha_\infty}{\alpha^*}\left(\frac{\alpha_0 + Re_t/R_\omega}{1 + Re_t/R_\omega}\right) \quad \text{Eq. 35}$$

$$R_\omega = 2.95\alpha^* \quad \text{Eq. 36}$$

$$Re_t = \frac{\rho \kappa}{\mu \omega} \quad \text{Eq. 37}$$

$$\Gamma_\kappa = \mu + \frac{\mu_t}{\sigma_\kappa} \quad \text{Eq. 38}$$

$$\Gamma_\omega = \mu + \frac{\mu_t}{\sigma_\omega} \quad \text{Eq. 39}$$

$$\mu_t = \frac{\rho \kappa}{\omega} \frac{1}{max\left[\frac{1}{\alpha^*}, \frac{\ddot{S} F_2}{a_1 \omega}\right]} \quad \text{Eq. 40}$$

$$\sigma_\kappa = \frac{1}{\frac{F_1}{\sigma_{\kappa,1}} + \frac{(1 - F_1)}{\sigma_{\kappa,2}}} \quad \text{Eq. 41}$$

$$\sigma_\omega = \frac{1}{\frac{F_1}{\sigma_{\omega,1}} + \frac{(1 - F_1)}{\sigma_{\omega,2}}} \quad \text{Eq. 42}$$

$$\alpha^* = \alpha^*_\infty \left(\frac{\alpha^*_0 + Re_t / R_\kappa}{1 + Re_t / R_\kappa}\right) \quad \text{Eq. 43}$$

$$F_1 = \tanh\left(\phi_1^4\right) \quad \text{Eq. 44}$$

$$F_2 = \tanh\left(\phi_2^4\right) \quad \text{Eq. 45}$$

$$\phi_1 = \min\left[\max\left(\frac{\sqrt{\kappa}}{0.09 \omega \gamma}, \frac{500 \mu}{\rho \gamma^2 \omega}\right), \frac{4 \rho \kappa}{\sigma_{\omega,2} D_\omega^+ \gamma^2}\right] \quad \text{Eq. 46}$$

$$D_\omega^+ = max\left[2 \rho \frac{1}{\sigma_{\omega,2} \omega} \frac{\partial \kappa}{\partial x_j} \frac{\partial \omega}{\partial x_j}, 10^{-10}\right] \quad \text{Eq. 47}$$

$$\phi_2 = max\left[2 \frac{\sqrt{\kappa}}{0.09 \omega \gamma}, \frac{500 \mu}{\rho \gamma^2 \omega}\right] \quad \text{Eq. 48}$$

$$\alpha_\infty = F_1 \alpha_{\infty,1} + (1 - F_1) \alpha_{\infty,2} \quad \text{Eq. 49}$$

$$\alpha_{\infty,1} = \frac{\beta_{i,1}}{\beta^*_\infty} - \frac{\psi^2}{\sigma_{w,1} \sqrt{\beta^*_\infty}} \quad \text{Eq. 50}$$

$$\alpha_{\infty,2} = \frac{\beta_{i,2}}{\beta^*_\infty} - \frac{\psi^2}{\sigma_{w,2} \sqrt{\beta^*_\infty}} \quad \text{Eq. 51}$$

$$Y_\kappa = \rho\beta^*\kappa\omega \quad \text{Eq. 52}$$

$$Y_\omega = \rho\beta\omega^2 \quad \text{Eq. 53}$$

$$\beta_i = F_1\beta_{i,1} + (1 - F_1)\beta_{i,2} \quad \text{Eq. 54}$$

$$D_\omega = 2(1 - F_1)\rho\frac{1}{\omega\sigma_{\omega,2}}\frac{\partial\kappa}{\partial x_j}\frac{\partial\omega}{\partial x_j} \quad \text{Eq. 55}$$

Γ_κ Effective Diffusivity of κ

Γ_ω Effective Diffusivity of ω

κ Turbulence Kinetic Energy

ω Specific Dissipation Rate of Turbulent Kinetic Energy into Thermal Energy

D_ω Cross-Diffusion Term

D_ω^+ Positive Portion of the Cross-Diffusion Term

G_κ Production of Turbulence Kinetic Energy

G_ω Generation of ω.

$\ddot{S}$ Strain Rate Magnitude

$\bar{S}$ Modulus of the Mean Stress Tensor

Y_κ Dissipation of κ due to Turbulence

Y_ω Dissipation of ω due to Turbulence

μ_t Turbulent Viscosity

σ_κ Turbulent Prandtl Number for κ

σ_ω Turbulent Prandtl Number for ω

γ Distance to Next Surface

M_{t0}	0.25	$\beta_{i,1}$	0.075
R_K	6	$\beta_{i,2}$	0.0828
R_β	8	σ_1	0.31
R_ω	2.95	$\sigma_{\kappa,1}$	1.176
f_{β^*}	1	$\sigma_{\kappa,2}$	1.0
f_β	1	σ_κ	2.0
α_0	1/9	$\sigma_{\omega,1}$	2.0
α_∞	0.52	$\sigma_{\omega,2}$	1.168
α_∞^*	1	σ_ω	2.0
β_∞^*	0.09	ψ	0.41

C. Material Database for Numerical Simulations

```
;;;;;;;;;;;;;;;;;;;;;;;;;;;;;;;;;;;;;;;;;;;;;;;;;;;;;;;;;;;;;;;;;;;;;;;;;;;
;;;                                                                    ;;;
;;;          Fluent USER DEFINED MATERIAL DATABASE                     ;;;
;;;                                                                    ;;;
;;; (name type[fluid/solid] (chemical-formula . formula)               ;;;
;;;          (prop1 (method1a . data1a) (method1b . data1b))           ;;;
;;;          (prop2 (method2a . data2a) (method2b . data2b)))          ;;;
;;;                                                                    ;;;
;;;;;;;;;;;;;;;;;;;;;;;;;;;;;;;;;;;;;;;;;;;;;;;;;;;;;;;;;;;;;;;;;;;;;;;;;;;

(

        (Igniter solid
                (chemical-formula . #f)
                (density (constant . 1506.))
                (specific-heat (polynomial piecewise-linear (323. . 1330.0) (343. .
1402.0) (363. . 1485.0) (383 . 1613.0)))
                (thermal-conductivity (polynomial piecewise-linear (293. . 0.395)
(323. . 0.450) (373. . 0.430)))

        )

        (P1 solid
                (chemical-formula . #f)
                (density (constant . 1670.))
                (specific-heat (polynomial piecewise-linear (333. . 1232.01) (353. .
1270.01) (373. . 1325.01) (393. . 1382.01) (403. . 1419.01)))
                (thermal-conductivity (polynomial piecewise-linear (303. . 0.470)
(323. . 0.480) (363. . 0.530) (373. . 0.550)))
        )

        (P2 solid
                (chemical-formula . #f)
                (density (constant . 1660.))
                (specific-heat (polynomial piecewise-linear (323. . 1229.01) (343. .
1368.01) (363. . 1478.01) (383. . 1579.01) (403. . 1652.01)))
                (thermal-conductivity (polynomial piecewise-linear (299. . 0.550)
(325. . 0.520) (351. . 0.515) (372. . 0.510)))
        )

        (P3 solid
                (chemical-formula . #f)
```

(density (constant . 1710.))
(specific-heat (polynomial piecewise-linear (333. . 1239.01) (343. . 1269.01) (363. . 1359.01) (383. . 1434.01) (403. . 1495.01)))
(thermal-conductivity (polynomial piecewise-linear (298. . 0.840) (324. . 0.800) (373. . 0.720) (410. . 0.670)))
)

(**P4** solid
(chemical-formula . #f)
(density (constant . 1810.))
(specific-heat (polynomial piecewise-linear (323. . 917.01) (343. . 944.01) (363. . 968.01) (383. . 992.01) (403. . 969.01) (423. . 977.01)))
(thermal-conductivity (polynomial piecewise-linear (295. . 0.650) (330. . 0.720) (372. . 0.705) (410. . 0.670)))
)

(**bitumen_liner** solid
(chemical-formula . #f)
(density (constant . 980.))
(specific-heat (polynomial piecewise-linear (298. . 1762.) (323. . 1982.) (453. . 2110.) (463. . 2179.)))
(thermal-conductivity (polynomial piecewise-linear (298. . 0.205)(323. . 0.180)))
)

(**4340_steel** solid
(chemical-formula . #f)
(thermal-conductivity (polynomial piecewise-linear (300. . 36.20000076293945) (470. . 38.70000076293945) (750. . 35.40000152587891)))
(specific-heat (constant . 434.))
(density (constant . 7850.))
)

(**Teflon** solid
(chemical-formula . #f)
(density (constant . 2160.))
(specific-heat (polynomial piecewise-linear (293. . 1400.) (313. . 1200.) (423. . 1300.)) (constant . 1200.))
(thermal-conductivity (constant . 0.25))
)

(**Eutectic-Bi-Sn** solid
(chemical-formula . #f)
(density (constant . 8000.))
(specific-heat (constant . 170.))

(thermal-conductivity (constant . 30.))
)

(**air** fluid
(chemical-formula . #f)
(density (constant . 1.225000023841858) (ideal-gas . #f)
(compressible-liquid 101325 1.225 142000. 1 1.1 0.9))
(specific-heat (constant . 1006.429992675781) (polynomial
piecewise-polynomial (100 1000 1161.48214452351 -2.36881890191577
0.0148551108358867 -5.03490927522584e-05 9.9285695564579e-08 -
1.11109658897742e-10 6.54019600406048e-14 -1.57358768447275e-17) (1000
3000 -7069.81410143802 33.7060506468204 -0.0581275953375815
5.42161532229608e-05 -2.936678858119e-08 9.237533169567681e-12 -
1.56555339604519e-15 1.11233485020759e-19)))
(thermal-conductivity (constant . 0.02419999986886978))
(viscosity (constant . 1.789400084817316e-05) (sutherland 1.716e-
05 273.11 110.56) (power-law 1.716e-05 273.11 0.666))
(molecular-weight (constant . 28.96599960327148))
(lennard-jones-length (constant . 3.711))
(lennard-jones-energy (constant . 78.59999999999999))
(thermal-accom-coefficient (constant . 0.9137))
(velocity-accom-coefficient (constant . 0.9137))
(formation-entropy (constant . 194336))
(reference-temperature (constant . 298.15))
(critical-pressure (constant . 3758000.))
(critical-temperature (constant . 132.3))
(acentric-factor (constant . 0.033))
(critical-volume (constant . 0.002857))
(therm-exp-coeff (constant . 0))
(speed-of-sound (none . #f))
)

(**aluminum_experiment** solid
(chemical-formula . #f)
(density (constant . 2700.))
(specific-heat (constant . 896.))
(thermal-conductivity (constant . 162.0))

)

(**aluminum__6061** solid
(chemical-formula . #f)
(density (constant . 2685.))
(specific-heat (polynomial piecewise-linear (323. . 878.6) (373. .
941.4) (423. . 962.3) (473. . 993.7)))

(thermal-conductivity (polynomial piecewise-linear (323. . 155.7) (373. . 160.9) (423. . 168.6) (473. . 173)))

(steel_4140 solid
(chemical-formula . steel_4140)
(density (constant . 7850.))
(specific-heat (constant . 460.))
(thermal-conductivity (constant . 42.59999847412109))
)

(**steel_1040** solid
(chemical-formula . #f)
(density (constant . 7845.))
(specific-heat (polynomial piecewise-linear (373. . 486.) (423. . 515.) (473. . 528.) (523. . 548.) (573. . 569.) (623. . 586.) (723. . 649.) (823. . 708.) (923. . 770.)) (constant . 871))
(thermal-conductivity (polynomial piecewise-linear (273. . 51.90000152587891) (373. . 50.70000076293945) (473. . 48.09999847412109) (573. . 45.70000076293945) (673. . 41.70000076293945) (873. . 38.20000076293945) (973. . 33.90000152587891) (1073. . 30.10000038146973) (1173. . 24.70000076293945)) (constant . 202.4))
(formation-entropy (constant . 164448.08))
(electric-conductivity (constant . 35410000.))
(magnetic-permeability (constant . 1.257e-06))
)

)

D. User Defined Functions (UDF) for Numerical Simulations

```
/**********************************************************************
  UDF for Source Term, Convective Heat Transfer Coefficient and Heating Profile
**********************************************************************
/
#include "udf.h"
```

#Source Term for Igniter

```
DEFINE_SOURCE(Igniter_Model_Free_method1, cell, thread, dS, eqn)
{
 real source_Igniter;
 real Eact_Igniter;
 real Aact_Igniter;
 real Qact_Igniter;
 real dens_Igniter;
 real conversion_Igniter;
 real Entalpi_Melting;

 Eact_Igniter=175615;
 Aact_Igniter=1.54e18;
 Qact_Igniter=1078000;
 dens_Igniter=1506;
 Entalpi_Melting=78638;

 {
 if (C_T(cell, thread)< 405.15)
        {
    source_Igniter = dens_Igniter*Qact_Igniter*Aact_Igniter*exp(-
1*Eact_Igniter/(8.314*C_T(cell, thread)));
    dS[eqn] = source_Igniter*(Eact_Igniter/(8.314*C_T(cell, thread)*C_T(cell,
thread)));
        }
    else if (C_T(cell, thread)< 409.15)
    {
        source_Igniter = dens_Igniter*Qact_Igniter*Aact_Igniter*exp(-
1*Eact_Igniter/(8.314*C_T(cell, thread)))-Entalpi_Melting;

    dS[eqn] = source_Igniter*(Eact_Igniter/(8.314*C_T(cell, thread)*C_T(cell,
thread)));
        }
    else
```

```
                {

        source_Igniter = dens_Igniter*Qact_Igniter*Aact_Igniter*exp(-
1*Eact_Igniter/(8.314*C_T(cell, thread)));
        dS[eqn] = source_Igniter*(Eact_Igniter/(8.314*C_T(cell, thread)*C_T(cell,
thread)));
        }
        }
return source_Igniter;
        }
```

#Source Term for P1 Explosive__Model_Based

```
DEFINE_SOURCE(P1_1st order_Method1, cell, thread, dS, eqn)
{
 real sourceP1;
 real EactP1;
 real AactP1;
 real QactP1;
 real densP1;
 real conversionP1;
   EactP1=203587;
 AactP1=3.35e19;
 QactP1=1352000;
 densP1=1670;
{
 if (C_T(cell, thread)<=401.4)
                {
        sourceP1 = densP1*QactP1*AactP1*exp(-1*EactP1/(8.314*C_T(cell,
thread)));
        dS[eqn] = sourceP1*(EactP1/(8.314*C_T(cell, thread)*C_T(cell, thread)));
        }
        else
        {
        conversionP1= 2.6527e-07*pow(C_T(cell, thread), 3.0)-2.982e-
04*pow(C_T(cell, thread), 2.0)+1.1172e-01*C_T(cell, thread)-13.944;
        sourceP1 = densP1*QactP1*AactP1*(1-conversionP1)*exp(-
1*EactP1/(8.314*C_T(cell, thread)));
        dS[eqn] = densP1*QactP1*AactP1*exp(-1*EactP1/(8.314*C_T(cell,
thread)))*(EactP1/(8.314*C_T(cell, thread)*C_T(cell, thread)))*(1-
conversionP1)+densP1*QactP1*AactP1*exp(-1*EactP1/(8.314*C_T(cell,
thread)))*((-3*2.6527e-07*pow(C_T(cell, thread), 2.0))+2*(2.982e-04)*C_T(cell,
thread)-1.1172e-01);
        }
 }
```

```
return sourceP1;

}
```

#Source Term for P1 Explosive__Isoconversional

```
DEFINE_SOURCE(P1_Model_Free_Method1, cell, thread, dS, eqn)
{
  real sourceP1;
  real EactP1;
  real AactP1;
  real QactP1;
  real densP1;
  real conversionP1;

  EactP1=185536;
  AactP1=1.93e17;
  QactP1=1352000;
  densP1=1670;

  sourceP1 = densP1*QactP1*AactP1*exp(-1*EactP1/(8.314*C_T(cell, thread)));
  dS[eqn] = sourceP1*(EactP1/(8.314*C_T(cell, thread)*C_T(cell, thread)));
return sourceP1;
}

DEFINE_SOURCE(P2_15C_h__melting__on, cell, thread, dS, eqn)
{
  real source_P2;
  real Eact_P2;
  real Aact_P2;
  real Qact_P2;
  real dens_P2;
  real conversion_P2;
  real Entalpi_deneme;


  Eact_P2=221190;
  Aact_P2=4.48e19;
  Qact_P2=1257000;
  dens_P2=1660;
  Entalpi_deneme=44483;

  {
  if (C_T(cell, thread)< 441.15)
                    {
```

```
        source_P2 = dens_P2*Qact_P2*Aact_P2*exp(-
1*Eact_P2/(8.314*C_T(cell, thread)));
        dS[eqn] = source_P2*(Eact_P2/(8.314*C_T(cell, thread)*C_T(cell,
thread)));
        }
        else if (C_T(cell, thread)< 442.15)
        {
        source_P2 = dens_P2*Qact_P2*Aact_P2*exp(-
1*Eact_P2/(8.314*C_T(cell, thread)))-Entalpi_deneme;;
        dS[eqn] = source_P2*(Eact_P2/(8.314*C_T(cell, thread)*C_T(cell,
thread)));
                }
        else
                {
        source_P2 = dens_P2*Qact_P2*Aact_P2*exp(-
1*Eact_P2/(8.314*C_T(cell, thread)));
        dS[eqn] = source_P2*(Eact_P2/(8.314*C_T(cell, thread)*C_T(cell,
thread)));
        }
        }


return source_PBP002;
}

DEFINE_SOURCE(P2_25C_h__melting__on, cell, thread, dS, eqn)
{
  real source_P2;
  real Eact_P2;
  real Aact_P2;
  real Qact_P2;
  real dens_P2;
  real conversion_P2;
  real Entalpi_deneme;


  Eact_P2=221190;
  Aact_P2=4.48e19;
  Qact_P2=1257000;
  dens_P2=1660;
  Entalpi_deneme=74139;

  {
  if (C_T(cell, thread)< 441.15)
                {
```

```
        source_P2 = dens_P2*Qact_P2*Aact_P2*exp(-
1*Eact_P2/(8.314*C_T(cell, thread)));
        dS[eqn] = source_P2*(Eact_P2/(8.314*C_T(cell, thread)*C_T(cell,
thread)));
        }
        else if (C_T(cell, thread)< 442.15)
        {
        source_P2 = dens_P2*Qact_P2*Aact_P2*exp(-
1*Eact_P2/(8.314*C_T(cell, thread)))-Entalpi_deneme;;
        dS[eqn] = source_P2*(Eact_P2/(8.314*C_T(cell, thread)*C_T(cell,
thread)));
                }
        else
                {
        source_P2 = dens_P2*Qact_P2*Aact_P2*exp(-
1*Eact_P2/(8.314*C_T(cell, thread)));
        dS[eqn] = source_P2*(Eact_P2/(8.314*C_T(cell, thread)*C_T(cell,
thread)));
        }
        }
return source_P2;
}

DEFINE_SOURCE(P3__5C_h__melting__on, cell, thread, dS, eqn)
{
 real source_P3;
 real Eact_P3;
 real Aact_P3;
 real Qact_P3;
 real dens_P3;
 real conversion_P3;
 real Entalpi_deneme;

 Eact_P3=183781;
 Aact_P3=1.26e16;
 Qact_P3=723000;
 dens_P3=1710;
 Entalpi_deneme=43000;

 {
 if (C_T(cell, thread)< 441.65)
                {
```

```
        source_P3 = dens_P3*Qact_P3*Aact_P3*exp(-
1*Eact_P3/(8.314*C_T(cell, thread)));
        dS[eqn] = source_P3*(Eact_P3/(8.314*C_T(cell, thread)*C_T(cell,
thread)));
        }
        else if (C_T(cell, thread)< 442.15)
        {
        source_P3 = dens_P3*Qact_P3*Aact_P3*exp(-
1*Eact_P3/(8.314*C_T(cell, thread)))-Entalpi_deneme;;
        dS[eqn] = source_P3*(Eact_P3/(8.314*C_T(cell, thread)*C_T(cell,
thread)));
                }
        else
                {
        source_P3 = dens_P3*Qact_P3*Aact_P3*exp(-
1*Eact_P3/(8.314*C_T(cell, thread)));
        dS[eqn] = source_P3*(Eact_P3/(8.314*C_T(cell, thread)*C_T(cell,
thread)));
        }
        }
return source_P3;
}

DEFINE_SOURCE(P3__15C_h__melting__on, cell, thread, dS, eqn)
{
  real source_P3;
  real Eact_P3;
  real Aact_P3;
  real Qact_P3;
  real dens_P3;
  real conversion_P3;
  real Entalpi_deneme;

  Eact_P3=183781;
  Aact_P3=1.26e16;
  Qact_P3=723000;
  dens_P3=1710;
  Entalpi_deneme=64500;
  {
  if (C_T(cell, thread)< 446.15)
                {
        source_P3 = dens_P3*Qact_P3*Aact_P3*exp(-
1*Eact_P3/(8.314*C_T(cell, thread)));
        dS[eqn] = source_P3*(Eact_P3/(8.314*C_T(cell, thread)*C_T(cell,
thread)));
```

```
        }
        else if (C_T(cell, thread)< 447.15)
        {
        source_P3 = dens_P3*Qact_P3*Aact_P3*exp(-
1*Eact_P3/(8.314*C_T(cell, thread)))-Entalpi_deneme;;
        dS[eqn] = source_P3*(Eact_P3/(8.314*C_T(cell, thread)*C_T(cell,
thread)));
                }
        else
                {
        source_P3 = dens_P3*Qact_P3*Aact_P3*exp(-
1*Eact_P3/(8.314*C_T(cell, thread)));
        dS[eqn] = source_P3*(Eact_P3/(8.314*C_T(cell, thread)*C_T(cell,
thread)));
        }
        }
return source_P3;
}

DEFINE_SOURCE(P3__25C_h__melting__on, cell, thread, dS, eqn)
{
 real source_P3;
 real Eact_P3;
 real Aact_P3;
 real Qact_P3;
 real dens_P3;
 real conversion_P3;
 real Entalpi_deneme;

 Eact_P3=183781;
 Aact_P3=1.26e16;
 Qact_P3=723000;
 dens_P3=1710;
 Entalpi_deneme=215000;
 {
 if (C_T(cell, thread)< 446.15)
                {
        source_P3 = dens_P3*Qact_P3*Aact_P3*exp(-
1*Eact_P3/(8.314*C_T(cell, thread)));
        dS[eqn] = source_P3*(Eact_P3/(8.314*C_T(cell, thread)*C_T(cell,
thread)));

        }
        else if (C_T(cell, thread)< 446.65)
```

```
        {

        source_P3 = dens_P3*Qact_P3*Aact_P3*exp(-
1*Eact_P3/(8.314*C_T(cell, thread)))-Entalpi_deneme;;
        dS[eqn] = source_P3*(Eact_P3/(8.314*C_T(cell, thread)*C_T(cell,
thread)));
                }
        else
                {
        source_P3 = dens_P3*Qact_P3*Aact_P3*exp(-
1*Eact_P3/(8.314*C_T(cell, thread)));
        dS[eqn] = source_P3*(Eact_P3/(8.314*C_T(cell, thread)*C_T(cell,
thread)));
        }
        }
return source_P3;
}
```

#Source Term for P4 Explosive

```
DEFINE_SOURCE(P4_Literature, cell, thread, dS, eqn)
{
 real source_P4;
 real Eact_P4;
 real Aact_P4;
 real Qact_P4;
 real dens_P4;
 real conversion_P4;

 Eact_P4=180000;
 Aact_P4=5.9e15;
 Qact_P4=1510000;
 dens_P4=1810;

        source_P4 = dens_P4*Qact_P4*Aact_P4*exp(-
1*Eact_P4/(8.314*C_T(cell, thread)));
        dS[eqn] = source_P4*(Eact_P4/(8.314*C_T(cell, thread)*C_T(cell,
thread)));
        return source_P4;
        }
```

#Source Term for Booster__Isoconversional

```
DEFINE_SOURCE(Booster_Method1, cell, thread, dS, eqn)
{
  real sourceBOOSTER;
  real EactBOOSTER;
  real AactBOOSTER;
  real QactBOOSTER;
  real densBOOSTER;
  real conversionBOOSTER;

  EactBOOSTER=220500;
  AactBOOSTER=5.0e19;
  QactBOOSTER=2092000;
  densBOOSTER=1810;

  sourceBOOSTER = densBOOSTER*QactBOOSTER*AactBOOSTER*exp(-
1*EactBOOSTER/(8.314*C_T(cell, thread)));
  dS[eqn] = sourceBOOSTER*(EactBOOSTER/(8.314*C_T(cell,
thread)*C_T(cell, thread)));
return sourceBOOSTER;
}
```

#Convective Heat Transfer Coefficient for Small Chamber

```
DEFINE_PROFILE(HTC_profile_Small_Chamber,thread,i)
{

face_t f;

real density;
real specific_heat;
real thermal_conductivity;
real dynamic_viscosity;
real kinematic_viscosity;
real radius;
real diameter;
real characteristic_length;
real velocity;
real prandtl_number;
real reynolds_number;
real nusselt_number;
real heat_transfer_coefficient;
```

```
radius=0.022;
diameter=0.044;
velocity=0.4;

begin_f_loop(f,thread)

{
density=4.8294e-06*pow(F_T(f,thread), 2.0)-5.847e-03*F_T(f,thread)+2.3225;

specific_heat=4.6044e-04*pow(F_T(f,thread), 2.0)-2.5218e-
01*F_T(f,thread)+1.0412*1000;

thermal_conductivity=-2.6069e-08*pow(F_T(f,thread), 2.0)+9.3089e-
05*F_T(f,thread)-6.7829e-04;

dynamic_viscosity=-2.7922e-11*pow(F_T(f,thread), 2.0)+6.5029e-
08*F_T(f,thread)-1.4647e-06;

kinematic_viscosity=dynamic_viscosity/density;

prandtl_number=specific_heat*dynamic_viscosity/thermal_conductivity;

reynolds_number=density*velocity*diameter/dynamic_viscosity;

nusselt_number=0.3+((0.62*pow(reynolds_number,0.5)*pow(prandtl_number,0.33
333))/pow((1+pow(0.4/prandtl_number,0.6666667)),0.25))*pow((1+pow(reynolds
_number/282000,0.625)),0.8);

heat_transfer_coefficient=nusselt_number*thermal_conductivity/diameter;

F_PROFILE(f,thread,i) = heat_transfer_coefficient;
}
end_f_loop(f,thread)
 }
```

#Temperature Profile of Igniter coupled with P1 Explosive (5°C/hour heating rate) for Small Chamber

```
DEFINE_PROFILE(temperature_profile____Igniter_FC_5C, thread, i)
{
face_t f;
begin_f_loop(f, thread)
{
real t = RP_Get_Real("flow-time");
if (t<=0.000)
```

```
F_PROFILE (f, thread, i) = 323.922;
else if (t<80000.10)
F_PROFILE (f, thread, i) = 323.922 +0.001443*t ;
else
F_PROFILE (f, thread, i) = 500. ;
}
end_f_loop(f, thread)
}
```

#Temperature Profile of Igniter coupled with P1 Explosive (15°C/hour heating rate) for Small Chamber

```
DEFINE_PROFILE(temperature_profile____Igniter_FC_15C_TEZ, thread, i)
{
face_t f;
begin_f_loop(f, thread)
{
real t = RP_Get_Real("flow-time");
if (t<=0.000)
F_PROFILE (f, thread, i) = 328.944;
else if (t<80000.10)
F_PROFILE (f, thread, i) = 328.944 +0.004141*t ;
else
F_PROFILE (f, thread, i) = 500. ;
}
end_f_loop(f, thread)
}
```

#Temperature Profile of Igniter coupled with P1 Explosive (25°C/hour heating rate) for Small Chamber

```
DEFINE_PROFILE(temperature_profile____Igniter_FC_25C_TEZ, thread, i)
{
face_t f;

begin_f_loop(f, thread)
{
real t = RP_Get_Real("flow-time");

if (t<=0.000)
F_PROFILE (f, thread, i) = 333.1975;
else if (t<80000.10)
F_PROFILE (f, thread, i) = 333.1975 +0.006809*t ;
else
F_PROFILE (f, thread, i) = 500. ;
```

```
}
end_f_loop(f, thread)
}
```

#Temperature Profile of P1 Explosive (5°C/hour heating rate) for Small Chamber

```
DEFINE_PROFILE(temperature_profile____P1__FC_5C, thread, i)
{
face_t f;
begin_f_loop(f, thread)
{
real t = RP_Get_Real("flow-time");
if (t<=0.000)
F_PROFILE (f, thread, i) = 328.2474;
else if (t<80000.10)
F_PROFILE (f, thread, i) = 328.2474 +0.001337*t ;
else
F_PROFILE (f, thread, i) = 500. ;
}
end_f_loop(f, thread)
}
```

#Temperature Profile of P1 Explosive (15°C/hour heating rate) for Small Chamber

```
DEFINE_PROFILE(temperature_profile____P1_FC_15C, thread, i)
{
face_t f;
begin_f_loop(f, thread)
{
real t = RP_Get_Real("flow-time");


if (t<=0.000)
F_PROFILE (f, thread, i) = 326.95;
else if (t<80000.10)
F_PROFILE (f, thread, i) = 326.95 +0.004211*t ;
else
F_PROFILE (f, thread, i) = 500. ;
}
end_f_loop(f, thread)
}
```

#Temperature Profile of P1 Explosive (25°C/hour heating rate) for Small Chamber

```
DEFINE_PROFILE(temperature_profile____P1_FC_25C, thread, i)
{
face_t f;
begin_f_loop(f, thread)
{
real t = RP_Get_Real("flow-time");
if (t<=0.000)
F_PROFILE (f, thread, i) = 328.04;
else if (t<80000.10)
F_PROFILE (f, thread, i) = 328.04+0.007074*t ;
else
F_PROFILE (f, thread, i) = 500. ;
}
end_f_loop(f, thread)
}
```

#Temperature Profile For Large_Scale_Test_Chamber

```
DEFINE_PROFILE(temperature_profile____Large_Scale_Test, thread, i)
{
face_t f;
begin_f_loop(f, thread)
{
real t = RP_Get_Real("flow-time");
real t1;
real t2;
real t3;
real t4;

t1=t;
t2=t;
t3=t;
t4=t;

if (t<=3980.100)
F_PROFILE (f, thread, i) = 336.15;
else if (t<42000.10)
F_PROFILE (f, thread, i) = 2.75555e-20*t*t1*t2*t3*t4-3.17015e-
15*t*t1*t2*t3+1.29017e-10*t*t1*t2-2.27510e-6*t*t1+2.27407e-2*t + 272.504 ;
else
F_PROFILE (f, thread, i) = 510. ;
}
end_f_loop(f, thread)
}
```

E. Repeatability of Small-Scale Slow Heating Tests

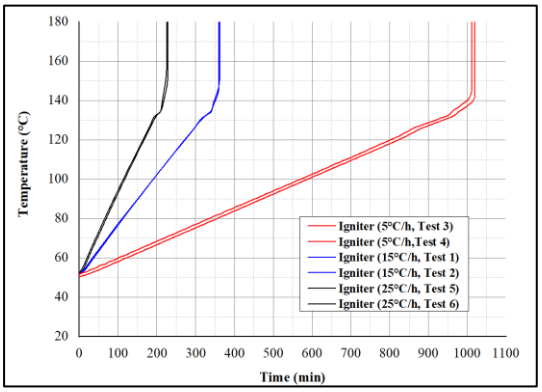

Figure AP.1. Igniter Coupled with P1 Explosive

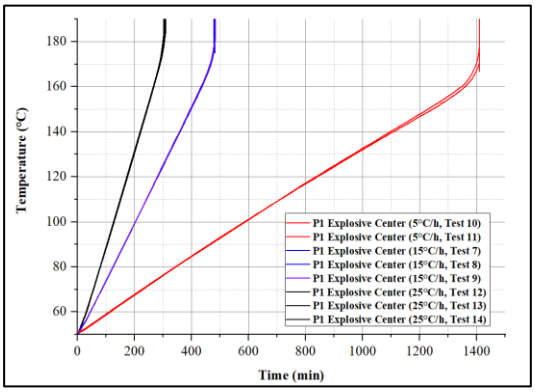

Figure AP.2. Bare P1 Explosive

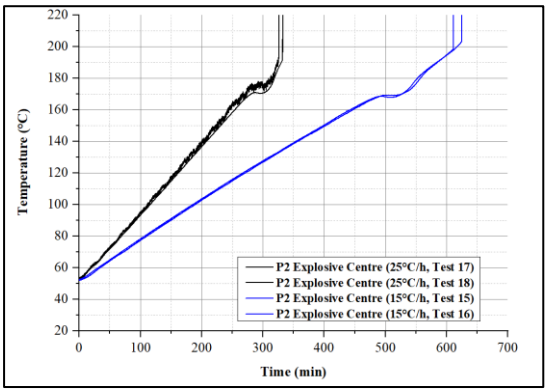

Figure AP.3. Bare P2 Explosive

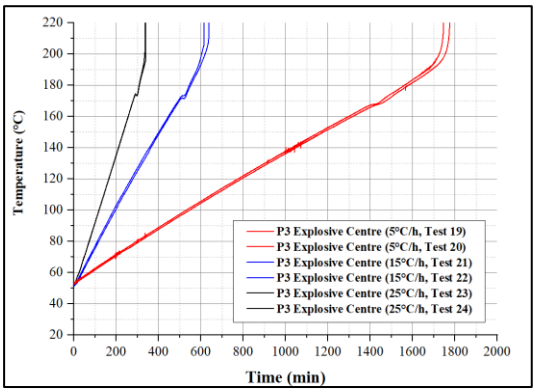

Figure AP.4. Bare P3 Explosive

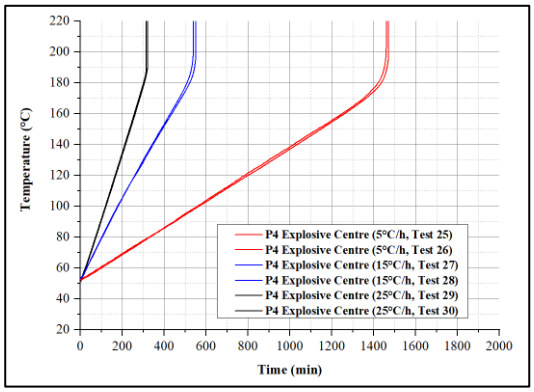

Figure AP.5. Bare P4 Explosive

F. Ignition Point Investigation of Small-Scale Test Item (P1 Explosive)

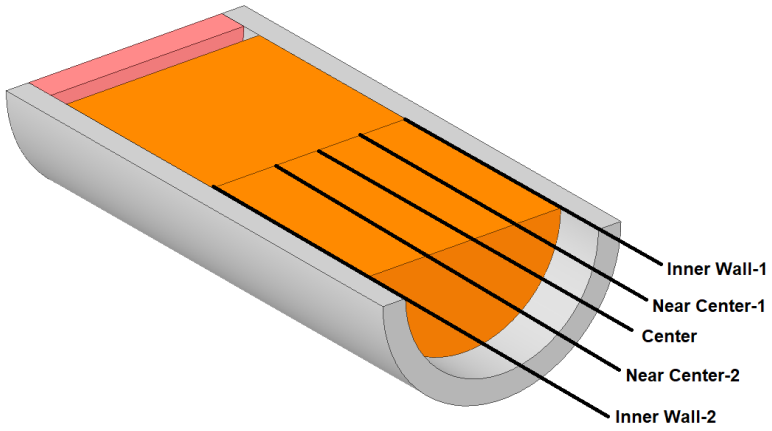

Figure AP.6. Investigation of Ignition Location of P1 Explosive for 15 °C/h Heating Rate

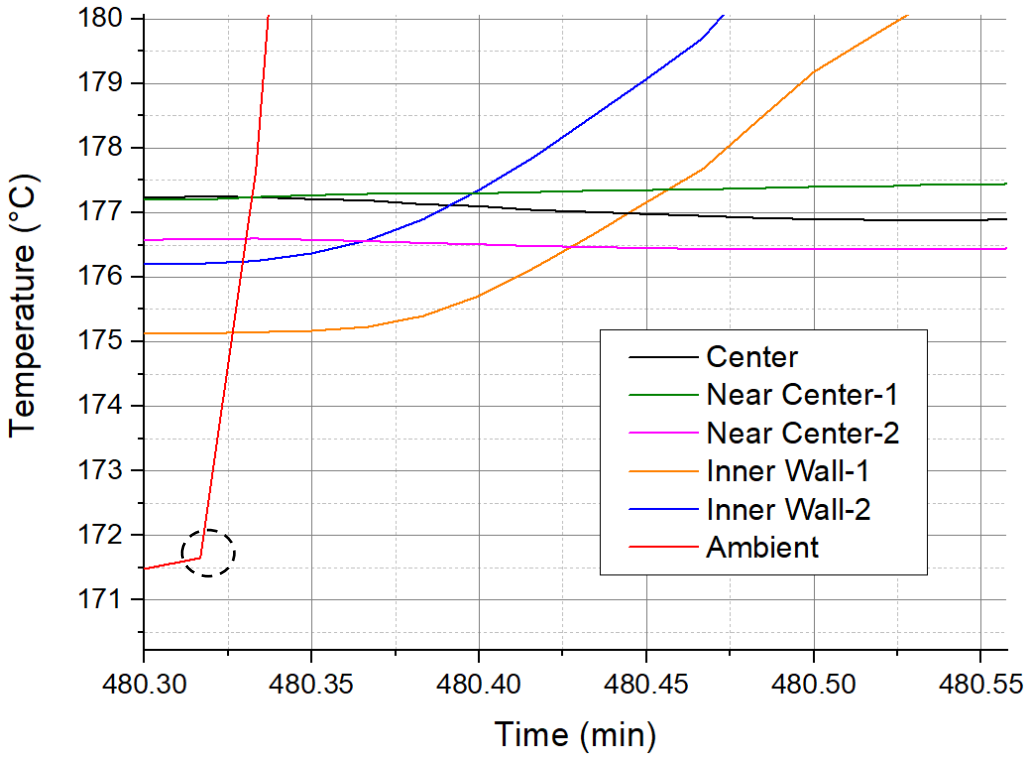

Figure AP.7. Ignition Point of P1 Explosive, Test 7 (15°C/h heating rate)

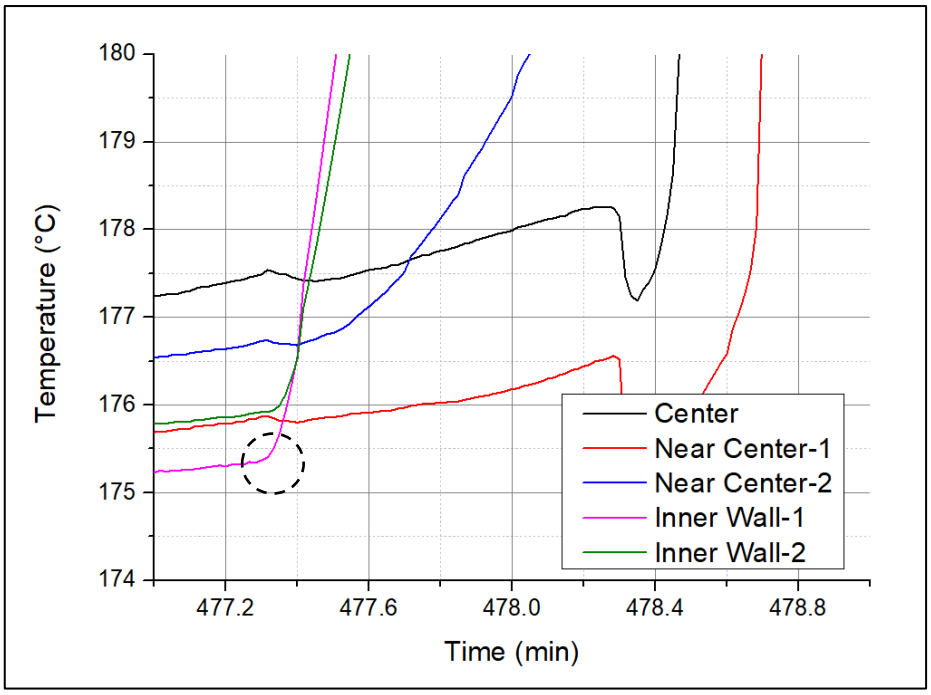

Figure AP.8. Ignition Point of P1 Explosive, Test 8 (15°C/h heating rate)

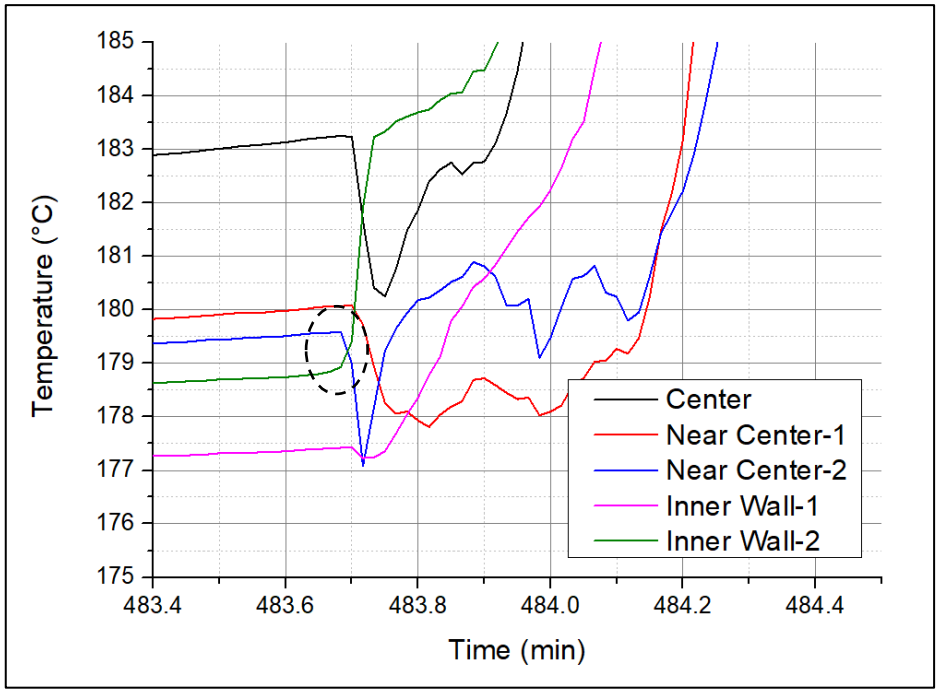

Figure AP.9. Ignition Point of P1 Explosive, Test 9 (15°C/h heating rate)

G. Effect of Convection Heat Transfer Coefficient on Temperature Profile for Bare P1 Explosive (Without Igniter)

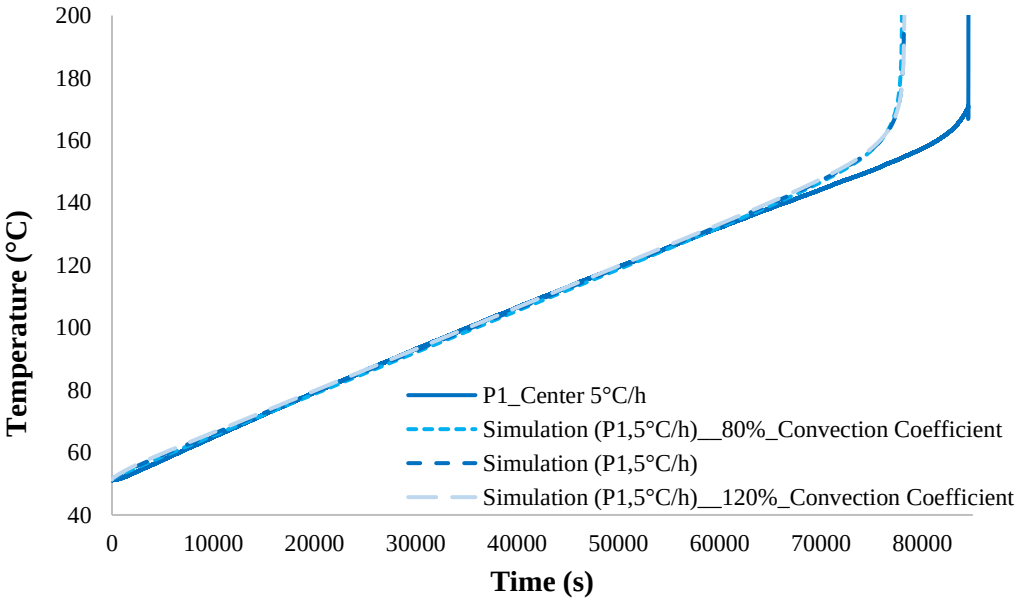

Figure AP.10. Effect of Convection Heat Transfer Coefficient on P1 Explosive Temperature Profile (Without Igniter) (5 °C/h)

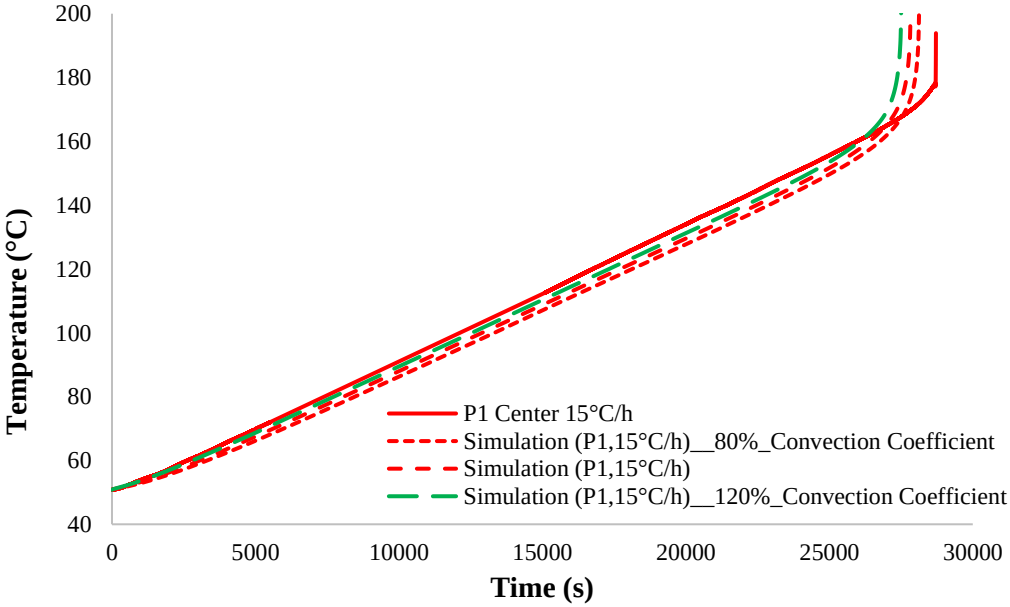

Figure AP.11. Effect of Convection Heat Transfer Coefficient on P1 Explosive Temperature Profile (Without Igniter) (15 °C/h)

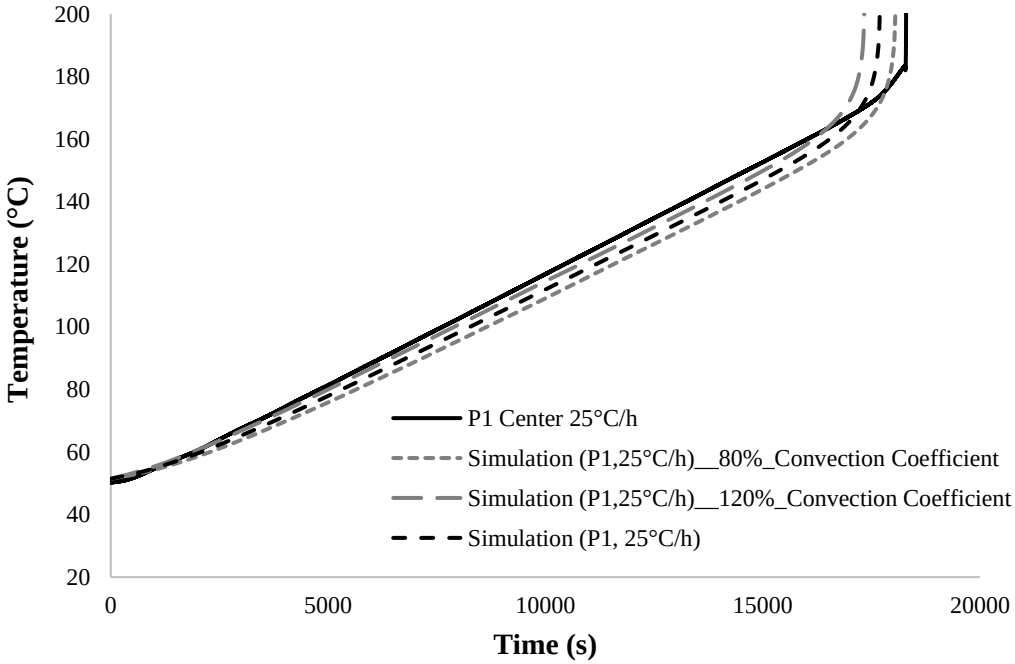

Figure AP.12. Effect of Convection Heat Transfer Coefficient on P1 Explosive Temperature Profile (Without Igniter) (25 °C/h)